Status report of EEVC WG 21 Accident Studies

P. Thomas
Loughborough University, UK
Y. Page
LAB France
G. Vallet
INRETS, France
D. Otte
Medical University of Hanover, Germany
R. Sferco
Ford of Europe , Germany
G. Della Valle
Elasis, Italy
M. Giunti
Fiat, Italy
B. Hoogvelt
TNO, Netherlands
J. Paez
INSIA, Spain
P. Magnusson
SNRA, Sweden
R. Cuerden
TRL Ltd, UK

07-0416

ABSTRACT

Working Group 21, Accident Studies, has been formed to bring together analysis of existing accident data in support of the work programme of the EEVC. Its members represent all of the major in-depth accident databases in Europe and have access to a large number of others. This paper presents some of its early work.

A major task has been to conduct an audit of the available accident databases and to record their key characteristics. A total of 45 accident databases from 8 countries are identified and the paper lists factors including proprietary, data content, selection criteria, vehicles studied and purpose of investigation.

In general larger quantities of accident data are more likely to give statistically significant results and a second objective of the group has been to evaluate the feasibility and analysis potential of combining data from several countries. A pilot study was conducted to combine data from France, Germany and the UK to estimate the effectiveness of side airbag systems. A logistic regression model was developed which showed side thorax airbags reduced AIS 2+ thoracic injuries by 17%, although this was statistically not significant.

In support of WG 12, biomechanics, WG 21 has been asked to provide data on the types of leg injury sustained in crashes by occupants of three different age groups of cars in relation to future designs of ATD. A parallel analysis of UK and Swedish data is presented which shows the changes in lower extremity injury location and type.

Finally the paper will describe some of the current work of the group which is to assist the new work plan of WG 13, Side Impact Protection in relation to the further development of test procedures and side impact barrier characteristics.

BACKGROUND

The European Enhanced Vehicles Committee seeks to improve the safety performance of vehicles in use in the European Union. In order to do this new test protocols are developed that address critical issues of impact types or injury causation. It is important that these issues apply generally across the EU so that changes to car design, which are also made on an EU basis, make the greatest contribution to casualty reduction. To support the work it is important to have a good knowledge of accident and injury priorities across the EU and therefore to base the EEVC work on a broad picture of accident analysis. This is in line with the increasing demand at international and national levels to ensure that government and EU policies are based on sound evidence and established safety benefits.

EEVC WG 21 Accident Studies has been established to serve as a resource centre and information provider to the other WGs regarding the collection, analysis and review of accident data in the wider EEVC work programme. Its Terms of Reference are summarised as follows:-

1) To conduct an audit of existing and future accident data needs of the EEVC Working Groups and to identify areas where poor quality information diminishes the value of accident and injury data and its subsequent analysis.

2) To redress these deficiencies by obtaining better data and analysis from within or outside the EEVC countries, especially to make use of work of the EU-funded Pendant and SafetyNet projects.

3) Through the analysis of existing accident databases make recommendations to the EEVC Steering Committee where future EEVC coordinated research could be undertaken, that would lead to reductions in both the number and severity of accidents and injury.

4) Through the analysis of existing accident databases monitor developments in advanced safety systems, and attempt to determine their efficacy and deficiencies, in liaison with the other EEVC Working Groups, and report to the EEVC Steering Committee on a regular basis.

5) Develop regular links with each of the EEVC Working Groups.

METHOD OF WORKING

EEVC WG 21 provides an accident data analysis service to the EEVC, bringing together data from the eight countries represented. Each country has its own national level data that is available for analysis but several countries have routine in-depth crash investigations while others have special studies of selected crash types. One requirement of the Working Group has been to construct an audit of these databases and their essential characteristics, the complete audit is available on the WG 21 web pages and an extract is presented in this report.

WG 21 will utilise this data to address specific issues of other EEVC Working Groups. Once a clear specification of the data needs has been reached WG 21 will conduct a co-ordinated analysis of several datasets where equivalent tables are produced from each, an example is the analysis of leg injuries conducted for EEVG Working Group 12, Crash Dummies. Alternatively Working Group 21 has examined methods where datasets can be combined for certain types of analysis to increase the confidence in the results and an example is the study on side airbag effectiveness. Most recently WG 21 has commenced an extensive analysis of side impacts in order to support the work of WG 13, Side Impact and the work schedules of both Working Groups have been synchronised so that the results from WG 21 feed directly into the deliberations of WG 13. Examples of each of these analyses is given below.

AUDIT OF DATABASES

An early task of WG 21 has been to conduct an audit of databases available to the group to facilitate the selection of suitable data sources for subsequent analysis. A total of 46 separate data systems have been identified and their main characteristics have been listed. The names and summary details of the databases are shown in Appendix A and the fields recorded for each are shown in Appendix B. The full list with details is available on http://www.eevc.org. Some of these databases have been used for combined or parallel analyses within the group so far , some of the results are outlined below.

ANALYSIS OF LEG INJURY PATTERNS – WG 12 (DUMMIES)

In order to focus its work on new dummy characteristics WG 12 requested an analysis of the patterns of injury to the lower extremities showing any changes relating to the introduction of EuroNCAP and the EC Directive on frontal impact

protection. The data from Sweden and the UK was used to address this issue and, since descriptive information only was required, a parallel analysis was conducted on each to a common specification. Although ideally the year of manufacture of the car would be a key parameter, describing the level of specification of the car, this is not available routinely on most of the crash injury databases so the data was categorised according to the year of registration of the vehicle. Each of these databases selects crashes that involve injury, but although there will be an injured casualty within the collision not all casualties are injured. The data cannot be used to assess the absolute changes on injury numbers but they do show any changes in frequency of injury of one body region compared to another. Table 1 shows the cases available from each dataset.

Table 1
Cases available for WG 12 leg injury analysis

Database	Year of Manufacture			Total
	1990-5	1996-9	2000+	
Swedish Strada data	449	258	410	1117
UK CCIS data	1060	1914	1288	4262
Total	1509	2172	1698	4379

A total of 4379 sets of occupant details were available for cars of the selected age ranges that were involved in frontal collisions. Figures 1 and 2 compare injuries to the lower extremity to other body regions for Swedish Strada and UK CCIS data. Since the lower extremity injuries that involve longer term impairment can have AIS values of 2 or higher the figures show the rates of such injuries to each body region.

Figure 1
Pattern of injuries – Strada

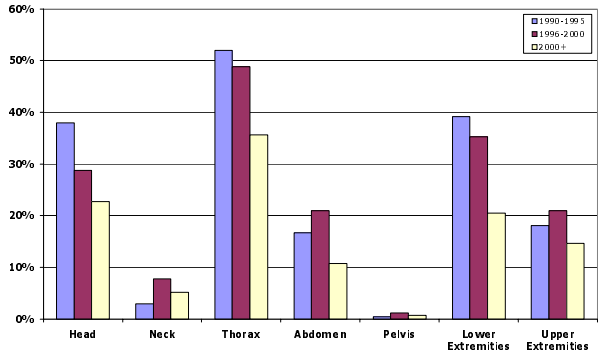

Figure 2.
Pattern of Injuries – CCIS

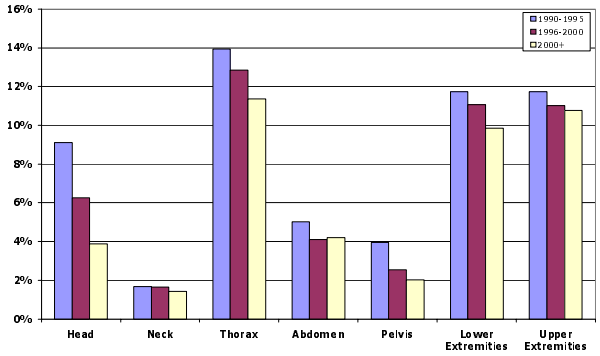

The case selection criteria for the three samples are different and the values cannot be directly compared, nevertheless consistent trends can be observed. All three datasets demonstrate a large reduction in rates of head and torso injuries. Injuries to the extremities were amongst the most common in all databases and mostly showed little or no decrease in relative frequency over the period studied.

The locations of injury are directly relevant to dummy design and determine the emphasis on specific locations for dummy instrumentation. The two datasets were also examined with respect to the injuries themselves, Table 2 shows the total AIS 2+ injuries from each group and Figures 3 and 4 show the locations of these injuries derived from each dataset.

Table 2
Injury details available for WG 12 leg injury analysis

Database	Year of Manufacture			Total
	1990-5	1996-9	2000+	
Swedish Strada data	141	70	71	282
UK CCIS data	283	413	413	1109
Total	424	483	484	1391

Figure 3.
Location of lower extremity injuries – Strada

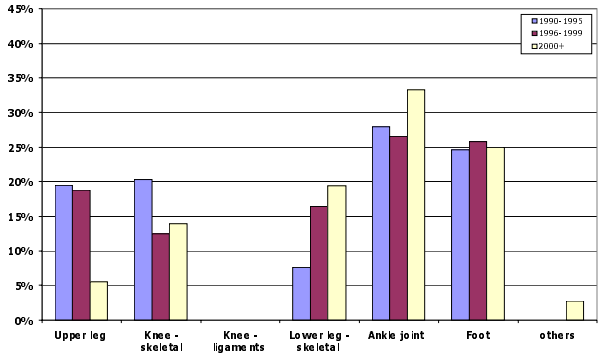

Figure 4.
Location of lower extremity injuries – CCIS

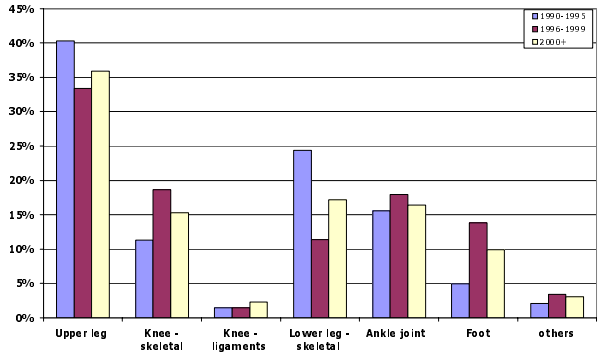

Although figures 3 and 4 show different distributions of injury location, possibly because of different vehicle fleets in the two countries both databases showed that ligament injuries to the knee were rare and also that the overall distribution of AIS 2+ injuries did not significantly change over the period 1990 – 2006. Otherwise the data from every country showed there remained a need for crash test dummies to measure the risks of injury at each part of the lower extremity.

PILOT STUDY ON ANALYSIS OF COMBINED DATASETS – SIDE AIRBAG EFFECTIVENESS.

WG 21 proposed to conduct a pilot study on the injury reduction effect of side airbags. It would also serve to evaluate the issues WG 21 would meet concerning parallel and combined data analyses from several sources in different countries. The group established that statistical modelling methods combined with case-by-case study would be the most suitable method.

During the last 5 years, the number of cars fitted with side airbags has dramatically increased. They are now standard equipment, even on many smaller cars or less luxurious vehicles. While some side airbags offer thoracic protection alone, there are those that combine thoracic and head protection (of which most deploy from the seat). Other systems employ separate airbags for head and thorax protection, which are designed to be effective noticeably in a crash against a pole. The Working Group 21 paper, presented at the ESAR Conference in September 2006[1], proposed an evaluation of the effectiveness of side airbags in preventing thoracic injuries to passenger car occupants involved in side crashes. Statistical analysis for head injuries was not possible due to the low number of accident cases with passenger cars fitted with head airbags in the databases.

First, the target population (who can take benefit of side airbag deployment and in what circumstances) was defined. Side airbags can be especially effective in cases of impacts on the door with intrusion at a certain impact speed. National data provides the overall magnitude of side impacts. For example, in France, side impacts account for about 25 % of fatalities (front and rear seats) and 18 % of seriously injured casualties in passenger cars. In the UK data 41% of fatally injured occupants died in side impacts and 37% of seriously injured casualties received their injuries in side impacts. 40 % of the French fatalities (respectively 60 % of those seriously injured) occur against another car, one third (respectively 30 %) against a fixed obstacle and 25 % (respectively 10 %) against a light or heavy truck.

70 % of the fatalities and 50 % of the seriously injured casualties in side impacts occur on the struck side with intrusion. Consequently, in France, 17 % of overall fatalities (70 % * 25 %) and 9 % of overall seriously injured casualties (50 % * 18 %) are the target population for side airbags, which are supposed to work for occupants seated against the struck door. This calculation was not done for either Germany or the UK.

Then, an example case of a side impact with side airbag deployment was given where side airbag deployment is thought to have had a positive effect on injury outcome. Actually, while statistical analysis and models can be used to derive a generalised view of accident data case by case reviews provide a complementary role. They are able to produce a fuller understanding of the real-world event and help to define key factors for use in subsequent modelling. An overall review of cases can help to define the most valuable selection criteria for cases to be

included in the model and to avoid outliers. They can also provide a qualitative view of the limits of protection with side airbags. An additional expert case review can also indicate injuries that would probably have occurred without side airbags and identify potential airbag induced injuries.

The CCIS database was searched for examples of cases of medium to high severity side impacts with low severity occupant thoracic injury, cases were side airbag deployment may have been effective for injury prevention and a higher injury outcome may have been expected. Two examples of the cases found were presented in the paper.

Then, the estimation of side airbag effectiveness (in terms of additional occupant protection brought exclusively by the airbag) was proposed by comparing injury risk sustained by occupants in (more or less) similar cars (fitted or non fitted with airbags). Comparing risks in similar cars was necessary since, during these years, car structure, and side airbag conception have considerably evolved.

In-depth accident data from France, the UK and Germany has been collected. Out of 2,035 side impact accident cases available in the databases, we selected 435 occupants of passenger cars (built from 1998 onwards) involved in an injury accident between year 1998 and year 2004 for EES (Energy Equivalent Speed) values between 20km/h and 50 km/h. The occupants belted or not, were sat on the struck side, whatever the obstacle and type of accidents (intersection, loss of control, etc.). For multiple impact crashes, the side impact was assumed to be the more severe one. Passengers cars were fitted with (96) or without (339) side airbags. Most of the potential risk explanatory variables were correctly and reliably reported in the databases (velocity – impact zone – impact angle – occupant characteristics, etc.).

The analysis compared injury risks for different levels of EES and different types of side airbags. A logistic regression model was also computed with injury variables (such as thoracic AIS 2+ or AIS 3+) as the dependant variable and other variables (including airbag type and EES) as explanatory injury risk factors. Results revealed statistically non-significant reductions in thoracic AIS 2+ and AIS 3+ injury risk in side airbag equipped cars in the impact violence range selected (odds ratio between 0.84 and 0.98 depending on types of airbags). The non-significance is assumed to be due to a low number of cases.

The GIDAS[23] [4]data was used to identify comparable in-depth cases with and without side airbags. These cases were used to illustrate the relative injury outcomes. An example is shown in Figure 6 below illustrating a case where the struck-side occupants sustained only minor injuries in the side collision. Overall the GIDAS analysis concluded side airbags gave a benefit in 41% of collisions and no benefit in 44% of collisions.

Figure 6.
GIDAS accident case example

SIDE IMPACTS

EEVC Working Group 13 has the objective to improve the safety performance of cars in side impacts. As part of a renewal of objectives and future work programme the EEVC Steering Committee has determined that analysis of crash injury data should form the basis of the work of WG 13. WG 21 has therefore been requested to conduct an extensive analysis of side impacts using a wide range of national level and in-depth datasets. This work is on-going but a sample of early results are presented below. These results are only available from analysis of the CCIS data at this stage and are therefore only indicative of any final conclusions, they may change as more data is examined. The analysis comprised an overview of the main characteristics of side impacts, comparing the frequency with that of other impact directions, followed by specific analysis of car to car impacts, pole impacts and non-struck side impacts. This paper presents only the interim results from part of the overview analysis.

Data in Table 3 shows the frequency of injuries according to the direction of impact. All casualties are occupants of cars registered after 1998, when the vast majority of new cars would have complied with the side impact regulation. Multiple impacts are

excluded to ensure the injuries are associated with the main impact alone.

Table 3.
Severity of injuries by collision direction – CCIS data

	Injury Severity							
	MAIS 0		MAIS 1&2		MAIS 3+		Fatal	
Front	343	68%	1594	68%	240	59%	71	49%
Rear	17	3%	109	5%	5	1%	3	2%
Side	144	29%	651	28%	159	39%	74	51%
of which SS	*65*	13%	*358*	15%	*114*	28%	*54*	38%
NSS	*79*	16%	*293*	12%	*45*	11%	*20*	14%

At lower injury severity levels front collisions are the most frequent source of injuries, only 28% – 29% are sustained in side impacts. However the more severe injuries are increasingly associated with side collisions, 39% of MAIS 3+ casualties are in side collisions and these accounted for slightly over 50% of fatalities. The table also categorises side impact casualties according to whether they are seated on the struck side or the far side. At each severity level the majority of side impacted occupants were seated on the struck side, 28% of fatally injured side impacted occupants were seated away from the impact on the non-struck side. Table 4 shows the nature of the collision partner according to the severity of injuries sustained by each occupant of a side impacted car.

Table 4.
Collision partner – struck-side casualties

	MAIS 3+	Fatal
Single Vehicle	43%	48%
Car/Car derivative	33%	30%
TWMV	2%	0%
MPV/LGV	7%	6%
HGV/Bus	12%	17%
3+ Vehicles	3%	0%
Total	100%	100%

The UK CCIS data indicates that nearly half of all struck-side fatalities are in single vehicle collisions while only 30% are in collision with another car. 17% are involved in impacts with large goods vehicles or buses. Of the single vehicle collisions only 27% struck a narrow road-side object, less than 41cm wide, broadly corresponding to a lamp-post or sign-post.

Figure 7 shows the mass of the collision partner when it was a car. Nearly 80% of all striking cars had a mass exceeding 950 kg, the mass of the deformable barrier however less than 10% were above 1500kg. The figure also shows how the distribution of mass varies according to the severity of the injuries of the struck-side casualties. In the absence of more detailed analysis there does not appear to be any link between mass of the striking car and injury outcome although these results have not yet been adjusted for collision severity.

Figure 7.
Mass of striking car.

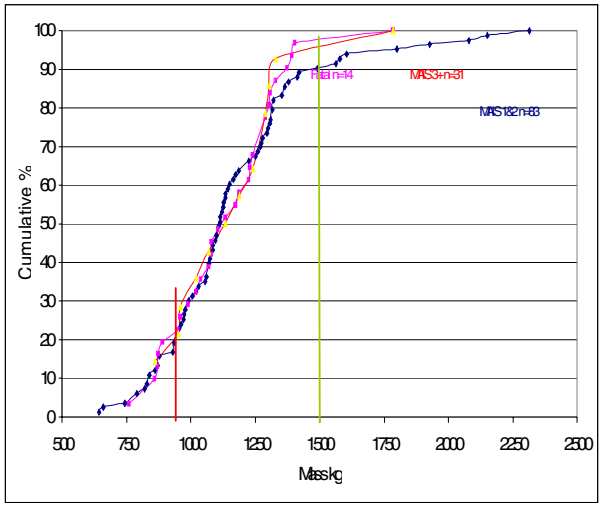

The standard test condition for side impacts in the EC directive and the EuroNCAP test involves a perpendicular impact to the vehicle, however the need for a different condition is still debated. Figure 8 shows the distribution of injury severity for the oblique and perpendicular impacts of struck side occupants.

Figure 8.
Perpendicular and oblique side impacts

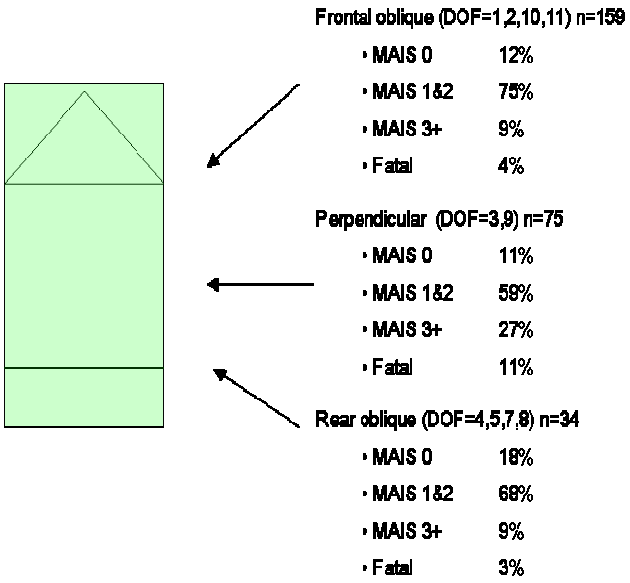

Analysis of the data shown in Figure 8 indicates that although oblique impacts to the front or rear were more common than perpendicular impacts they were less likely to involve severe injury. 70% of the total impacts in Figure 8 were oblique but the numbers of fatalities in each configuration were equal. The risk of fatality in perpendicular collisions was 10% compared with only 4% in oblique impacts. Similarly the rate of MAIS 3+ injury in perpendicular collisions was 25% compared with 9% in oblique.

The same distribution was obtained for impacts with poles and the data for Germany and the UK is shown in Figure 9 below. This diagram illustrates that perpendicular collisions are the most likely to result in injury.

Figure 9.
Impact direction and injury severity

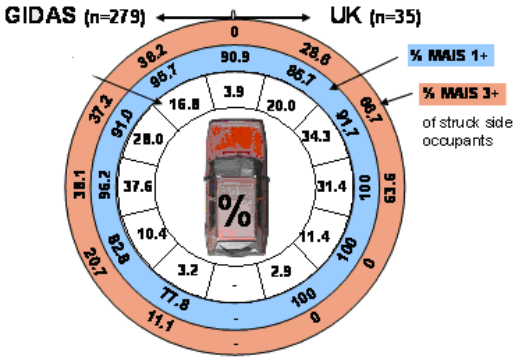

CONCLUSION

The work of EEVC Working Group 21 focuses on a wide range of subjects, of which a sample have been presented in this paper. The group is able to conduct detailed analysis of many datasets to a common end. These analyses can cover several datasets using a set of common specifications or be based on a combined dataset where certain outcome parameters can be modelled.

Over 45 different datasets of a variety of levels of detail can be accessed by the group including national and in-depth data. This data is gathered using a wide variety of case selection procedures, while this mixture may limit detailed comparability it also may mean that a much wider range of analysis questions can be addressed.

ACKNOWLEDGEMENT

This paper uses accident data from the United Kingdom Co-operative Crash Injury Study. CCIS is managed by TRL Ltd on behalf of the Department for Transport (Transport Technology and Standards Division) who fund the project with Autoliv, Ford Motor Company, Nissan Motor Europe and Toyota Motor Europe. The data were collected by teams from the Birmingham Automotive Safety Centre of the University of Birmingham, the Vehicle Safety Research Centre at Loughborough University, and the Vehicle & Operator Services Agency of the Department for Transport. Further information on CCIS can be found at http://www.ukccis.org.

This paper contains data and analysis from the German In Depth Accident Study (GIDAS). GIDAS is a joint project between FAT (Forschungsvereinigung Automobiltechnik or Automotive Industry Research Association) and BASt (Bundesanstalt für Straßenwesen or the Federal Road Research Institute).

Appendix 1: list of available accident databases

Database name	Full Name	Owner
EACS	European Accident Causation Survey	ACEA + ACEA Members
PVM-90	Fatal Accident Analysis 1990	LAB
PVM-2000	Fatal Accident Analysis 2002	LAB
ETAC	European Truck Accident Causation	IRU + EU
EDA	LAB In-Depth Car Accident Investigation	LAB
LAB	LAB - in house	LAB
CHILD	Advanced methods for improved Child Safety	European project consortium
RISER	Roadside Infrastructure for Safer European Roads	EU
TRUCK	In-Depth Truck Accident Analysis	RENAULT TRUCKS
BUS	In-Depth Bus Accident Analysis	IRISBUS
EDA	INRETS In-Depth Car Accident Analysis	INRETS
MAIDS	Motorcycle Accident In-Depth Study	ACEM
RIDER	In-Depth Motorcycle accident research	French Government (Department of Research), CEESAR
OTS	On The Spot accident research project	UK Department for Transport
GIDAS	German In-Depth Accident Study	GIDAS consortium (BASt and several manufacturers/suppliers)
PENDANT	Pan European co-ordinated Accident and Injury Databases	EU
CARE	Community Road Accident Database	EU
CCIS	Co-operative Crash Injury Study	UK Department for Transport with industry co-sponsors (see Acknowledgement)
SAFETYNET	European Road Safety Observatory	EU
TRAMS	Tram Accidents	Dutch Transport Safety Board
SUV	Sport Utility Vehicles	TNO
TRUCKS	Truck Accidents	SCANIA
UK Travel Survey	UK Travel Survey	
STAT 19 enhanced	STATS 19	UK Department for Transport
SSIS	Sistema Integrato Sicurezza Stradale	Milan province, Sorrento city and Salerno city
BAAC	French Injured Accident Analysis Report	French Government (Department of transport)
OGPAS	Official German Police Accident Statistics	Federal Statistical Offices of the German States
GMS2002	German Mileage Survey 2002	BASt
VW- In house	VW - In house	VW
GNS	Greek National Statistics	National Statistical Service of Greece
DGT database	Spanish General Directorate of Traffic - Road Accidents Database	Spain Government (Department of Transport)
DIANA	Proyecto de Investigación y Análisis de Accidentes	CIDAUT
LMU - FARS	Getötetendatenbank. Accidents with fatal injuries in Bavaria	LMU
KISS	Kraft Informations Statistik System der Allianz	Allianz Insurance

Database name	Full Name	Owner
ROLLOVER	Improvement of Rollover Safety for Passenger Vehicles	European project consortium
AJBCN	Ajuntament de Barcelona (Barcelone Council)	Barcelone Council
BUS - SP	In-depth accident investigation with buses involved in Spain	DGT-Applus + IDIADA
PED - BCN	Pedestrian Barcelone	Barcelona Council - Applus + IDIADA
SINGULAR CASES	Singular cases - Isolated incidents	Applus + IDIADA
SCT	Servei Català del Trànsit	Catalonia Government
BIA	Barcelona Investigació d'Accidents (Accident Investigation Barcelone)	Càtedra Applus
TROHOGNOMON	Trohognomon (traffic accidents investigator company) database	Trohognomon company
IRTAD	International Road Traffic and Accident Database	EU
DEKRA	DEKRA Accident Database	DEKRA
In-depth studies of fatal accidents	In-depth studies of fatal accidents	Swedish Road Administration
STRADA	Swedish TRaffic Accident Data Acquisition	Swedish Road Administration
SEWIK	Polish State Police Accident Database	Polish State Police
ITS Accident database	Institute for Transport Studies database	Institute for Transport Studies, Poland

Appendix 2: Main characteristics recorded for each database.

Database name	
Full Name	
Owner	
Investigation Teams	
Principle focus (active, passive, both etc)	
Main Objective	
Type of investigation	In-Depth Acc. On the spot
	In-Depth Acc. Delayed Time
	Police Report Anal.
	Exposure Data
	Stat. Data
Vehicle types covered	Car
	Two Wheelers
	Ped.
	Truck
	Bus
Years of accidents	
Selection criteria	
Sampling details	
Most suitable applications	
Status	
Nb Acc/year (average)	
Total no of vehicles on database (up to now) or expected	
No of vehicles year model >= 2000	
Use of Data	Any special condition
	Raw data available
	Own Team processes
Comments on application for passive or active safety research on modern vehicles?	
Any other information	
Software	
Available export format	
Language	
Region covered	Region
	Comment
Documentation	Methodology
	Coding Convention
	Statistical Sampling plan
	Questionnaire
	Glossary of terms
Data Content	Pictures available
	Cause of accidents
	Cause of injuries
	Human Factors
	Vehicle technology
	Accident situation

	Road user
	Reconstruction

REFERENCES

[1] Y. Page, P. Thomas, V. Hervé, A. Kirk The Effectiveness of Side Airbags in Preventing Thoracic Injuries in Europe. 2nd Expert Symposium on Accident Research, Hanover, 2006

[2] Otte, D.; Krettek, C.; Brunner, H.; Zwipp, H.: Scientific Approach and Methodology of a New In-Depth-Investigation Study in Germany so called GIDAS, ESV Conference, Japan, 2003

[3] Otte, D.; Krettek, Ch.:Rollover Accidents of Cars in the German Road Traffic – An In-Depth Analysis of Injury and Deformation Pattern by GIDAS
19. ESV Conference in Washington D.C., ESV paper no 05-0093-0, 2005

[4] Brühning, E.; Otte, D.; Pastor, C.: 30 Jahre wissenschaftliche Erhebungen am Unfallort für mehr Verkehrssicherheit
Zeitschrift für Verkehrssicherheit 51, 175-181, 2005

TECHNOLOGIES TO IMPROVE IMPACT RELATED FIRE SAFETY

Kennerly H. Digges
Motor Vehicle Fire Research Institute (MVFRI)
United States

Paper Number 07-0480

ABSTRACT

The research reported in this paper is a follow-on to a five year research program conducted by General Motors in accordance with an administrative Settlement Agreement reached with the US Department of Transportation. In a subsequent Judicial Settlement, GM agreed fund more than $4.1 million in fire-related research over the period 2001-2004. The purpose of this paper is to provide a public update report on the projects that have been funded under this latter research program, along with results to date. This paper is the sixth in a series of technical papers intended to disseminate the results of the ongoing research.

The projects and research results reported in this paper include statistical analyses of vehicle fires based on FARS and NASS and summaries of technologies to reduce crash induced fires

INTRODUCTION

The GM/DoT Settlement research program has been documented elsewhere [NHTSA 2001]. The research reported in this paper is a follow-on to that project.

The Fatality Analysis Reporting System (FARS) is a database maintained by the US Department of Transportation. It contains records of all fatal crashes that occur on public roads in the United States. The FARS database has been used to document the variations in fatal injuries annually since 1975.

The FARS database documents all fatalities that occurred as a result of the crash including those where a fire resulted. In this paper, the term "FARS Fatalities" designates the fatalities in which a fire occurred in the vehicle, regardless of whether or not the fire caused the fatality. Since 1979, FARS also coded the "most harmful event" (MHE). If the fire event has been coded as the most harmful event, burn or inhalation injuries are the most likely cause of the fatality. In many crashes, it may be difficult to discern the cause of the fatality (biomechanical trauma vs. fire trauma). This distinction was not investigated and the coding was taken directly from FARS. Previous studies have attempted to investigate the uncertainty and difficulty in coding fire as the most harmful event [Davies 2002].

Earlier papers reported that between 1979 and 2000, when fire was coded as the most harmful event (MHE), the fatality rates for vehicles less than 5 years old had declined by 72.4% [Friedman 2003 and 2005; Digges 2003]. The MHE fire rates for pickups less than 5 years old had reduced by 82.4%, but their rates were still higher than the rate for passenger cars.

A follow-on analysis grouped years of FARS data to examine changes in the fatal crashes with fires [Bahouth, 2007]. The figures presented in the earlier papers showed that the fire rates of vehicles generally decreased during the decade of the 1980's but have remained relatively constant since 1990. To examine these trends, the FARS years were aggregated into three groups – 1979-1989; 1990-1999; and 2000-2005. Figure 1 shows the FARS fire rate and FARS MHE fire rate using billions of annual vehicle miles traveled (VMT) as the denominator.

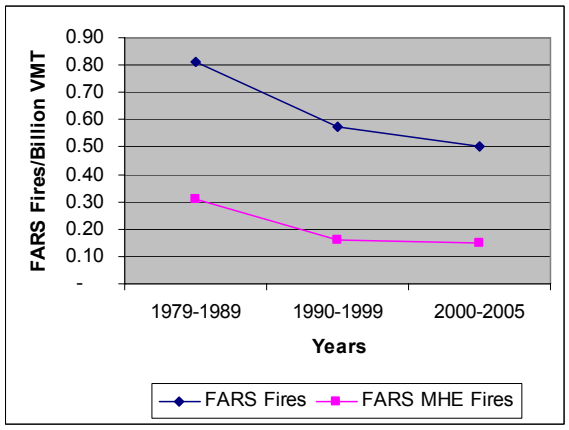

Figure 1. Fatalities in Vehicles with Fires and in Vehicles with Fire as the Most Harmful Event per Billion Vehicle Miles Traveled Annually - FARS

FARS does not record the direction of force in the crash. However, the location of principal damage is coded. In this coding, rollovers with damage from impacts with fixed objects or with other vehicles are coded according to the location of the damage. If the damage comes from ground contact, the crash is classified as a non-collision. Rollovers are classified according to the event during which it occurred (i.e. Non-rollover, rollover during 1st harmful event, or rollover during subsequent events). Most of the rollovers have damage to the front or sides of the vehicle. This damage may have been caused by impacts with fixed or non-fixed objects before or

during the rollover. In some cases, these impacts may have been the cause of the fatality. The FARS can be examined by damage area only and without identifying the rollovers. However, in the analysis to follow, all rollovers are grouped together, regardless of the area of damage. No crashes with rollover are included in the front, side or rear damage areas. When FARS is analyzed in this way, the average annual fatalities are shown in Figure 2.

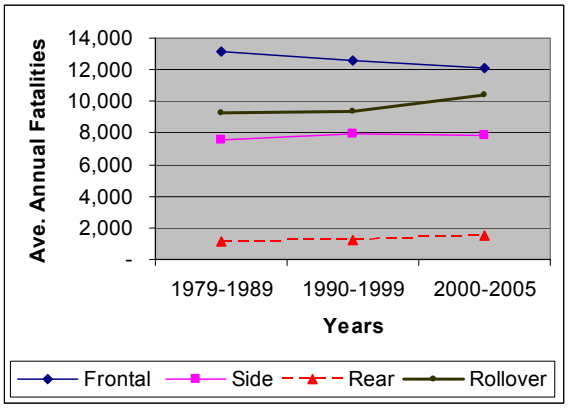

Figure 2. Average Annual Fatalities in Vehicles by Damage Area, with Rollover Separated - FARS

Using the same separation of rollovers as in Figure 2, the changes in fatalities when fire was the most harmful event can be examined. The results are plotted in Figure 3.

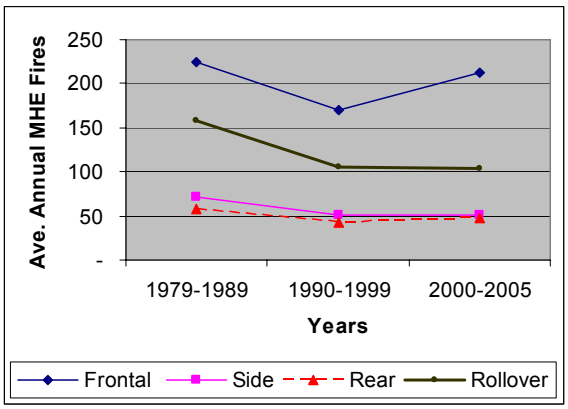

Figure 3. Average Annual Fatalities with Fire as the Most Harmful Event by Damage Area, with Rollovers Separated – FARS

Figure 4 shows the distribution of damage for the rollover fatalities in FARS years 2000 to 2005. The figure compares all rollover fatalities and rollover fatalities with fires. In the figure, non-collision and top damage were combined under "Roll". Left and right side damage were combined. "UCarr" is an abbreviation for undercarriage damage.

FARS does not provide data on fire origin and the designation of crash direction is by damage area. NASS provides better information on these variables and can be used in conjunction with FARS to gain a better understanding of collision related fires.

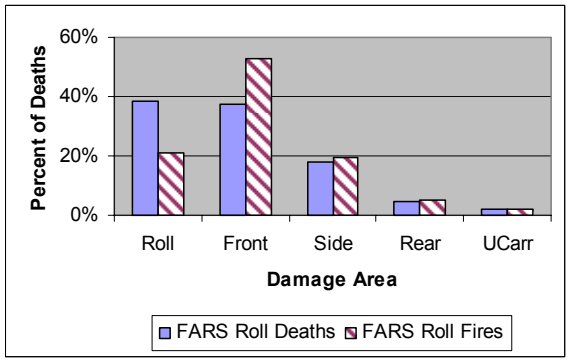

Figure 4. Damage Areas in Rollovers with Fatalities and Rollovers with Fires and Fatalities – FARS 2000-2005

NASS/CDS is a sample of tow away crashes that occur on US roads each year. The sample scheme stratifies cases by the severity of the crash. The sample rate for minor crashes is much lower than for severe crashes. In order to expand the stratified sample to the entire population it represents, an inflation factor is assigned to each case in the NASS/CDS sample. When the data is processed using the actual number of cases investigated, the data is referred to as "unweighted" or "raw." When the data is processed using the total of the inflation factors, the results should represent the total population of vehicles involved in tow-away crashes and the data is referred to as "weighted." In the analysis to follow weighted data estimates are reported. The figures to follow are based on a more detailed analysis of fires in NASS from George Washington University [Kildare, 2006]. This report contains both weighted and unweighted estimates.

One of the most significant variables in the analysis of fire occurrence is crash direction (mode). This variable specifies whether a crash is frontal, near side, far side, rear or rollover. Crash direction was defined using a combination of documented variables - principal direction of force (PDOF), general area of damage (GAD1) and rollover (ROLLOVER). The following criteria were used to establish crash direction.

Frontal - Frontal crashes were determined to be any crash where the PDOF was 1, 11, or 12 o'clock or was at either 10 or 2 o'clock with the highest deformation location coded as front (F).

Side - Side crashes were determined to be any crash where the PDOF was 3 or 4 o'clock or was at 2 o'clock with the highest deformation location not coded as front (F) or where the PDOF was 8 or 9 o'clock or was at 10 o'clock with the highest deformation location not coded as front (F).

Rear - Rear crashes were determined to be any crash where the PDOF was 5, 6 or 7 o'clock.

Rollover - Rollover crashes were determined to be any crash where a rollover was indicated by the variable ROLLOVER. It is important to note that crashes with any involvement of rollover were included as a rollover crash. Multiple impacts with any other planar impact occurring first would be included as a rollover crash.

Other - All Crashes not meeting the criteria of the other aforementioned crash directions was labeled as 'Other.' Some of the vehicles in NASS do not have a PDOF assigned. These vehicles with unknown PDOF were included in the 'Other" category.

NASS/CDS classifies fires as either Minor or Major. These fire severities are defined as the following:
A Minor Fire is a general term used to describe the degree of fire involvement and is used in the following situations:

- Engine compartment only fire
- Trunk compartment only fire
- Partial passenger compartment only fire
- Undercarriage only fire
- Tire(s) only fire.

A Major Fire is defined as those situations where the vehicle experienced a greater fire involvement than defined under "minor" above, and is used in the following situations:

- Total passenger compartment fire
- Combined engine and passenger compartment fire (either partial or total passenger compartment involvement)
- Combined trunk and passenger compartment fire (either partial or total passenger compartment involvement)
- Combined undercarriage and passenger compartment (either partial or total passenger compartment involvement)
- Combined tire(s) and passenger compartment (either partial or total passenger compartment involvement)

About 50% of the fires in NASS/CDS are classified as "Major". This is true for both weighted and unweighted data [Kildare 2006].

Figure 5 shows the distribution of all crashes (with and without fires) and crashes with major fires by crash direction. The distribution of minor fires is generally similar to major fire distribution [Kildare 2006].

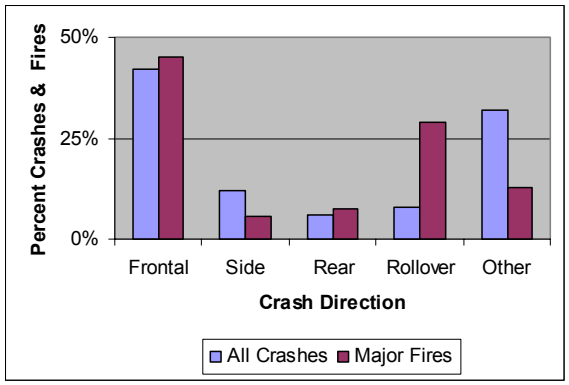

Figure 5. Distribution of Crashes and Crashes with Major Fires, by Crash Direction – NASS 1995-2004

Figure 6 shows the frequency of fires per 100 crashes for each crash mode. The denominator for the rate calculation is the total number of crashes in the crash mode under consideration.

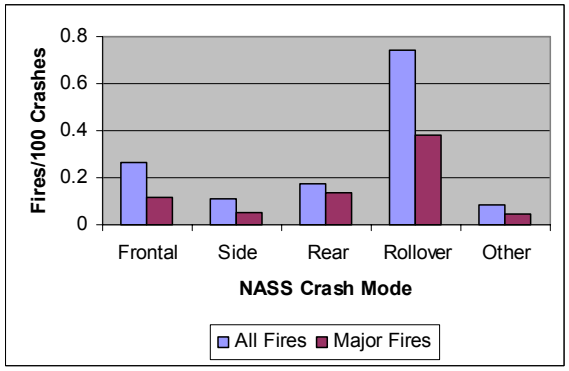

Figure 6. Rates of Crashes with Fires and Crashes with Major Fires, by Crash Direction – NASS 1995-2004

NASS also codes the fire origin. The distribution of the origins for major fires is shown in Figure 7. Over 60% of major fires originate in the engine compartment.

A further breakdown of major fire origins by frontal and rollover crash mode is shown in Figure 8. The engine compartment was the most frequent major fire origin for both the frontal and rollover crash modes. For the rollover crash mode, the fuel tank origin was a close second in major fire frequency.

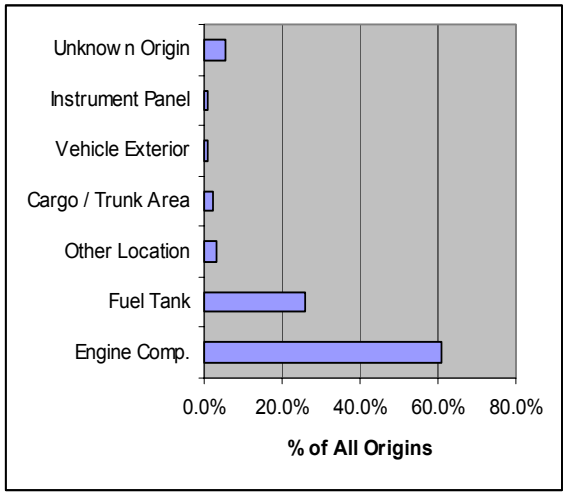

Figure 7. Distribution of Origins for Major Fires, All Crash Modes– NASS 1995-2004

Examination of individual cases of major fires in NASS 1997-2004 rollovers found that impacts prior to the rollover occurred in all cases with fuel tank fire origins for model year 1997 and later vehicles (Digges & Kildare, 2007). The study also found that seventy percent of the cases had engine compartment fire origins. About half of the cases with major engine compartment fires in rollovers did not involve significant impacts prior to the rollover.

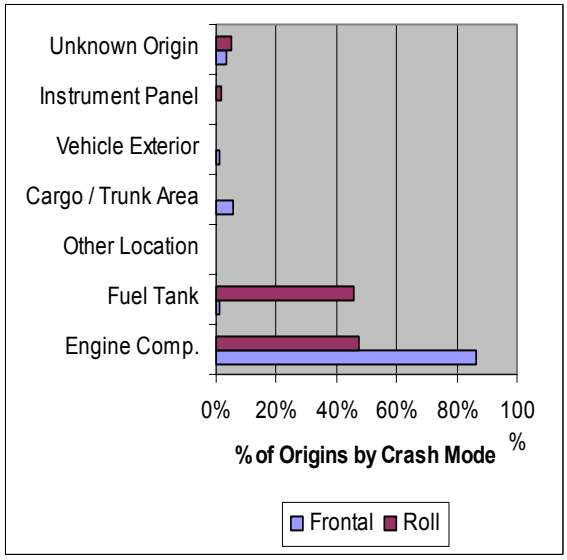

Figure 8. Distribution of Origins for Major Fires, Frontal and Rollover Crashes– NASS 1995-2004

The vehicle damage patterns exhibited by vehicles with fires in NASS have been analyzed and the results reported in a recent paper [Bahouth, 2006].

DISCUSSION OF FIRE DATA

As with other highway crash types, the rate of fires in fatal crashes per billion annual vehicle miles traveled has decreased significantly during the past twenty-five years. The decline is displayed in Figure 1.

During the same period, the annual average number of fatalities in vehicles with frontal damage has decreased, while fatalities in rollovers have increased. These trends are shown in Figure 2.

Except for frontal crashes, there is a downward trend in the annual number of fatalities where fire was the most harmful event (MHE). This trend is shown in Figure 3. However, for frontal damage crashes, the trend for fatalities with fire as the most harmful event has been upward during the past five years. During this same period, Figure 2 shows that the overall trend in fatalities in vehicles with frontal damage has been downward.

Figure 4 presents data on the location of vehicle damage in fatal rollover crashes. An examination of the vehicle damage areas in rollovers shows that the majority of FARS rollovers with fires also have frontal damage. These rollovers with frontal damage also have the highest fire rates. The lowest fire rates are in rollovers that have top damage or damage from the ground (non- collision). These latter two classes contribute about 20% of the rollovers with fires and fatalities.

The NASS data for major fires generally confirms the FARS data with regard to frequency of fires by crash direction or vehicle damage area. Figure 5 shows that nearly half of major fires are in frontal crashes. Rollovers contribute about 30% of the major fires and have the highest fire rate. The high fire rates for rollovers relative to the other crash modes are displayed in Figure 6.

Figures 7 and 8 provide information on the origins for major fires. Figure 7 shows that over 60% of major fires in NASS have their origins in the engine compartment. Figure 8 shows that for frontal crashes, over 80% of the major fires originate in the engine compartment. For rollovers, 47% originate in the engine compartment. This data indicates an opportunity to further improve fire safety by controlling engine compartment fires.

The lethality of engine compartment fires depends on the time available between the ignition of the fire and the time required for it to penetrate the occupant compartment. In the event occupants are trapped or

immobile due to injuries, the rescue time also becomes a critical factor. Data on rescue times has been published earlier [Digges 2005]. The 75% percentile rescue time for FARS rural cases was 24 minutes.

Data on the fire penetration time for selected tests conducted by General Motors has also been published [Tewarson, SAE 2005-01-1555]. In three tests of crashed vehicles with fires ignited in the engine compartment, the time to occupant compartment fire penetration varied from 10 to 23.5 minutes. The tests showed that once flames from the engine compartment penetrated the occupant compartment, the time to untenability was extremely short – a maximum of 3 minutes. This short tenability time of the occupant compartment when exposed to intense flames further amplifies the need to prevent or control engine compartment fires and delay their penetration of the occupant compartment.

The challenge of controlling engine compartment fires has increased with time due to the increasing amount of plastics used in motor vehicles. The amount of combustible materials has increased from 20 lbs per vehicle in 1960 [NAS 1979] to 200 lbs in 1996 [Twearson, 1997, Abu, 1998,]. Combustible plastics now constitute the major fire load (twice the weight and heat content of the gasoline) in a typical vehicle and these combustible materials are often ignited and contribute to the intensity of an automobile fire [Aherns, 2005; Friedman, 2005].

SUMMARY OF ENGINE COMPARTMENT FIRE TESTS AND MATERIALS FIRE PROPERTIES

Under a contract with MVFRI, the GM/DOT Settlement research program in motor vehicle fire safety has been summarized by a team of fire experts led by FM Global [Tewerson, Vols I, II and III, 2005]. Of particular interest has been the analysis of eleven, highly instrumented burn tests using crashed vehicles. These tests included underhood ignition scenarios and spilled fuel fires of an intensity that could be possible after a crash. The test results were summarized in an earlier ESV paper [Digges 2005].

Three of the vehicles that had undergone frontal crashes were then subjected to underhood fires with ignition sources either at the battery location or by the ignition of sprays and pools of mixtures of hot engine compartment fluids from a propane flame located in and below the engine compartment.

For the three crashed vehicle burn tests with ignition in and under the engine compartment, flame penetration time into the passenger compartment varied between 10 to 23.5 minutes. Once the flame penetrated the passenger compartment, the environment rapidly became untenable. The time between flame penetration and untenability of the passenger compartment varied from 48 seconds to 3 minutes.

The windshield and the bulkhead were the principal ports of entry for the flame spread into the occupant compartment. If the hood remained relatively intact, the fire tended to enter through openings in the bulkhead. The windshield was the principal flame entry port when it was directly exposed to flame as a consequence of openings in the hood near the base of the windshield. Whether the windshield is intact or broken as a result of the crash will also influence the rate of flame spread into the passenger compartment.

Additional research summarized test procedures to determine fire behavior of materials [Tewerson Vol 2 2005] and thermophysical properties of automotive plastics and engine compartment fluids [Tewerson Vol 3, 2005 and SAE 2005-01-1560, 2005]. Data on the toxicity and thermophysical properties of automotive plastics was reported by Southwest Research under a related research project funded by NHTSA and MVFRI [Battipaglia, 2003; Griffith, 2005]. A comparison of the fire properties of plastics used in aircraft with those used in automotive applications was reported by Lyon and Walters [Lyon 2005].

ENGINE COMPARTMENT FIRE SAFETY FEATURES

Possible countermeasures for engine compartment fires fall into three categories: (1) fire prevention, (2) delay in fire penetration of the occupant compartment and (3) fire suppression. The three areas will be discussed separately.

Fire Prevention

Considerable fire prevention technology is present in vehicles on the road. To assess this technology, a database of 2003 model year vehicles was assembled and the technologies were documented in a database [Fournier 2001]. Lists of available fire prevention technologies were summarized in subsequent papers [Fournier, SAE 2005-01-1423 and Report R06-20, 2006]. The design considerations discussed included:

- Structural crashworthiness of the vehicle frame
- Tank placement
- Fuel line routing/compliance
- Tank materials selection
- Fuel filler connections
- Electrical grounding
- Battery placement

The technologies that were reviewed included:

- Check valves for the tank filler tube
- Roll-over valves
- Shut-off mechanisms for electronic fuel pumps
- Returnless fuel systems that reduce the exposure to damage
- Crash sensing battery disconnects or cut-offs
- Collapsible drive shafts

Research was initiated to explore possible ignition sources for engine compartment fires. Tests were conduced by Biokinetics to measure engine compartment and exhaust component surface temperatures of four different classes of vehicles during driving conditions and when the vehicle was stopped after driving [Fournier, R04-13, 2004 and R06-23, 2006]. While driving uphill, the maximum temperature measured on the surface of the exhaust manifold varied from a low of 241 ^{o}C for a minivan to a high of 550 ^{o}C for a passenger car. Tests of underhood fluids showed that the minimum temperature of a hot surface to cause ignition was in the order of 310 ^{o}C for lubricants and 518 ^{o}C for coolants [Tewarson, SAE 2005-01-1650].

The Friedman Research Corporation used state police reported accident data to examine the frequency of fires in pickup trucks of the same model but with different engines. The state data showed that the eight cylinder (V-8) engines had a higher fire rate than the inline six cylinder engines. An obvious difference is the increased exposure of the exhaust manifold in the V-8 [Friedman, 2006].

A considerable difference was noted in the maximum temperature of exhaust components for different vehicles under similar operating conditions. Control of the maximum underhood temperature, as exhibited by the vehicle with the lowest exhaust temperature, could provide an opportunity for improved fire safety, by reducing the intensity of a possible ignition source.

The prevention of fluid leakage offers another opportunity for improved fire safety. A research program by Biokinetics investigated and documented the technology in present day vehicles to prevent fuel leakage when lines from the fuel tank are severed [Fournier, R0-6-20, 2006].

Biokinetics conducted leakage tests on 20 fuel tanks to study the fuel containment technologies employed and their performance. The tests simulated a vehicle rollover by rotating a tank, filled to capacity, about an axis that when installed in a vehicle would be parallel to the vehicle's longitudinal axis. The tanks were rotated to seven discreet positions during the rollover simulation. None of the tanks leaked when all hoses were intact. In each position, the fuel system hoses were disconnected one at a time to represent a damaged or severed line and the resulting leaks were observed. The results of the testing showed that six of the tanks leaked in every orientation and ten leaked in some orientations. However, four did not leak with each of the lines severed and when subjected to all orientations. The results of these tests are discussed in more detail in earlier papers [Fournier, R04-06c, 2004; Digges, 2005].

Another recent paper by Biokinetics has documented in detail the technology that prevents leakage when lines are severed [Fournier R06-20, 2006]. This report also evaluates the technology available to prevent siphoning of the fuel from the tank after a fuel line is severed.

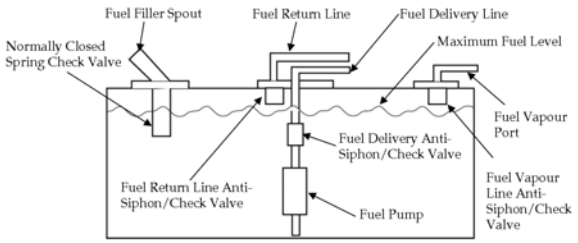

Figure 9 - Fuel Tank Leakage Prevention Components Found in Service (after Fournier, July 2006)

Some leakage prevention technologies currently incorporated in vehicles are illustrated in Figure 9. They include a check valve in the fuel filler spout, and check and anti-siphon valves in the fuel delivery line, the fuel vapor port and the fuel return line. Other leakage prevention technologies include inertia shut-off switches, logic built into engine computer controls and other monitoring devices that automatically shut down the fuel pump when a concern is detected. Some vehicles have eliminated the fuel return line, thereby reducing the opportunity for fuel to escape.

Delay of Fire Penetration

Test data and inspection of crashed vehicles with engine compartment fires indicates that there are two principal areas for fire entry into the occupant compartment – the firewall and the windshield. Once the flames breach the hood and impinge on the windshield, there is a large vulnerability to rapid occupant compartment penetration via a broken and collapsed windshield. If the flames are contained under the hood, the firewall becomes a vulnerable fire penetration area.

An opportunity for reducing the firewall vulnerability is by minimizing the area of openings through which the fire can penetrate. One approach to reduce openings studied during the GM/DoT research program was the use of intumescent materials that would expand with heat and close openings [Hamins, 2007]. The research was not successful with the intumescent materials that were used. Another suggested approach was to apply mechanical devices to close the largest openings. This approach was not investigated.

Even if technology is not applied to the firewall fire penetration problem, there are designs that may be beneficial. Competitive vehicles display large differences in the area of openings in the metal firewall. Typical examples are shown in Figures 10 and 11. Figure 10 shows a large opening on the left side for the heating and air conditioning system. The ducting for the system is flammable and could burn away in an engine compartment fire, providing an entry to the occupant compartment. The firewall in Figure 11 has a much smaller opening and, therefore, should be beneficial in resisting the penetration of flames into the occupant compartment.

Another path for flames to enter the occupant compartment is through the windshield. The fire shield offered by the firewall, hood and cowl can delay the spread of fire in the direction of the windshield. However, in recent vehicles, the metal in the cowl area has been replaced with combustible plastics. As a consequence, the opportunity for fire to burn through the cowl area and impinge on the windshield is increased.

Figure 12 illustrates that the plastic cowl between the hood and firewall burns away during an engine compartment fire. For crashes in which the hood remains intact, cowl designs to resist fire penetration could extend the time until flames impinge on the windshield and expose the occupant compartment to the fire.

Figure 10 – Vehicle Firewall with Large Openings

Figure 11 – Vehicle Firewall with Small Openings

Figure 12 –Vehicle with Plastic Cowl Consumed

During the MVFRI survey of fire safety technologies in new vehicles, several car sales personnel indicated that the underhood liners on their vehicles could serve as fire blankets and act to smother engine compartment fires. These claims prompted a research project to evaluate the fire resistant properties on underhood insulation materials. During

this project, Biokinetics measured the heat release rate of twenty different underhood liners to examine the extent that these materials might mitigate or aggravate the containment of an underhood fire [Fournier R06-23, 2005; Digges, 2006]. The results showed that the differences in heat release rate ranged over two orders of magnitude. The materials with the lowest heat release rate resisted combustion and could have aided in reducing the fire intensity. Those with the highest heat release rate contributed fuel to the engine compartment fire. There appeared to be no correlation between the cost of the vehicle and the heat release rate of the underhood liner. Additional specifications to improve the fire resistance of underhood liners could reduce the fuel load in the engine compartment and might contribute to reducing the fire growth rate.

Fire Suppression

Fire suppression of underhood fires is in the early stages and offers considerable promise. Several technologies have been researched and there are fire suppression products for a variety of applications on the market [Hamins, 2007]. In an earlier research project, University of Maryland demonstrated a foam based underhood fire suppression system [Gunderson 2005]. The system demonstrated the ability to extinguish an 80kW fire fed by a pool of fuel located near the battery.

One of the impediments to the deployment of an underhood fire suppression system is the lack of specifications to determine its efficacy. To assist in understanding the requirements for suppression systems specifications, a research project was undertaken by NIST. A summary report outlined the requirements and considerations for motor vehicle fire suppression, including suppression of underhood fires [Hamins, 2007]. Some of the considerations are as follows:

- Post-crash vehicle fires differ from fires in intact vehicles, as the geometric configuration may be modified by the collision in ways that cannot be precisely defined beforehand.
- The final orientation of the crashed vehicle may influence the fire ignition and growth rate, and the suppression system requirements.
- Underhood fires occur in a compartment that is partially open to the environment, which can lead to suppressant loss.
- The time of initiation of a fire after a collision can vary.
- Re-ignition of the fire may occur if the fire sources remain after the suppressant has been expended.
- Ambient factors such as temperature, wind, and incline of the road may influence suppression system performance.

CONCLUSIONS

Frontal and rollover crashes account for most major fires in NASS. The engine compartment is the most frequent origin of major fires in frontal and rollover crashes. The fuel tank is also a frequent origin of major fires in rollovers, but impacts prior to the rollover may be a major cause of fuel tank spillage in these events.

When examining 2000-2005 FARS fatalities with fire as the most harmful event, frontal damage crashes account for more that half of the population. Rollovers account for another twenty-five percent.

Controlling fires in frontal and rollover crashes offers the largest opportunity for fire safety improvements. A number of present-day vehicles incorporate technologies to prevent fuel leakage in rollovers. There are other technologies to delay the fire penetration into the occupant compartment. However, these technologies are not universally employed. Additional attention to the fire safety in frontal and rollover crashes is needed to offset the increased fuel load from combustible plastics that is present in today's motor vehicles.

ACKNOWLEDGMENTS

The author would like to recognize that funding for this research was provided by General Motors in accordance with the White, Monson and Cashiola vs. General Motors Settlement Agreement. The author also recognizes the valuable contributions of Dr. R. R. Stephenson in reviewing this paper in monitoring some of the research contracts on which the paper was based.

Further details of research and progress associated with this work may be obtained at: www.mvfri.org

REFERENCES

Abu-Isa, I., Cummings, D., LaDue, D., and Tewarson, A., "Thermal Properties and Flammability Behavior of Automotive Polymers," Paper No. 98-54-P-17, *16th International Technical Conference on Enhanced Safety of Vehicles*, Windsor, Canada, June, 1-4, 1998.

Ahrens, M., "U.S. Vehicle Fire Trends and Patterns," National Fire Protection Association, Quincy, MA, August, 2005.

Bahouth, G., **"**Analysis of Fire Related Crash Fatalities and Crashed Vehicle Rescue Times", MVFRI Report, March, 2007, www.mvfri.org

Bahouth, G., "Post Crash Exterior Crush Patterns and Motor Vehicle Fire Occurrence" SAE 2006-01-0789, 2006

Bahouth, J., and Kuzentsov, A., "Automotive and Fire Safety Research", The George Washington University, January, 2005. www.mvfri.org

Battpaglia, K., Griffith, L., Huczek, J., Janssens, M., Miler, M. and Wilson, K., "Comparison of Fire Properties of Automotive Materials and Evaluation of Performance Levels", SwRI Project No. 01.05804, October 2003. www.mvfri.org

Committee on Fire Safety Aspects of Polymeric Materials, "Fire Safety Aspects of Polymeric Materials, Volume 8, Land Transportation Vehicles," National Materials Advisory Board, National Academy of Sciences, Publication NMAB 318-8, Washington, D.C., pp. 158, 1979.

Digges, K., and Kildare, S., "Fire Occurrence in Rollover Crashes Based on NASS/CDS", SAE 2007-01-0875, April, 2007.

Digges K., and Stephenson, R., "Summary of Recent Research in Crash-Induced Vehicle Fire Safety," SAE 2006-01-0551, April, 2006.

Digges, K. and Stephenson, R. "A Research Program to Study Impact Related Fire Safety" *19th International Technical Conference on the Enhanced Safety of Vehicles*, Washington DC., May, 2005.

Digges, K, Stephenson, R., and Bedewi, P., "Research Programs in Crash-Induced Fire Safety," SAE 2005-01-1425, April, 2005

Digges, K., Stephenson, R., and Bedewi, P., "A Research Program in Crash-Induced Fire Safety," SAE 2004-01-0475, March, 2004.

Digges, K., Stephenson, R., and Bedewi, P., "Fire Safety Performance of Motor Vehicles In Crashes," *18th International Technical Conference on the Enhanced Safety of Vehicles*, May, 2003.

Fell, J., "Interim Report to MVFRI on FARS Missing Data", Pacific Institute for Research and Evaluation, prepared for MVFRI, November 2004. www.mvfri.org

Fournier, E., and Bayne, T., "Anti-siphoning and Leak Prevention Technology Review," Prepared for Motor Vehicle Fire Research Institute by Biokinetics and Associates, Ltd., Report R06-20, September, 2006. www.mvfri.org

Fournier, E., and Bayne, T., "Assessment of Thermocouple Attachment Techniques for Measuring Exhaust Manifold Temperature" Prepared for Motor Vehicle Fire Research Institute by Biokinetics and Associates, Ltd., Report R06-23, September 2006. www.mvfri.org

Fournier, E. and Bain, T., "Cone Calorimeter Testing of Under Hood Insulation", Prepared for Motor Vehicle Fire Research Institute by Biokinetics and Associates, Ltd., Report R05-13b, August, 2005. www.mvfri.org

Fournier, E., Kot, J., and Sullivan, D., "Assessment of Fuel System Technology Use in 2003 Model Year Vehicles", SAE 2005-01-1423, April, 2005

Fournier, E. and Bain, T., "Underhood Temperature Measurements of Four Vehicles", Prepared for Motor Vehicle Fire Research Institute, by Biokinetics and Associated Ltd., Report R04-13, September, 2004. www.mvfri.org

Fournier, E., and Kot, J., "Comparison of Internal Tank Components – 20 Fuel Systems," Prepared for Motor Vehicle Fire Research Institute by Biokinetics and Associates, Ltd., Report R04-06c, July, 2004. www.mvfri.org.

Fournier, E., Bayne, T., and Kot, J., "Survey of the State-Of-The-Art in Fuel System Fire Safety – Phase II," Prepared for Motor Vehicle Fire Research Institute by Biokinetics and Associates, Ltd., R03-01, May, 2003. www.mvfri.org.

Fournier, E., and Keown, M. "Survey of the State-Of-The-Art in Fuel System Fire Safety – Phase I," Prepared for Motor Vehicle Fire Research Institute by Biokinetics and Associates, Ltd., R02-04 April, 2002. www.mvfri.org.

Friedman, K., Holloway, E., and Kenny, T., "Impact Induced Fires: Pickup Feature Design Analysis", SAE 2006-01-0550, April, 2006.

Friedman, K., Holloway, E., and Kenny, T., "Impact Induced Fires: Statistical Analysis of FARS and State Data Files (1978-2001)", SAE 2005-01-1421, April, 2005

Friedman, K., Holloway, E., and Kenny, T., "Final Report, Impact Induced Fires & Fuel Leakage: Statistical Analysis of FARS and State Data Files (1978-2001)", prepared for MVFRI by Friedman Research Corporation, July, 2003. www.mvfri.org

Griffith, L., Janssens, M., and Wilson, K., "Evaluation of Smoke Toxicity of Automotive Materials According to Standard Small-Scale Test Procedures", SAE paper 2005-01-1558, April, 2005.

Gunderson, J., and di Marzo, M., "Feasibility Study for a Vehicle Under Hood Nitrogen Foam Fire Suppression System," SAE paper 2005-01-1789, April, 2005.

Hamins, A., "Vehicle Fire Suppression Research Needs", NIST Report for MVFRI, February 23, 2007. www.mvfri.org

Judicial District Court "Agreement of Settlement, White, Monson and Cashiola vs. General Motors", Number 42,865, DIV."D", 18th Judicial District Court, Parish of Iberville, Louisiana, June 27, 1996.

Kildare, S, and Digges, K., "Analysis of Fire Occurrence in Automotive crashes Using NASS CDS Data (1994-2004), GWU Report, November, 2006. www.mvfri.org,

Lyon, R., and Walters, R., "Flammability of Automotive Plastics", Report prepared for MVFRI, August, 2005. www.mvfri.org

National Highway Traffic Safety Administration, "U.S. DOT/General Motors Settlement Agreement Status Report, Year 4", NHTSA 2001.

Tewarson, A., Quintiere, J., and Purser, J., "Post Collision Motor Vehicle Fires." Report prepared for MVFRI by FM Global Technical Report #0003018009, Volume I, October 2005. www.mvfri.org

Tewarson, A., Quintiere, J., and Purser, J., "Theory and Testing for the Fire Behavior of Materials for the Transportation Industry" Report prepared for MVFRI by FM Global Technical Report #0003018009, Volume II, October 2005. www.mvfri.org

Tewarson, A., Quintiere, J., and Purser, J., "Thermophysical and Fire Properties of Automobile Plastic Parts and Engine Compartment Fluids" Report prepared for MVFRI by FM Global Technical Report #0003018009, Volume III, October, 2005. www.mvfri.org

Tewarson , A., Quintiere , J., and Purser, D., "Fire Behavior of Materials in Vehicle Crash Fires and Survivability of the Passengers", SAE paper 2005-01-1555, April, 2005.

Tewarson , A., "Thermophysical and Fire Properties of Engine Compartment Fluids", SAE paper 2005-01-1560, April, 2005.

A. Tewarson, "A Study of the Flammability of Plastics in Vehicle Components and Parts, Technical Report FMRC J.I. 0B1R7.RC, Factory Mutual Research Corporation, Norwood, MA, October, 1997.

USE OF HIGH EFFICIENT ENERGY ABSORPTION FOAM IN SIDE IMPACT PADDING

Gerhard Slik
Dow Automotive
Germany
Gavin Vogel
Dow Automotive
USA
Paper Number 07-0185

ABSTRACT

In side impact events padding is often utilised to not only absorb energy but also push the dummy into motion. The padding is usually applied in the pelvic, the abdomen and the thorax area. The amount of absorption versus push load is important to obtain acceptable levels of the injury parameters as stipulated by legislation (e.g. ECE R95, FMVSS 214) and consumer tests (e.g. EURO/US-NCAP and IIHS). Practice shows many types of foam padding designs which fulfil the requirements, often in combination with side airbags.
In this paper the advantage of applying high efficient energy absorption foams in padding is presented. This enables designers of passive safety systems not only to save space, weight and cost but also increase safety (ratings) by having a better defined and more easily tune-able loading system on the dummy during side impact crashes. Computer Aided Engineering (CAE) simulation methodology can be used efficiently to optimise part design. A case showing the benefits of high efficient energy absorption foam padding is discussed.

INTRODUCTION

Side impact crashes are one of the most severe accidents and account for roughly 30% of all fatalities in road accidents involving passenger cars and light trucks. For this reason, in many countries legislation has been put into place with minimum requirements for injury parameters in side impact crash tests. On top of this, consumer test ratings like Euro-NCAP and insurance testing have generally put higher requirements on side impact crash performance of cars. For example the recent upgrade of the IIHS side impact test in which the deformable barrier impactor has comparable dimensions to those of the front of a light truck, giving a much more severe impact collision than it used to be with the old barrier.

In addition, an increasing consumer awareness of safety is allowing automakers to utilize consumer and insurance test reports as a powerful marketing tool.

In view of all this, the trend of increasing level of passive safety measurements is clear. Even in the lower end vehicle segments, airbags are incorporated more often for frontal and side impact protection. In higher end vehicle segments, active safety systems are being introduced to the market and have found their application. However there is still a large number of vehicles built without side airbags, in specific regions such as North America and emerging markets. Therefore it is still necessary to engineer passive energy absorbing countermeasures utilizing foams solutions to provide occupant protection during side impact collisions.

Since the layout of safety systems greatly influences the design and styling of a vehicle it is important to know the performance of such systems and have a reliable tool for evaluation early in the design stage.

In the present study the advantage of using high efficient energy absorption foam in side impact protection is presented. First, an example of a recently developed energy absorbing foam is discussed. Then the development of the material models to accurately simulate this material in LS-DYNA is described. Subsequently a case is presented and conclusions are listed.

HIGH EFFICIENT ENERGY ABSORPTION FOAM

The foam considered in the present paper is a closed cell, styrenic foam, specially developed for energy absorption in automotive applications. It is produced via an extrusion manufacturing process and commercialised under the trade name IMPAXX™ energy absorbing (EA) foam. The continuous extrusion production process ensures a constant quality and a high level of consistency of the material properties. Foam boards are formed in the extrusion process from which parts (pads) can be cut by hot wire or abrasive wire cutting technology. This fabrication technique offers the additional benefit of eliminating the need for

™ IMPAXX is a trademark of The Dow Chemical Company and its subsidiaries.

expensive forming tools associated with traditional foam solutions.

A typical quasi-static stress-strain characteristic of the foam is depicted in Figure 1.

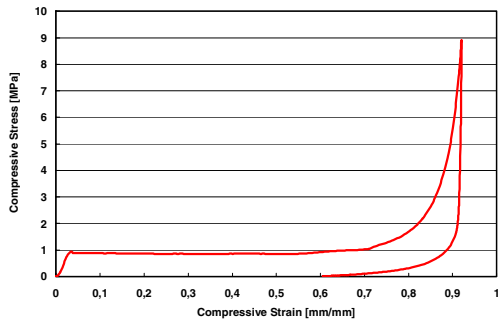

Figure 1. Quasi-static stress-strain curve for IMPAXX™ foam.

The stress ramps up rather fast and then remains constant, up to 70~80% compression. From then on the material densifies and the stress increases rapidly. Due to this behaviour, the material can be categorised as high efficient energy absorbing since the stress-strain curve is nearly a block curve and an ideal absorber would show a square wave response.

In Figure 2, a comparison is given between IMPAXX™, expanded Polypropylene (ePP) and semi-rigid Polyurethane (PUR) foam, all of similar densities.

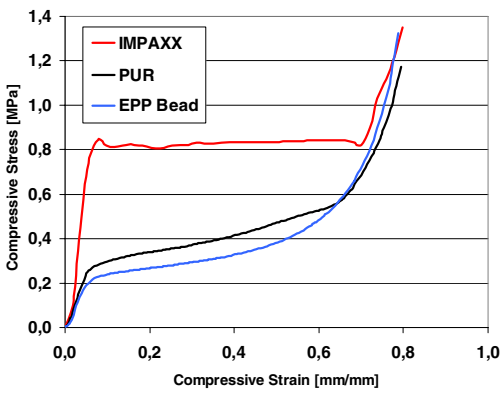

Figure 2. Compression curves of IMPAXX™ in comparison with ePP and PUR foam for equal density.

Due to the square-wave response of IMPAXX™ foam it is clear that it is a more efficient solution compared to ePP and PUR foams. This is illustrated in Figure 3 where the efficiency curves of the mentioned materials are shown.

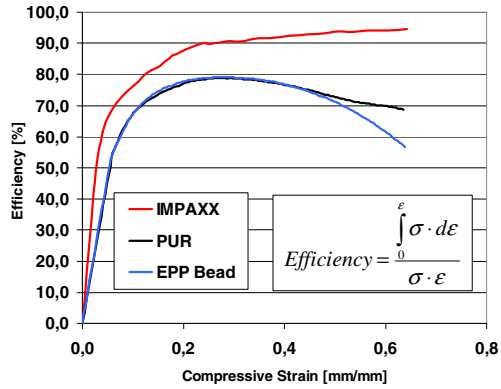

Figure 3. Comparison of efficiency curves.

Increasing the density of ePP or PUR to achieve the same compressive strength of IMPAXX™ foam would, not only increase the effective weight of the EA part, but also speed up the densification, thereby further decreasing their efficiencies. Therefore, besides maximising the energy absorption and minimising the packaging-space required to absorb a given amount of energy using IMPAXX™ foam, significant weight savings can be realized as well.

Another positive attribute is the stable performance over a wide temperature range as illustrated in Figure 4.

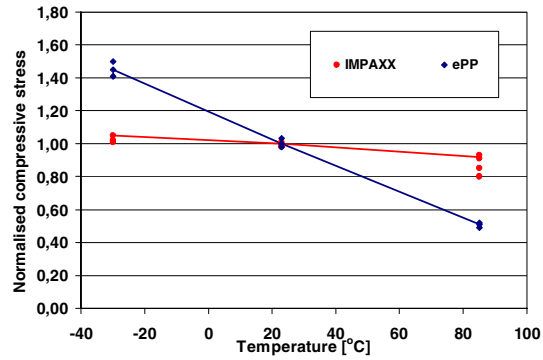

Figure 4. Normalised compressive stress over temperature.

It shows that over a wide temperature range from -35 °C up to 85 °C IMPAXX™ has a constant performance.

MATERIAL MODELS FOR CAE

Because computer simulations play a big role in modern vehicle development, it is important that trustworthy material models are available. This section describes briefly the material model validation of IMPAXX™ EA foam.

Parameters for LS-DYNA material model Type 63 (*MAT_CRUSHABLE_FOAM) [1] were identified for each foam grade from drop tower tests with a flat impactor, see Figure 5, to obtain high strain rate stress-strain curves, see Figure 6.

Figure 5. Drop tower test set-up.

The smoothened average compressive stress-strain curves were used as input load curves for the material models.

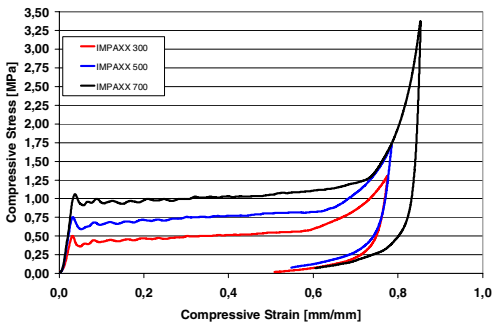

Figure 6. Average dynamic compressive stress-strain responses for IMPAXX™.

Pelvic shaped impactor tests, see Figure 7, were performed for validation of the models.

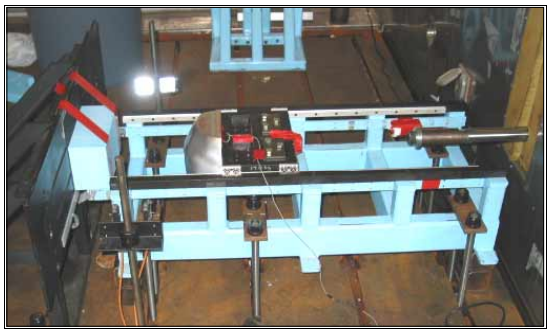

Figure 7. Pelvic impactor test set-up.

These tests were done on several sample geometries: blocks, cones and pyramids, see Figure 8.

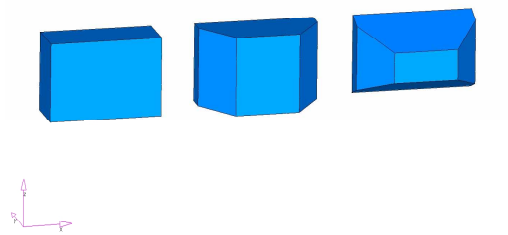

Figure 8. Sample geometries for the pelvic impactor tests: block, cone and pyramid.

Finite element models for the drop tower test, see Figure 9, and the pelvic impactor test, see Figure 10, were created and the tests were simulated.

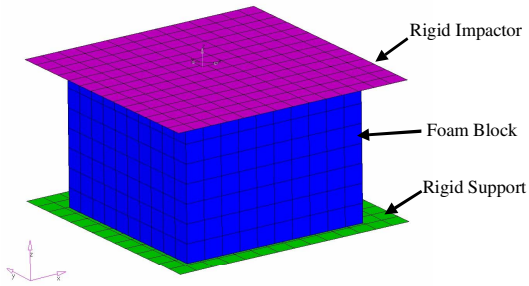

Figure 9. Finite element model of the drop tower test set-up.

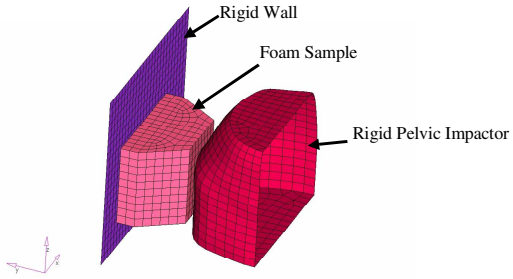

Figure 10. FE Model of the pelvic impactor test set-up.

Figure 11 to Figure 14 show simulation results versus tests for IMPAXX™ 700 of drop tower tests and pelvic impactor tests.

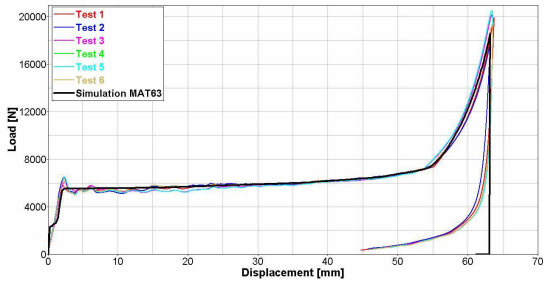

Figure 11. Drop Tower Test vs. Simulation for IMPAXX™ 700.

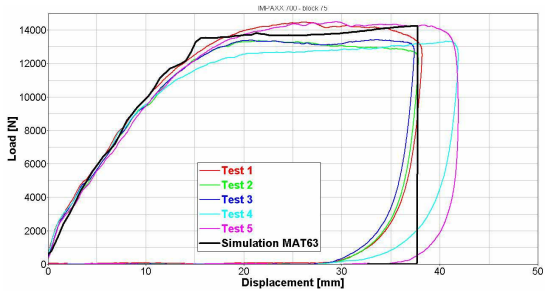

Figure 12. Pelvic impactor tests vs. simulation on 75 mm thick IMPAXX™ 700 blocks.

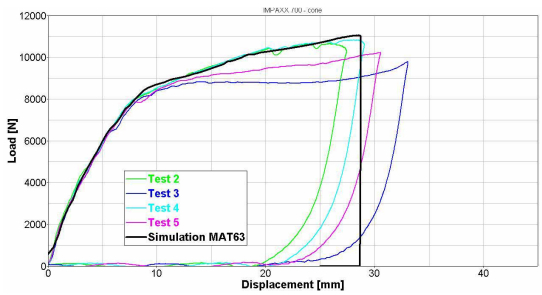

Figure 13. Pelvic impactor tests vs. simulation on IMPAXX™ 700 cone samples.

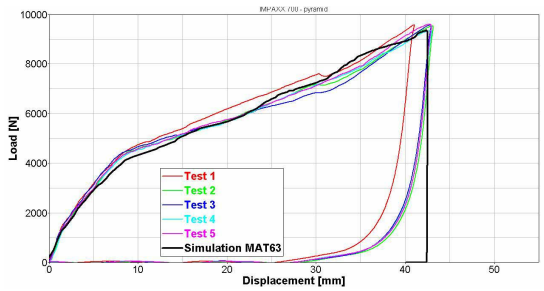

Figure 14. Pelvic impactor tests vs. simulation on IMPAXX™ 700 pyramid samples.

All cases show a very good correlation of the impactor's load and displacement level between test and simulation. The models can be used with confidence.

SIDE IMPACT CAE OPTIMISATION CASE

In many cases car manufactures obtain door modules from a supplier who is then also responsible for the development with respect to safety. In these cases, the door system is required to give a certain load-intrusion characteristic to a rigid impactor. This characteristic is then defined for the pelvic, abdomen and thorax area and is such that it will achieve the appropriate loads during side impact to the dummy to result in the targeted level of injury parameters. Figure 15 illustrates a typical pelvic impactor load-intrusion requirement for a door panel.

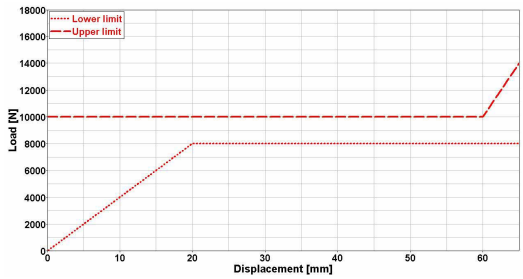

Figure 15. Typical load corridor specified for rigid pelvic impactor.

The door module supplier is required to prove the right load-intrusion characteristic by CAE simulations and by testing. Testing is defined on the door module as follows. A rigid pelvic shaped impactor hits the door module with a defined initial velocity and the impactor acceleration is recorded.

Acceleration and displacement are calculated from the load and thus obtained load versus displacement must fit in the defined corridor. The test is usually done on a drop tower or on a sled test set-up. Figure 16 illustrates a drop tower test set-up with a rigid pelvic shaped impactor.

Figure 16. Drop tower with pelvic impactor.

The pelvic impactor test set-up of the discussed door module is modelled, see Figure 17 and contains all components of the door, the door-in-white and the rigid pelvic impactor.

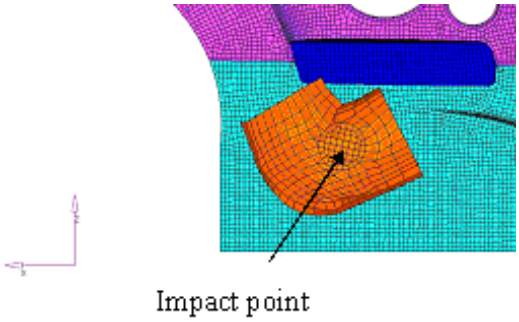

Figure 17. Side impact CAE door model.

Starting with a relatively large foam pad, the optimum shape is found by reducing the size and changing the location. The optimum shapes from fabrication point of view are square parts (blocks). Usually the door trim is rather flat which means that if the pad is attached to that side, it also can be flat. Usually the door-in-white has a complex geometry, however if during a side impact crash the barrier starts pushing the car, the door-in-white is pushed and deforms and will move as a flat surface, even if it is not flat in the original position. This means that also on the side of the door-in-white, the foam padding can be flat. Usually, the whole part can be kept simple and block shaped. For the case discussed here, the size of the part was optimised, such that the pelvic load response was in the corridor, see Figure 18.

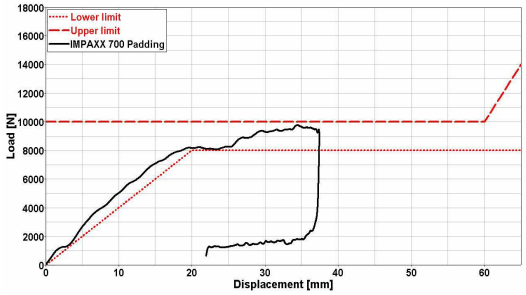

Figure 18. Pelvic impactor load response for an optimised foam pad.

In Figure 19 a cross section of the simulation model at four stages during the pelvic impact is shown.

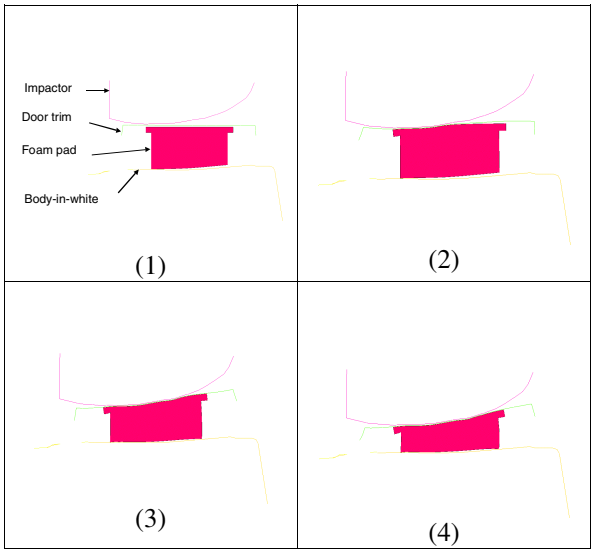

Figure 19. Pelvic impactor intrusion; horizontal cross section through the H-point.

At stage (1) the impactor has just made contact with the door trim, displacement is 0 mm. At stage (2) the impactor has moved further, the load has ramped up and is going towards 8 kN at 20 mm displacement. At stage (3) the impactor has moved 20 mm and the contact area between impactor and foam pad is maximal. When the impactor moves further, the load does not increase significantly; the compression area is constant and the stress level is constant until the foam enters the densification area at about 70% compression. This means that up to that point a nearly perfect load control is possible, see Figure 18.

This case illustrates a relatively easy method of optimizing the part design of an energy absorbing foam countermeasure pad using an efficient solution such as IMPAXX™ foam.

CONCLUSIONS

Use of high efficient energy absorption foam for side impact protection is presented. These materials have great advantages to be used in development of side impact padding:

- Improved load control. Due to the square-like compression stress-strain response of the foam, a nearly perfect load control can be established. This enables design of robust side impact pads.
- Accurate material models exist to simulate parts in CAE analyses. This means that in the development process CAE can be leveraged to optimise an EA countermeasure part design using both geometry and density.
- Short development times. First, with use of accurate CAE models enables more accurate, virtual testing and save on testing time and cost. Secondly, prototypes can be produced easy, quick and cost effective since no tooling is necessary.
- Prototypes are equal to production parts since the way to produce both are the same; by hot or abrasive wire cutting technology. Also during testing it is easy to modify prototypes and an optimum can be found iteratively on the testing spot as well.
- Weight savings up to 50% are possible since high efficiency results in smaller part with same performance. On top of the smaller part size, the density is general lower. For example, to obtain the same load response with ePP the densities need to be twice as high. Although this is not safety related, fuel consumption efficiency as a result of lower car weights is nowadays highly appreciated.
- Packaging space saving since the padding can be smaller. If this is taken into account early in the design process, it is possible to use the extra space, e.g. for enlarged door pockets.

REFERENCES

[1] LS-DYNA User Manual, Livermore Software Technology Corporation.

Dow Automotive is a business unit of The Dow Chemical Company and its subsidiaries

"This information is considered accurate and reliable as of March 1st, 2007 and is presented in good faith. No warranty, expressed or implied, is given nor is freedom from any patent owned by The Dow Chemical Company or others to be inferred. Since Dow has no control over how this information may ultimately be used, all liability is expressly disclaimed; Dow assumes no obligation or liability therefor".

CURTAIN AIRBAG GAS DELIVERY SYSTEM DEVELOPMENT USING CFD ANALYSIS

Hyunsok Pang
Joseph Massa
Key Safety Systems, Inc.
United States
Paper Number 07-0208

ABSTRACT

This paper describes curtain airbag gas delivery system development work using CFD analysis. The objective of developing gas delivery system was to achieve uniform inflation and reasonable time to position for oblique pole test with 5th %ile female. CFD analysis has been conducted to design gas delivery system of 3 row curtain airbag. The gas delivery system consists of T-diffuser and flexible gas delivery tube. T-diffuser hole sizes and the hole sizes in flexible gas delivery tube system have been determined through CFD simulations. Confirmation static deployment test has been conducted to confirm the design specification from CFD analysis. In the static deployment test, pressure ports were installed to measure the pressure at several locations in the curtain airbag. It was found that the bag kinematics and pressures in the test were close to the simulation kinematics and results.

INTRODUCTION

In developing a curtain airbag system for head protection in side impact condition, gas delivery system development work is very important to achieve uniform inflation and reasonable time to position. In this paper, a 3 row curtain airbag is considered to design a gas delivery system which consists of T-diffuser and two flexible gas delivery tubes connected to the T-diffuser. Madymo CFD simulations are conducted to design a gas delivery system. Through Madymo CFD simulations, T-diffuser hole size and hole size in flexible gas delivery tube are determined, which achieve uniform inflation and reasonable bag positioning time. Then, static deployment test is conducted to confirm the design specification from CFD simulations. In the static deployment test, pressure ports are installed to measure the pressures at three locations in the curtain airbag. The curtain airbag kinematics and pressure curves from the static deployment test are compared to the ones from the CFD simulation which produced the design specification.

Curtain Airbag System

Figure 1 shows the 3 row curtain airbag system which has been considered here.

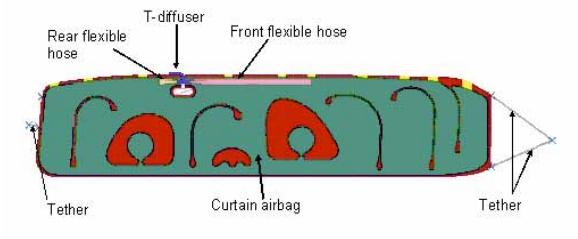

Figure 1. A 3 row curtain airbag system.

The 3 row curtain airbag system considered here consists of T-diffuser, front flexible hose, rear flexible hose, curtain airbag and external tethers. The right side is the vehicle front. A inflator is connected to the T-diffuser inlet. The front and rear flexible hoses are connected to the T-diffuser inside the curtain airbag as shown in Figure. 1. Gas flows into T-diffuser from the inflator and is distributed into front and rear flexible hoses. The right end of front flexible hose has a hole and three holes can be made on the front flexible hose. Gas flows through holes into curtain airbag. The left end of rear flexible hose has a hole through which gas flows into curtain airbag. The front and rear flexible hoses have some permeability. Therefore, some gas flows into curtain airbag through hose walls.

MADYMO CFD Simulations for a 3 Row Curtain Airbag System Design

Madymo CFD code has been used to design T-diffuser hole size for rear flexible hose and 3 hole sizes on front flexible hose. Other design factors such as hose lengths, hole locations on front flexible hose and T-diffuser hole size for front flexible hose have already been decided, based on the experiences. For Madymo CFD analysis, inflator modeling and DOE simulations have been conducted.

Inflator Modeling - In order to obtain the mass flow rate and inflator exit temperature data which are Madymo inputs for CFD simulations, Madymo MTA analysis has been conducted. Figure 2 shows the inflator mass flow rate and Figure 3 shows the tank pressure simulation which justifies the mass flow rate and inflator exit temperature which generate the same tank pressure curve as in the tank test.

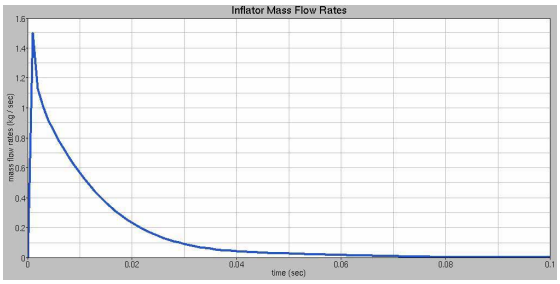

Figure 2. Inflator mass flow rate.

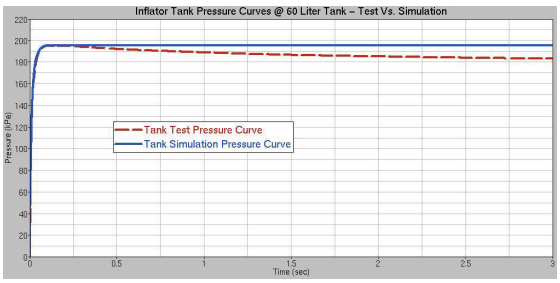

Figure 3. Tank pressure curves @ 60 liter tank – Test vs Simulation.

Madymo CFD Curtain Airbag System Model - Madymo CFD curtain airbag system model has been built, which is close to the real curtain airbag system. Figure 4 shows the Madymo CFD curtain airbag system model.

Figure 4. Madymo CFD curtain airbag system model.

The model in Figure 4 consists of 4 chambers which are the T-diffuser chamber, front hose chamber, rear hose chamber and curtain airbag chamber. Inflator is fired at the inflator inlet of the T-diffuser using a jet. Therefore the inflator gas flows into the T-diffuser and then from T-diffuser into both front and rear hose chamber and then from front and rear hose chamber into curtain airbag chamber. The front hose chamber can have 3 downward holes on the hose surface. Therefore, gas can flow through 3 holes from front hose chamber into curtain airbag chamber. Both the front and rear hose chambers have the permeability which allow gas to flow into the curtain airbag chamber. The curtain airbag chamber is roll-folded to simulate the real situation as close as possible. The MADYMO CFD solver is used, which does not provide uniform pressure inside chambers. Therefore, the pressures can be different at different locations inside one chamber.

CFD Simulation Matrix - Running time of a Madymo CFD model is usually very long. In this work, running time is around 11 hours. Therefore, the number of design parameters should be reduced. The design parameters considered here are the rear diffuser hole size and the vent hole size on the front flexible hose. The rear diffuser hole connects the diffuser to the rear flexible hose. The rear diffuser hole size affects the bag kinematics and pressure in the rear part of curtain airbag. The vent hole size of three holes on the front flexible hose affects the kinematics and pressure in the front part of curtain airbag. Table 1 show the CFD simulation matrix.

Table 1.
CFD Simulation Matrix

No.	Rear Diffuser Hole Size	Hose Size On Front Hose
1	6 mm	0 mm
2	6 mm	9 mm
3	6 mm	12 mm
4	6 mm	15 mm
5	8 mm	0 mm
6	8 mm	9 mm
7	8 mm	12 mm
8	8 mm	15 mm
9	10 mm	0 mm
10	10 mm	9 mm
11	10 mm	12 mm
12	10 mm	15 mm

Madymo CFD Simulation - From the previous experiences, it has been noticed that the permeability of the flexible hose plays an important role. Therefore, the permeability of flexible hose fabric has been obtained through tests in the lab. The obtained data was the permeability function which is dependent on pressure. The pressure vs permeability function data have been introduced in the front and rear flexible hose models.

Curtain Airbag Kinematics And Data Analysis

- The goal of this CFD simulation work was to obtain a curtain airbag gas delivery system specification with which the bag can deploy fully within 25 msec after firing, considering the 20mph-5th %ile oblique pole test condition. Therefore, the bag kinematics comparison is the most important one in this work. The figures below show the bag kinematics at 25msec after firing.

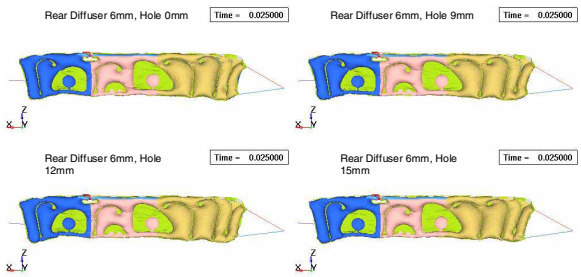

Figure 5. Curtain airbag kinematics at 25msec – 6mm rear diffuser hole – 0, 9, 12, 15mm holes on front hose.

In the Figure 5, it is noticed that there are no significant kinematics differences at 25msec between 0mm, 9mm, 12mm and 15mm holes at 25msec and all cases meet the bag kinematics requirement for the 5th %ile oblique pole test condition.

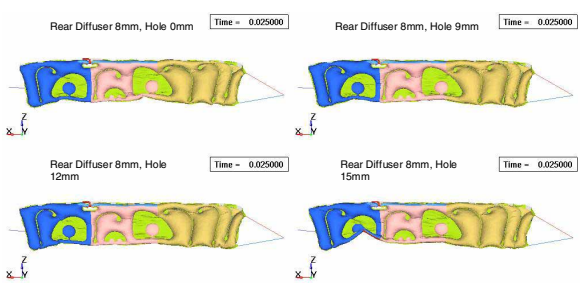

Figure 6. Curtain airbag kinematics at 25msec – 8 mm rear diffuser hole – 0, 9, 12, 15mm holes on front hose.

In the Figure 6, it is noticed that there are no significant kinematics at 25msec differences between 0mm, 9mm and 12mm holes, except the 15mm hole. However, it is considered that all cases meet the bag kinematics requirement for 5th %ile oblique pole test condition.

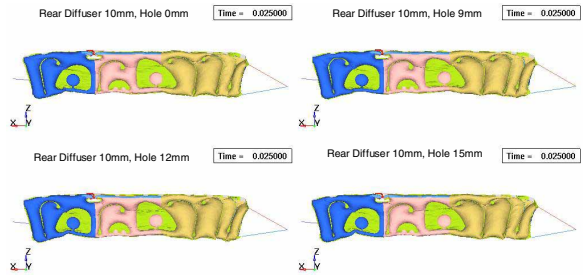

Figure 7. Curtain airbag kinematics at 25msec – 10mm rear diffuser hole – 0, 9, 12, 15mm holes on front hose.

In the Figure 7, it is noticed that there are no significant kinematics differences at 25msec between 0mm, 9mm, 12mm and 15mm holes and all cases meet the bag kinematics requirement for 5th %ile oblique pole test condition.

Considering that all cases in Figure 5, Figure 6 and Figure 7 meet the kinematics requirement for 5th %ile oblique pole, it is temporarily concluded that the holes do not necessarily be introduced on the front flexible hose. Therefore, only the cases of no holes on front hose are considered to determine the rear diffuser hole size. First, the gas mass flows in T-diffuser are compared between 6mm, 8mm and 10mm rear diffuser holes.

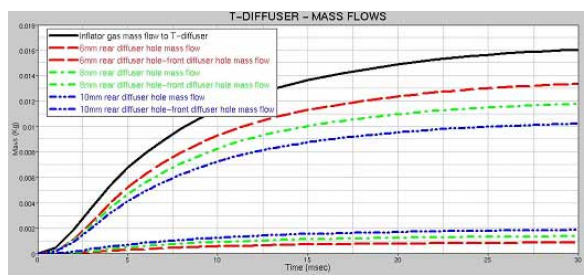

Figure 8. Mass flows in front and rear diffuser holes with 6mm, 8mm and 10mm rear diffuser hole sizes.

Figure 8 shows the mass flows in front and rear diffuser holes as expected. As the rear diffuser hole size increases, the mass flow in rear diffuser hole increases and the mass flow in front diffuser hole decreases. The next step is to investigate the pressures inside the curtain airbag. Three locations were chosen to investigate the pressures as seen in the Figure 9.

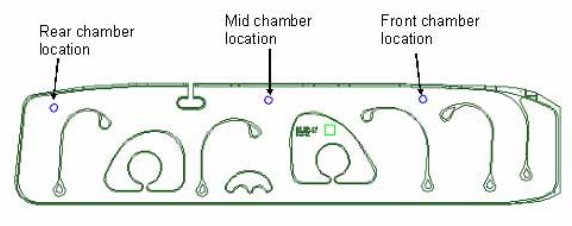

Figure 9. Three locations inside curtain airbag for pressure investigation.

In three locations, the pressures were investigated for the 6mm, 8mm and 10mm rear diffuser hole cases.

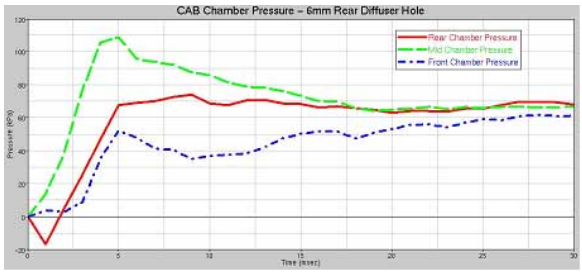

Figure 10. Pressure curves at three locations inside curtain airbag with 6mm rear diffuser hole.

From the Figure 10, it is noticed that the mid chamber pressure is the highest among three locations and three pressure curves tend to converge to equilibrium pressure.

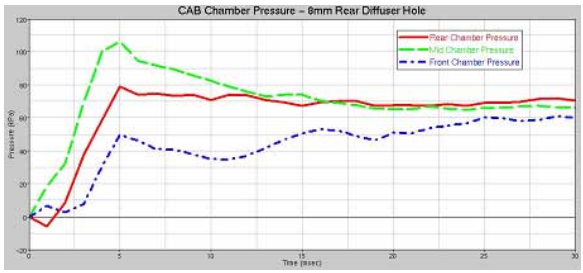

Figure 11. Pressure curves at three locations inside curtain airbag with 8mm rear diffuser hole.

Considering Figure 10 and 11, it is noticed that at 5msec, the rear chamber pressure with 8mm rear diffuser hole is higher than the one with 6mm rear diffuser hole and the mid chamber pressure with the 8mm rear diffuser hole is lower than the one with the 6mm rear diffuser hole. And the pressure converging to equilibrium with the 6mm diffuser hole is observed to be faster than the one with the 8mm diffuser hole.

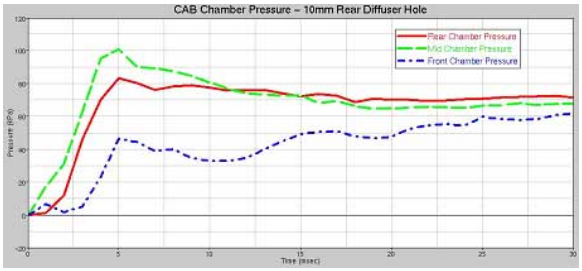

Figure 12. Pressure curves at three locations inside curtain airbag with 10mm rear diffuser hole.

Comparing Figure 10, 11 and 12, as the rear diffuser hole size increases, the mid chamber pressure decreases and rear chamber pressure increases. And with the increase of the rear diffuser hole size, the pressure converging to equilibrium becomes late. If the pressure converging to equilibrium is fast, it means quick and even unfolding of curtain airbag which is desirable. At 20msec, the pressure differences between mid and front chambers were 11.7 kPa for the 6mm, 14.2 kPa for the 8mm and 17.1 kPa for the 10mm rear diffuser hole. Therefore, the rear diffuser hole of 6mm was chosen for testing.

Curtain Airbag System Static Test

A curtain airbag system static test was conducted in a vehicle and the pressures were measured at the locations shown in Figure 9. Figure 13 shows the test environment at t=0 msec.

Figure 13. Curtain airbag system static test set-up at t=0 msec.

Figure 14 shows the measured pressures at the location shown in Figure 9.

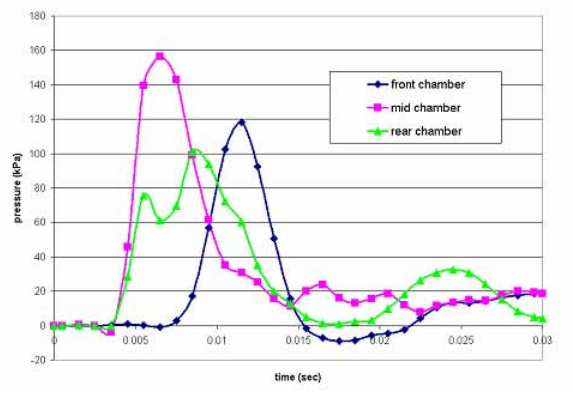

Figure 14. Pressure curves with the 6mm rear diffuser hole from system static test.

Considering Figure 14 and 10, it seems that the pressure curves from the test are different from the pressure curves from the simulation. The difference seems to come from the folding difference and the cover. The folding in simulation has more initial volume than the real, in order to avoid initial penetration which causes numerical instability. And the cover was not modeled in the simulation. However, as predicted in the simulation, in early time, the mid chamber pressure was the highest among three and the rear chamber pressure was higher than the front chamber pressure. Therefore, the curves characteristics in the test are the same as the one in the simulation. This fact made the chamber inflating order in test to be the same as in the simulation.

Deployment Kinematics Comparison

The figures below show the curtain airbag kinematics comparison between simulation and test.

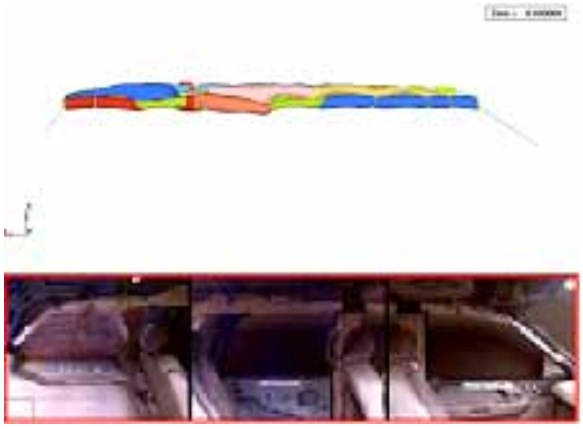

Figure 15. Curtain airbag kinematics at 5msec – simulation vs test.

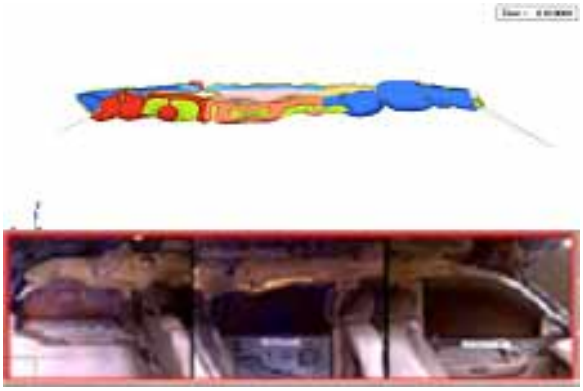

Figure 16. Curtain airbag kinematics at 10msec – simulation vs test.

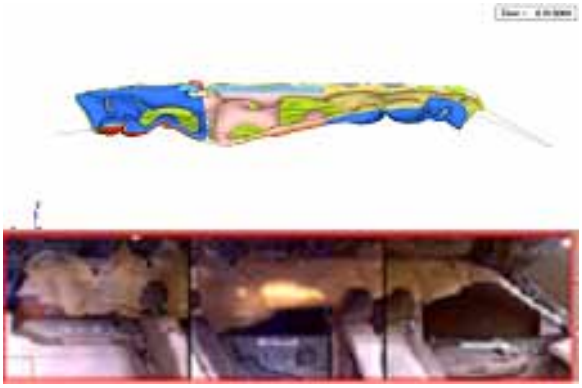

Figure 17. Curtain airbag kinematics at 15msec – simulation vs test.

Figure 18. Curtain airbag kinematics at 20msec – simulation vs test.

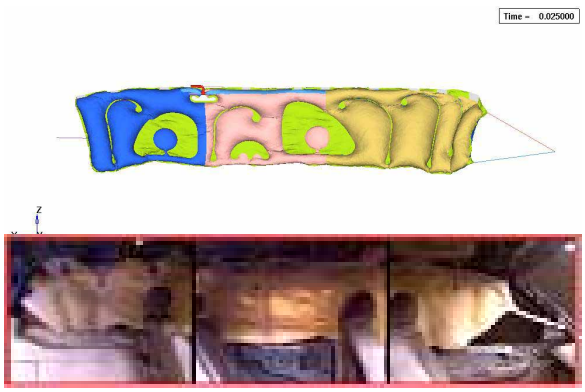

Figure 19. Curtain airbag kinematics at 25msec – simulation vs test.

From Figure 15 to Figure 19, the CAB deployment kinematics of simulation are seen to generally match the test. However, as seen in Figure 19, the right bottom corner of front chamber in the test did not be as fully unfolded as in the simulation. The reason is that the folding in test is tighter than in the simulation and the cover wraps the curtain airbag in the test. In the test, the right bottom corner of front chamber was unfolded fully at 40msec as seen in the Figure 20.

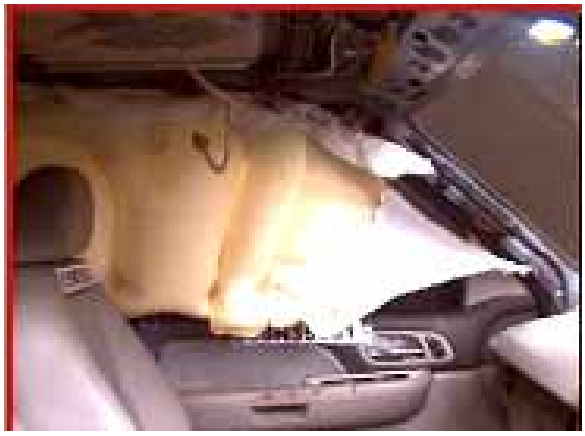

Figure 20. Front chamber kinematics at 40msec.

CONCLUSIONS

In this work, the following conclusions are made.

- Madymo CFD code can simulate gas flows in gas delivery system (T-diffuser, front flexible hose and resr flexible hose) plus curtain airbg.
- Madymo CFD code could be used to predict the curtain bag kinematics.
- Madymo CFD code could produce the pressure data inside curtain airbag which show some difference from but the same trend as the test pressure data.
- To minimize differences in pressure data and kinematics, the bag folding close to the real and adding cover on the curtain are needed.
- Madymo CFD code could prove that the permeability function of flexible hose plays an important role.
- Madymo CFD code could be successfully used to design curtain airbag gas delivery system.

ACKNOWLEDGEMENTS

I thank Bruce Kalandek and Chang Ju for providing data and helping bag kinematics analysis.

REFERENCES

[1] TNO Automotive, MADYMO v6.2 Theory Manual

[2] TNO Automotive, MADYMO v6.2 Reference Manual

[3] Key Safety Systems, Inc., Curtain Airbag System Static Test Data and Film

AN OVERVIEW OF NHTSA'S CRASH RECONSTRUCTION SOFTWARE WinSMASH

Dinesh Sharma
Seymour Stern
John Brophy
National Highway Traffic Safety Administration, USA
Eun-Ha Choi
Rainbow Technology, USA
Paper Number 07-0211

ABSTRACT

The National Highway Traffic Safety Administration (NHTSA) uses WinSMASH computer software to estimate the change in velocity, delta-V, of the vehicles involved in crashes. The software uses detailed measurements from the crash scene, vehicle damage and vehicle stiffness characteristics to compute energy absorbed by the vehicle and estimate the delta-V and Barrier Equivalent Speed (BES). The WinSMASH is a Microsoft Windows based, enhanced and updated version of the accident reconstruction software CRASH3 previously used by NHTSA. The purpose of this paper is to describe the new enhancements in the program.

The damage algorithm used in CRASH3 has been reformulated in WinSMASH. The new damage algorithm in WinSMASH is based on an assumed linear relationship between crash energy and crush and uses intercept d_0 and slope d_1 to describe vehicle stiffness. The software uses generic vehicle size and stiffness categories based on the vehicle's wheelbase. However, the program also allows the users to enter the vehicle specific stiffness coefficients. The stiffness coefficients for a large number of vehicles have been calculated from crash test results and integrated into WinSMASH. An automated procedure to select the vehicle specific stiffness coefficients is currently under development. A statistical model is also being developed for estimating the stiffness coefficients of a vehicle that is not crash tested. The paper provides an overview of these procedures.

The WinSMASH estimated delta-V of the vehicles is compared with the corresponding delta-V obtained from the Event Data Recorder (EDR) installed in the crashed vehicles to assess the accuracy of the software. The staged crash tests used to validate the software are also discussed in the paper.

INTRODUCTION

The NHTSA's National Center for Statistics and Analysis (NCSA) has been collecting nationally representative data on motor vehicle traffic crashes through the National Automotive Sampling System/Crashworthiness Data System (NASS/CDS), since 1979. The purpose of this data collection effort is to understand the real world motor vehicle crash performance and the injury risk as a function of crash severity. The most commonly used measure of crash severity is the change in velocity, delta-V of vehicles involved in a collision. It is defined as the change in velocity of the crashed vehicle during the collision phase. The delta-V is considered a good indicator of the crash severity because it is related to the impact forces of the collision and to the vehicle deceleration.

In the 1970s, Calspan Corporation developed the program CRASH (Calspan Reconstruction of Accident Speeds on the Highway) for NHTSA to assist SMAC (Simulation Model of Automobile Collisions) users in determining a first estimate of impact speeds. It was subsequently utilized as stand-alone software to estimate the delta-V of the vehicles involved in a crash and make a standardized assessment of the severity of an impact. The program had two separate and independent methods, trajectory analysis and damage analysis. The trajectory analysis method required detailed measurements from a crash scene and vehicle to compute the delta-V using the principle of conservation of linear momentum for the collision.

The damage analysis method was based on Campbell's observation that for full frontal impacts into a fixed rigid barrier, the delta-V has a linear relationship with residual crush [1]. It used detailed measurements of the structural deformation of each vehicle to estimate the approach energy, which was then used to estimate the delta-V.

The NASS/CDS began coding the delta-V of crashed vehicles in 1979 using the CRASH program. The program was updated and revised several times in the 1980s to a widely used and distributed mainframe version:CRASH3. In the late 80s, the program was migrated to a DOS based PC platform and the version was called CRASHPC. No algorithm changes were made in the translation. The CRASH3 program was

based on crash tests conducted on older (1971-1974) GM full frame body cars. Later model year cars have significant changes in the structure and materials and many have a unitized body. In the 1990s, the NHTSA Vehicle Research and Test Center (VRTC) used repeated test techniques on later model year (1980-1992) cars to verify the relationship between the crush energy and residual crush. Based on these results the damage analysis algorithm of the CRASH3 program was reformulated and the new program was called SMASH. The SMASH program was written for the Microsoft Windows environment. Finally, in 1995, Volpe National Transportation System Center made some user-friendly enhancements to SMASH and integrated the program with the NASS/CDS data entry software and called the program WinSMASH. Since then several versions of the program were released for internal use, but all of those releases were mostly cosmetic changes and error corrections. The WinSMASH is written in the Delphi programming language under the Microsoft windows environment. One of the key features of the WinSMASH software is the user-oriented, menu-driven, interactive input mode. The interactive input option allows the user to supply all input data, edit the data and run the program. A mouse can be used to navigate through the program. The results of the analysis are displayed in numerical and graphical forms. The NASS/CDS system began using SMASH/WinSMASH in 1995. This paper describes WinSMASH version 2.42, which is currently being used by NHTSA.

The new additions in WinSMASH, since the last version of CRASH3 was released, include:

- Reformulated damage algorithm
- Updated stiffness coefficients
- Input fields for substitution of default data including stiffness coefficients
- New algorithm for missing vehicle reconstruction
- Estimation of Barrier Equivalent Speed

OBJECTIVES

The purpose of this paper is to describe the new enhancements in the WinSMASH software since the last PC-based version of CRASH3 was released. This paper provides an overview of different calculation procedures of WinSMASH and their application in the NASS/CDS. The accuracy of the program is assessed by comparing the WinSMASH estimated delta-V with the corresponding delta-V obtained from the EDR installed in the crashed vehicles and with the delta-V from staged crash tests. The use of vehicle specific stiffness is proposed and a statistical method for estimating the stiffness coefficients of a vehicle model that is not crash tested is being developed and is discussed here briefly.

WinSMASH PROCEDURES

The WinSMASH software has two separate and independent algorithms (Trajectory Analysis and Damage Analysis) to estimate the delta-V of the vehicles involved in a crash. Each method has options to reconstruct vehicle-to-vehicle and vehicle-to-object crashes. The software also has a reformulated missing vehicle algorithm that is used to estimate the delta-V when the damage to one of the vehicles is unknown.

All of the simplifying assumptions of CRASH3 remain in WinSMASH. The algorithms assume the impact was instantaneous and at some point during the impact both vehicles reached a common velocity. Due to these assumptions, WinSMASH can not be used for rollovers, sideswipes, non-horizontal forces, severe over-ride/under-ride, under-carriage impacts, multiple impacts to the same area, and towed trailer or vehicles.

The WinSMASH algorithms are discussed in the following sections.

Trajectory Analysis Algorithm

The trajectory analysis algorithms of WinSMASH and CRASH3 are identical. The algorithm is based on work-energy relationships for the spinout and the conservation of linear momentum for collisions. It estimates the vehicle separation speed from the information about the rest position, skid marks, coefficient of friction, and point of collision. The momentum equations are then used to compute the impact speed and delta-V of the vehicles.

For oblique impacts where the line of action of the collision force is not perpendicular to the damaged side or end, the algorithm uses spinout and the conservation of linear momentum to compute the delta-V and impact speeds. For those impacts, WinSMASH also computes the delta-V using the damage analysis algorithm. The delta-V from the two algorithms will seldom be precisely equal. However, the NASS researcher assumes that a satisfactory agreement exists between the two estimates when their delta-V components differ by no more than 4 kmph or ten percent, whichever is greater.

For the axial impacts, delta-V is computed using the damage analysis algorithm. The trajectory algorithm then uses separation conditions and damage delta-V to compute the impact speeds of the vehicles.

The Trajectory Simulation Option of CRASH3/CRASHPC is also available in WinSMASH. This option can be used to improve the agreement between the predicted post crash trajectory and documented physical evidence. The algorithm changes the magnitude and direction of linear velocity of the vehicles at separation until agreement is reached between the predicted and actual rest positions and heading angles. In WinSMASH, the users have control of the number of trajectory runs, instead of up-to-5 automatic runs completed in the trajectory simulation option of CRASH3.

Required Input

To use the trajectory option in WinSMASH, the NASS researcher thoroughly examines the crash scene for physical evidence, and obtains coordinates of the rest and impact positions, heading angle, slip angle, rotation direction, end rotation position, coordinates of a point on the path if the trajectory is in a curved path, friction coefficients and rolling resistance at each tire, for each vehicle. The vehicle damage data, described later in this paper, are also required for axial impacts.

NASS/CDS Application

Due to the statistical case selection process of the NASS program, a lag time exists between the crash date and the date the crash researcher begins data collection. Scene evidence, tire marks, and other witness marks tend to diminish with time. Moreover, Anti-lock Braking System (ABS) equipped vehicles generally do not leave readily visible skid marks at the scene. As such, this evidence may be overlooked or not documented. Due to the difficulties associated with the scene data collection, the trajectory option is rarely used by the NASS researcher. Less than one percent of the coded delta-Vs in NASS/CDS are computed using the trajectory algorithm. Since the trajectory option is rarely used, no initiative was taken to update this portion of the algorithm in WinSMASH.

The major enhancements to the trajectory option in WinSMASH are the implementation of a user friendly interface and graphical output. The detailed description of the trajectory analysis algorithm can be found in the CRASH3 manual [2].

Damage Analysis Algorithm

The damage analysis algorithm uses the damage measurement of the vehicle to estimate the approach energy absorbed by the vehicle, which is then used to estimate the delta-Vs by using the principal of conservation of momentum. The damage algorithm of CRASH3 was based on the assumed linear relationship between the impact velocity and crush and was derived from the crash tests conducted on old (1971-1974) General Motors full frame body cars. The later model year cars have unitized body and have significant changes in material and structures. Similar crash tests on late model year cars were needed to study their crush behavior.

In the 1990s, VRTC performed several crash tests on late model year cars [1980-1992] at delta-V in the range of 16-64 kmph [4,5,6]. A repeated test technique was used to confirm the linear relationship between the terms $\sqrt{\frac{2E_A}{w}}$ and crush. Where E_A is the energy absorbed by the vehicle structure and w is the width of the crush. The technique was based on the assumption that the vehicle deforms under repeated impacts in a manner similar to that of a single test at higher speeds having the same absorbed impact energy [3]. Based on the results from the crash tests, the damage analysis algorithm of CRASH3 was reformulated in WinSMASH. The new damage algorithm in WinSMASH is based on an assumed linear relationship between crash energy and crush [4,5,6].

The linear relationship between $\sqrt{\frac{2E_A}{w}}$ and residual crush is represented by Figure 1. In this model two parameters intercept, d_0 and slope, d_1 characterize the vehicle stiffness.

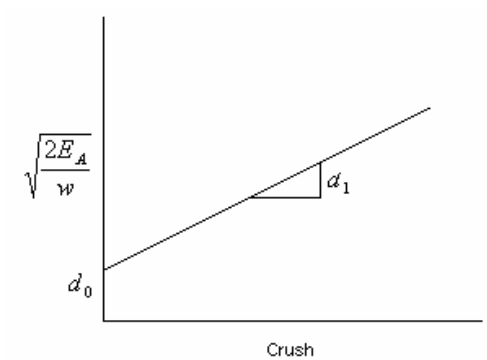

Figure 1. Assumed linear relationship between crush and crash energy.

The expression for the straight line in Figure 1 is given by:

$$\sqrt{\frac{2E_A}{w}} = d_0 + d_1 \times C \qquad (1).$$

Where C is the residual crush.

The energy absorbed during the approach period that is defined as the time between the initial contact and the time when common velocity is achieved, can be calculated by integrating the expression over the crush profile C(w):

$$E_A = \int_0^w \frac{1}{2} \times (d_0 + d_1 \times C)^2 \, dw \qquad (2).$$

In WinSMASH the integration is performed numerically by assuming piecewise linear approximation of the crush profile. The crush profile can be defined by two, four, or six equidistant points along the damage plane.

Equation (2) is used to compute the absorbed energy (E_A) for each vehicle. The total energy (E_T, sum of energy absorbed by each vehicle) is then used to compute the delta-V of each vehicle at the center of gravity (c.g.) using the principle of conservation of linear momentum. The delta-V of the approach period is given by:

$$\Delta V_1 = \sqrt{\frac{2E_T\gamma_1}{M_1\left(1 + \frac{\gamma_1 M_1}{\gamma_2 M_2}\right)}} \qquad (3).$$

$$\Delta V_2 = \sqrt{\frac{2E_T\gamma_2}{M_2\left(1 + \frac{\gamma_2 M_2}{\gamma_1 M_1}\right)}} \qquad (4).$$

M_1 and M_2 are the masses of the vehicles and

$$\gamma_1 = \frac{k_1^2}{k_1^2 + h_1^2} \quad \text{and} \quad \gamma_2 = \frac{k_2^2}{k_2^2 + h_2^2} \qquad (5).$$

Where:
k_1 and k_2 are the radius of gyration of vehicles 1 and 2
h_1 and h_2 are the moment arm of impact force [Figure2].

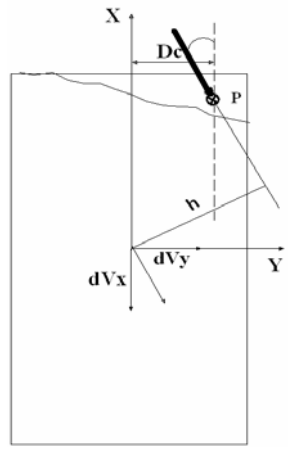

Figure 2. Moment Arm in non-central collision

The moment arm of impact force depends on the location of the centroid of the damage area relative to the center of gravity of the vehicle and the Principal Direction of Force (PDOF). For central impacts, where the line of action of the collision force passes through the center of mass of the two vehicles, the moment arms are zero, and γ_1 and γ_2 are equal to 1. The procedure to determine the h_1 and h_2 can be found in the CRASH3 Technical Manual [2].

The stiffness coefficients A, B and G used in CRASH3 are replaced by d_0 and d_1 in WinSMASH. The new coefficients are conceptually more direct and simpler. It avoids the need to reduce the experimental results to force-deflection formulation and models the energy crush behavior directly. The WinSMASH stiffness coefficients can be converted to CRASH3 coefficients A and B as follows:

$$A = d_0 \times d_1 \quad \text{and} \quad B = d_1^2 \qquad (6).$$

The WinSMASH damage reformulation consists mainly of the addition of new crash test data points and a rework of the formula to use different symbols [7]. Nonetheless, the updated algorithm allows a general procedure for front, rear, and side impacts. The observed improvement in results of the WinSMASH is due to the use of vehicle-specific dimensions, inertial properties, and updated stiffness coefficients.

The damage algorithm in WinSMASH only estimates the velocity change in the approach period. The velocity change during the separation period defined as the period between the maximum crush and complete separation of the vehicles is not considered in the analysis. The residual crush is used to compute the energy absorbed to the point of common velocity.

Required Input

The input required to use damage analysis option are Field L, Damage Offset, Crush Profile, PDOF, heading angle, Collision Deformation Classification (CDC), and Stiffness Coefficients. The NASS/CDS uses SI units for all measurements. The following sections briefly describe the input variables.

Field L and Field L-D

The Field L, also known as damage length or width, is defined as the length of the direct and induced damage measured parallel to the damage plane. The Field L is used for Damage Length in WinSMASH for side plane impacts and for end plane impacts where the damage does not extend across the entire end plane. For end impacts where contact and induced damage includes the entire width of the end plane, the undeformed end width (UEW) of the vehicle is entered as the Damage Length in WinSMASH. The UEW is the distance on an undamaged end plane measured bumper corner to bumper corner from an exemplar vehicle.

The Field L-D (D_{FL}) is the distance from the center of the Field L to vehicle's damaged end plane center or the damaged wheelbase center, measured parallel to the vehicle's lateral or longitudinal axes for front and side impacts, respectively [Figure 3]. The Field L-D measurement is primarily used to specifically locate the damage on the vehicle diagram.

Damage Offset

The damage offset also known as Direct D (Dc) is the distance from the center of the direct damage width to either the vehicle's damaged end plane center or the damaged wheelbase center [Figure 3]. It is measured along the general slope of the damaged plane. The center of gravity (c.g.) of the vehicle is typically located forward of the center of the wheelbase. For side plane damage, the WinSMASH program adjusts the D_C to account for different location of c.g. and the center of wheelbase. The D_C measurement is used to compute the moment arm of the impulse force.

In non-central frontal collisions (i.e. offset), the line of action of the collision forces passes through a point P in the region of direct contact [Figure 2]. This point P (centroid of direct damage area) is at a distance, Dc, away from the c.g. of the vehicle in a lateral direction. The point is between the undamaged plane (undamaged box) and damage plane (damaged box) in the region of direct contact. The force acting at a distance from the c.g. creates a moment arm and in turn affects the calculated delta-V of the vehicles, since this moment arm tends to produce rotation as well as translation. Assuming the same force is acting, a larger moment arm produces a lower delta-V but a higher rate of rotation.

Crush Profile

In NASS/CDS the basis for field data collection is the point-to-point vehicle measurement technique which specifies the actual distance a specific component moved within its damage plane. The crush profile measurements are obtained by establishing a reference line, measuring residual crush, and subtracting the undeformed bumper/body taper to obtain the resultant crush profile. The emphasis is placed on the damage level at which the stiffness coefficients were determined. For end impacts, measurements are taken at bumper level and for side impacts the measurements are typically taken along the door guard beam. Typically, the crush measurements are taken at six equidistant points obtained by dividing the Field L into five equal lengths [Figures 3, 4]. The depths of the crush are measured from the original outline of the vehicle to the final crush position in the perpendicular direction.

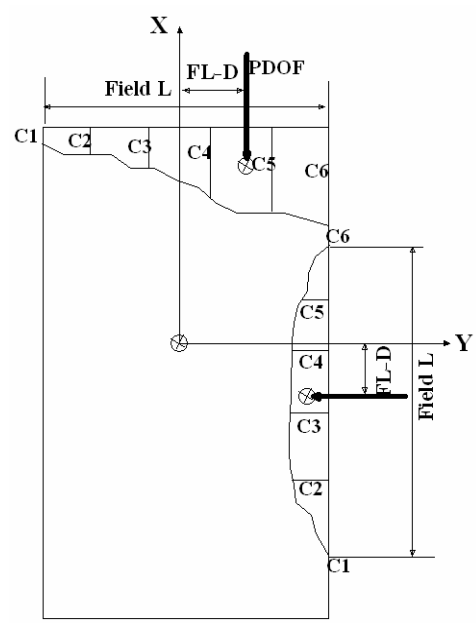

Figure 3. Crush Profile Approximation

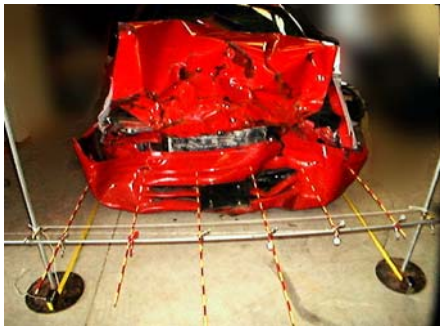

Figure 4. Measurement taken during vehicle inspection

PDOF and Heading Angle

The PDOF is defined as the angle of the direction of Impulse Force acting on the vehicle, measured relative to the longitudinal axis. It determines the direction of delta-V. The delta-V computed by WinSMASH is most sensitive to PDOF and yet it is the most difficult measurement to obtain. The NASS investigator considers the general flow of sheet metal crush of the vehicle, weight and impact speed, pre and post impact trajectories and occupant kinematics to determine the PDOF. In NASS/CDS, PDOF is estimated to the nearest 10 degrees and entered as an improved PDOF to the clock direction specified in columns 1 and 2 of the CDC. The PDOF estimated from the CDC clock direction may be off by as much as 30 degrees.

The heading angle is the direction of travel and it specifies the orientation of the vehicle at the impact location. For vehicle-to-vehicle impacts, the WinSMASH requires that the Force Vectors on the vehicle must be within 15 degrees of perfectly collinear or along the same line. The WinSMASH performs a collinearity check before proceeding with the calculation and an error message is displayed if the PDOFs are apart by more than 15 degrees.

CDC

The CDC value is used to determine the type of collision that occurred in the crash, e.g. frontal, side, rear or rollover. The CDC is a seven character alpha-numeric code that describes the vehicle deformation detail concerning the direction, location, size of the damage area, and extent of damage. A CDC is required for each vehicle for a WinSMASH run. The program uses CDC information to validate the consistency of PDOF and crush measurements. The information is also used to properly locate the damage on the vehicle diagram. If the vehicle is not available for measurement, WinSMASH has an option to use CDC information to compute a crude estimate of delta-V. The CDC is completely described in SAE Recommended Practice (SAE J224 MAR 80).

Vehicle Stiffness Coefficients d_0 and d_1

In WinSMASH, the stiffness characteristics of vehicles are defined by coefficients d_0 and d_1 as opposed to A, B and G in CRASH3. The stiffness parameters for passenger cars are categorized according to the wheelbase in similar ways as in CRASH3. The stiffness category automatically assigns the generic d_0 and d_1 according to the general structural characteristics of the vehicle.

The CRASH3 assumption, vehicles of similar size have similar stiffness characteristics, also applies to WinSMASH. The program assumes a homogeneous stiffness along the front, side and rear structures of the vehicle. The vehicles are divided into nine sets of stiffness coefficients (d_0, d_1) corresponding to seven vehicle size categories. The data from NHTSA's crashworthiness database that contains data from mostly New Car Assessment Program (NCAP) and Compliance crash tests is used to compute the stiffness coefficients for each category. First, a method developed by Prasad [4,5,6] is used to compute the d_0 and d_1 values for each vehicle in the database. The method is based on using two data points on the straight line describing $\sqrt{\frac{2E_A}{w}}$ vs. crush to determine the intercept d_0 and slope d_1. A zero crush intercept is used for the low speed data point and the high speed data point is obtained from the NHTSA's crash test. For frontal impacts, a low speed data point is assumed to be zero crush at 12 kmph. The NCAP tests at 56 kmph and Federal Motor Vehicle Safety Standard (FMVSS) No. 208 tests at 48 kmph are used for the high speed data point. For rear impacts, a low speed data point is assumed to be zero crush for the impactor speed of 16 kmph (i.e. delta-V of 8 kmph). The FMVSS No. 301 tests at 48 kmph and 80 kmph are used for the high speed data point. For side impacts FMVSS No. 214 tests at 54 kmph are used for the high speed data point. The value of d_0 is assumed to be $63.3\sqrt{\text{Newton}}$ (which is equivalent to a barrier approach velocity of approximately 16 kmph with vehicle and barrier weighing 1360 kg. each) [6]. This data point provides a reasonable estimate for low speed impacts and avoids the errors introduced by curve-fitting multiple data points clumped together at 48-56 kmph.

Figure 5 shows the crush energy relationship for a 2005 Volvo V70 which is a NHTSA frontal NCAP test number 5242.

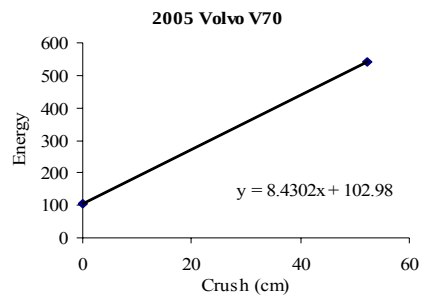

Figure 5 Crush Energy plot for NHTSA test 5242

Once the stiffness coefficients for all the vehicles are computed, the vehicles are then assigned to six passenger car categories (1 to 6) according to wheelbase and two categories for vans (category 7) and pickups (category 8). A generic set of d_0 and d_1 values are computed for each category by averaging the known values in that category. The generic stiffness coefficients used in WinSMASH are listed in Tables 1 and 2. For frontal impacts, a separate stiffness category (category 9) is used for front wheel drive (FWD) vehicles. The stiffness in category 9 is the average of all the front wheel drive passenger cars.

For side impacts, all vehicles including pickup trucks and vans are divided into six stiffness categories based on wheelbase size.

The NHTSA' crashworthiness database is constantly updated as newer models are tested by NHTSA for Compliance and NCAP. The generic stiffness coefficients shown in Tables 1 and 2 were created in 1995 using test data from NHTSA's crashworthiness database. The stiffness coefficients are currently being updated to include later model year vehicles which have been crash tested by NHTSA.

Table 1.
Vehicle Size Categories

Category	Wheelbase (cm)
1	<= – 240.8
2	240.8 – 258.0
3	258.0 – 280.4
4	280.4 – 298.4
5	298.4 – 312.9
6	> – 312.9
7 (vans)	276.8 – 330.2

Table 2.
Generic Vehicle Stiffness Categories

Cat.	Front		Rear		Side	
	d_0 $\sqrt{\text{Newton}}$	d_1 $\frac{\sqrt{\text{Newton}}}{\text{cm}}$	d_0 $\sqrt{\text{Newton}}$	d_1 $\frac{\sqrt{\text{Newton}}}{\text{cm}}$	d_0 $\sqrt{\text{Newton}}$	d_1 $\frac{\sqrt{\text{Newton}}}{\text{cm}}$
1	91.4	6.7	93.88	5.43	63.3	6.83
2	97.0	7.22	96.23	5.28	63.3	8.02
3	102.1	7.25	99.49	5.56	63.3	7.50
4	107.0	6.36	99.99	5.37	63.3	7.21
5	109.6	6.18	99.97	4.50	63.3	5.19
6	116.0	5.75	74.86	6.94	63.3	5.69
7 (vans)	109.7	8.51	98.69	7.79	-	-
8 (pickup)	105.7	7.98	101.42	7.77	-	-
9 (FWD)	99.18	6.46	-	-	-	-

NASS/CDS Application

The damage analysis option is used most often by NASS investigators to estimate the delta-V because it can be accomplished from the vehicle inspection alone and it does not require scene data. It is a practical means of independently determining the delta-V of a vehicle when good accident site data are unavailable. For 2000-2005 NASS/CDS cases, fifty-three percent of the highest severity impacts (by vehicle) have delta-V values. The other unknown delta-Vs could not be computed for reasons including non-horizontal impacts, side swipe, rollover, severe over-ride, overlapping damage, insufficient data, vehicle beyond scope, and no vehicle inspection. Ninety-nine percent of those coded delta-V are computed using one of the options of the damage analysis algorithm including Standard (vehicle-to-vehicle impacts), Barrier (vehicle-to-object impacts), Missing Vehicle or CDC-Only. Of those coded delta-Vs, about fifty-eight percent are calculated using the standard or barrier option also known as Damage-Only in NASS/CDS.

Input Fields for Substitution of Default Data

The CRASH3 program used generic vehicle parameters based on vehicle size category. These data represent an average within a specified wheelbase range. A specific vehicle sometimes has properties which differ significantly from the generic data. The vehicle dimension can result in incorrect computation of damage offset, h. These inaccuracies can cause inaccuracy in the computed delta-V. The

WinSMASH has a facility to substitute for the generic data.

The use of vehicle-specific dimensions and inertial properties has improved the WinSMASH results. The radius of gyration used in the reformulated damage algorithm of WinSMASH is based on an investigation done at VRTC as a part of the Crash Avoidance Inertial Parameter Measurement Program and is given by

k = 0.3 x (vehicle length) (7).

The generic d_0 and d_1 stiffness coefficients automatically assigned by the crush stiffness category may not apply for all collisions. As in the case of bumper over-ride and under-ride crashes, the frames of one vehicle engage with the softer part of the other vehicle. The WinSMASH allows for replacement of generic coefficients with the vehicle specific stiffness coefficients. The NHTSA's Special Crash Investigation (SCI) teams use vehicle specific coefficients when available. However, NASS/CDS only uses generic stiffness coefficients in WinSMASH for delta-V estimations.

Correction Factor

During the vehicle inspection, the depths of the crush are measured from the original outline of the vehicle to the final crush position in a perpendicular direction. However, in oblique impacts the distance through which the PDOF act is greater than the measured crush. Therefore, in CRASH3 the value of the energy absorbed by the vehicles is multiplied by a correction factor given by ($C_f = 1 + \tan^2 \alpha$) where α is the angle between the PDOF and surface normal. The usage of correction factor (C_f) increases the value of absorbed energy (E_A) and therefore, causes CRASH3 to over-predict the value of delta-V in the oblique side impacts. In reconstructing an oblique side impact that has α of 45°, eliminating the correction factor reduced the delta-V error to less the 10 percent from 40 percent [5].

In WinSMASH, the user can specify whether to use or ignore the correction factor. An option "End Shift" can be checked to include the correction factor in the damage algorithm of WinSMASH. In NASS/CDS the end shift is only used for oblique impacts where the vehicle end structure (both frame rails) shifts more than 10 cm.

Missing Vehicle Option

The missing vehicle option is used to estimate the delta-V when the damage to one of the vehicles is unknown in a vehicle-to-vehicle impact. The missing vehicle algorithm, OLDMISS of CRASH3 has been reformulated and completely integrated in WinSMASH. The new algorithm uses a simple expression directly relating the energies absorbed by the known vehicle and missing vehicle, bypassing the need to estimate the crush profile of the missing vehicle, and then integrate across that profile. The method also accounts for the energy absorbed by the induced damage. The new algorithm is based on crash tests conducted at VRTC to update the CRASH3 damage algorithm [8]. The new missing vehicle algorithm uses the following expressions to estimate the energy of the missing vehicle:

For an impact involving damage to only the front or rear of vehicle:

$$E_{missing} = \frac{(d_1^2)_{measured}}{(d_1^2)_{missing}} E_{measured} \quad (8).$$

For an impact involving damage to sides and front of the vehicles:
Case 1: Vehicle with front/rear damage available, side damage missing:

$$E_{missing} = 2.1 \frac{(d_1^2)_{measured}}{(d_1^2)_{missing}} E_{measured} \quad (9).$$

Case 2: Vehicle with side damage available, front/rear damage missing

$$E_{missing} = \frac{(d_1^2)_{measured}}{(d_1^2)_{missing}} \frac{E_{measured}}{(2.1)} \quad (10).$$

The damage analysis algorithm is used to compute the absorbed energy for the measured vehicle. Once the energy absorbed by the missing vehicle is computed, the total energy (E_T) is used in equation 3 and 4 to estimate the delta-V. In NASS/CDS thirty seven percent of the coded delta-Vs are computed using the missing vehicle option of WinSMASH. This option only requires the vehicle specifications and damage location for the un-inspected or missing vehicle.

CDC-Only Option

The CDC-Only option is used for vehicle-to-vehicle collisions when insufficient damage data are documented for one of the vehicles. The option requires a complete CDC for both vehicles, and complete damage data for one vehicle. The algorithm computes the crush profile of the second vehicle by using the damage length and damage extent coded in CDC. Only four percent of the coded NASS delta-Vs are computed using the CDC-Only option of WinSMASH.

Barrier Equivalent Speed

The WinSMASH also estimates the Barrier Equivalent Speed (BES) for each vehicle. The BES is defined as the speed with which a vehicle would have to collide with a fixed barrier in order to absorb the same amount of energy or produce same amount of crush to the vehicle as in the crash. The BES is a direct representation of the amount of energy the vehicle structure has to absorb and therefore approximates the amount of crush sustained by the vehicle. The same energy absorption could come out of collisions with different delta-Vs, leading to different potential for injuries. The BES therefore is typically a more appropriate way of comparing collisions with similar struck objects.

Nonetheless, BES is also considered a reliable indicator of crash severity. The NASS/CDS cases are used in Figure 6 to show the injury relationship with the delta-V and BES. The cumulative frequency of MAIS 2+ injuries to the belted occupant in crashes that have an air bag deployment is plotted against delta-V and BES of the vehicles. The chart shows sixty percent of the MAIS2+ injuries occurred at BES of 34 kmph and less. Similarly, sixty percent of the MAIS2+ injuries occurred at Delta-V of 38 kmph and less.

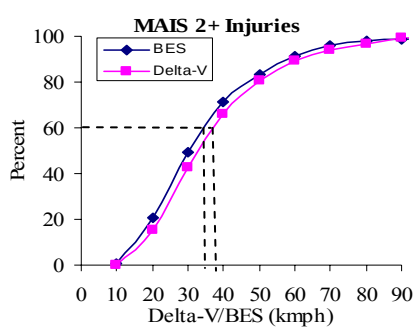

Figure 6. The cumulative distribution of MAIS 2+ injuries .vs. delta-V and BES.

The BES is calculated using mass and energy absorbed by each vehicle. No information is required of collision partner for BES calculations. Whereas, total amount of energy (both vehicle 1 and vehicle 2) is required to calculate approach delta-V.

For each vehicle the BES is given by,

$$\mathrm{BES} = \sqrt{\frac{2 E_A \gamma}{M}} \qquad (11).$$

Since 1995 the NASS/CDS was coding BES for all cases where delta-V estimates were available. The vehicle collisions with yielding objects, moving trains, larger trucks, large animals, pedestrians and cyclists that results in a measurable crush to the vehicle are set-up with the Barrier option and only the BES is coded for the vehicle.

Pole Option

The WinSMASH also has an option to set up vehicle impacts with a pole. This option uses the same damage analysis algorithm described above. However, the categorical stiffness coefficients are modified by multiplying the values by a correction factor. These factors are computed based on a series of repeated centered pole impact tests carried out on eight late model year (1987-1992) vehicles. The results were compared to the performance of these vehicles in full frontal impacts. An examination of the d_0 data showed that the values for pole impacts are much smaller than the values for full front impacts. For the pole option d_0 is set to zero and value for d_1 is multiplied by 1.5 for small cars and 2.0 for all other cars.

The pole option is not validated and is not used by the NASS researchers to calculate delta-V. All pole impacts are set up with barrier option in NASS/CDS.

Validation of Damage Algorithm
<u>Staged Crash Tests</u>

The accuracy of the reformulated damage algorithm of WinSMASH was assessed by comparing the delta-V estimates from the software with the delta-V from the crash tests conducted under controlled conditions. These staged crash tests were based on both vehicle-to-barrier impacts and vehicle-to-vehicle impacts. The vehicles were instrumented with accelerometers at various locations for direct computation of delta-V. The algorithm was validated by reconstructing nine staged vehicle-to-vehicle impacts and five crash tests involving oblique and

rear impacts. The details of validation are available in a report by VRTC [5]. Since, the damage algorithm in WinSMASH only estimates the velocity change in the approach period, delta-V at the point of common velocity was compared for validation.

For frontal impact tests, overall on average, the WinSMASH underestimated the delta-V by 5 percent. For 10 of 11 frontal impact tests, the errors in delta-V from WinSMASH were well below 10 percent.

For rear impact tests, overall on average, the WinSMASH underestimated the delta-V by 11 percent. For two of the three rear impact tests, the errors in delta-V from WinSMASH were less than 5 percent.

For validating the WinSMASH in side impacts, seven vehicle-to-vehicle 270 degree side impacts and five oblique impacts were reconstructed. These tests involved both vehicles moving prior to the impact. In eight of the twelve tests the percent errors in delta-V were less than or close to 10 percent. Overall on average, WinSMASH overestimated the delta-V by 12 percent for side impacts.

Real World Collisions

The real world collisions are complex and very seldom match the perfect configuration of staged collisions used for software validation. The WinSMASH software was developed to compute the delta-V estimates of the vehicles involved in real world collisions and hence, the accuracy of the program should be assessed for these crashes. The EDR now installed as standard equipment by several vehicle manufacturers, provide a direct measurement of the delta-V of the crashed vehicle. Several authors have investigated and written about the accuracy of delta-V estimates from EDR [9,10].

In a study of 121 real world crashed vehicles, Niehoff and Gabler compared the delta-V measured by EDRs with the delta-V estimated by WinSMASH, and found that WinSMASH underestimates longitudinal delta-V by 25 percent on average [12]. A similar analysis was carried out in parallel at NHTSA using 135 NASS files from year 1997-2003. In this analysis, the NASS cases with questionable WinSMASH delta-V estimates were excluded. The delta-V estimates ranged from 20 kmph to 50 kmph. The overall average difference between the WinSMASH and EDR delta-V was about 21 percent. Figure 7 compares the delta-V estimated by WinSMASH using generic stiffness coefficients [Table 2] with the corresponding delta-V computed from EDR data. The symbols falling on the dotted line drawn diagonally across the plot are cases where the EDR and WinSMASH delta-V perfectly matched with each other. The symbols falling below this line represent underestimated WinSMASH delta-V, that is, the WinSMASH delta-V estimate is lower than the EDR delta-V. The other two dashed lines correspond to +/- 20 percent difference between the WinSMASH and EDR delta-V.

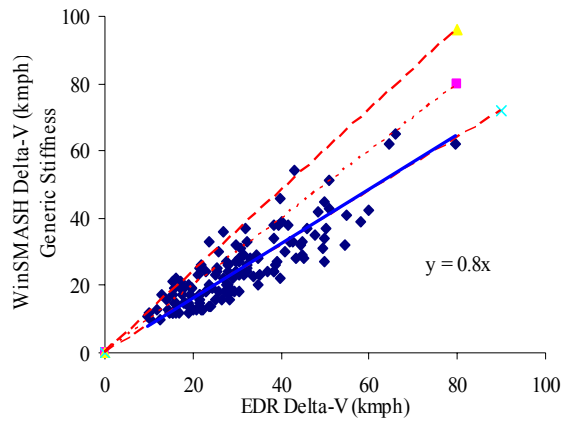

Figure 7. EDR vs. WinSMASH delta-V using generic stiffness.

The average difference was lower in NHTSA's analysis because the cases with questionable WinSMASH runs were excluded in their analysis. As mentioned earlier in the paper, the damage algorithm in WinSMASH only estimates the delta-V in the approach period, i.e. at the point of common velocity. This may have contributed to the difference seen in the comparison of delta-V from WinSMASH and EDR. The consideration of restitution may improve the WinSMASH results.

The stiffness coefficients of WinSMASH are best applicable to crash configurations that match with the crash tests used to develop the coefficients. The offset impacts, side impacts at the wheel and axle, under-ride and over-ride impacts should be examined carefully. The WinSMASH was not designed to be a simulation program but rather a consistent, uniform method of judging accident severity in terms of the change in velocity. It should be emphasized that the WinSMASH program, as CRASH3, should be statistically valid for a large number of cases; it may not provide accurate results in a particular case. The software should only be used with caution for individual cases. Good engineering judgment must always be used to ensure the validity of any simulation results.

RECENT DEVELOPMENTS IN WinSMASH

Abandoning Stiffness Category 9

In WinSMASH, for frontal impacts, a separate stiffness category (category 9) is used for front wheel drive passenger cars. The stiffness coefficients for category 9 are computed by averaging the known stiffness coefficients of all the front wheel drive passenger cars.

The data used to compute the average generic stiffness for each category suggest that drive axle (front or rear) is no longer a distinguishing feature. The larger cars tend to be rear wheel drive cars and smaller cars tend to be front wheel drive. In WinSMASH, the average stiffness in each category is calculated from crash tested vehicles that are mostly front wheel drive. To test the applicability of the category representing the front wheel drive vehicles, the NHTSA barrier crash tests of front wheel drive vehicles from size categories 2, 3 and 4 [Table 1] were reconstructed with WinSMASH. Each crash test was reconstructed twice, first using stiffness category based on wheelbase size and again using stiffness category 9. All data except the stiffness category were the same for both reconstructions. The delta-V estimates from using category 9 were six percent lower than the delta-V estimates using size based stiffness categories 2 and 3 [Table 2].

Based on these observations, the category 9 has been eliminated in NASS/CDS since data collection year 2006. The category 9 is absorbed in wheelbase size.

A new class of vehicles known as Sports Utility Vehicles (SUV) has emerged since the WinSMASH categories were developed. The computed average stiffness coefficients for SUVs matched closely to the stiffness coefficients of vans. Therefore, category 7 is currently used for SUVs until a separate category is created for SUVs.

Using Vehicle Specific Stiffness Coefficients

The 135 NASS/CDS cases used in the real world collision validation were selected to study the effect of replacing the generic stiffness coefficients with the vehicle specific coefficients in WinSMASH. Figure 8 compares the delta-V estimated by WinSMASH using vehicle stiffness coefficients with the corresponding delta-V computed from EDR data. Again symbols falling on the dotted line drawn diagonally across the plot are cases where the EDR and WinSMASH delta-V perfectly match with each other. The other two thin lines correspond to +/- 20 percent difference between the WinSMASH and EDR delta-V estimates. The plot clearly shows that more cases moved between the 20 percent error bounds (dashed lines) after the vehicle specific coefficients were used in the WinSMASH runs.

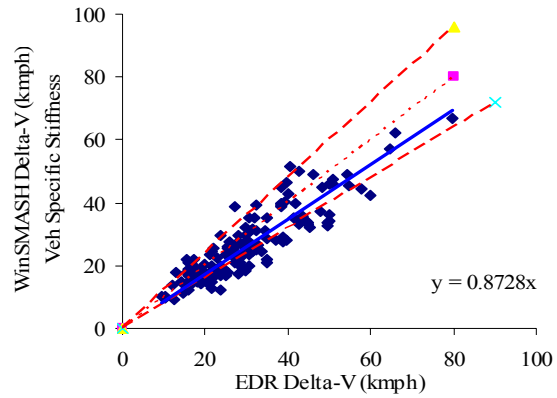

Figure 8. EDR vs. WinSMASH delta-V using vehicle specific stiffness.

The overall average difference between the WinSMASH and EDR delta-V is reduced to about 17 percent from 21 percent. This accounts for an improvement of about 4 percent, when vehicle specific coefficients were used in the WinSMASH software. The study also examined and compared the data by different impact and crash configurations including front-to-front, front-to-side, and front-to-barrier and pole crashes. In those cases, the WinSMASH delta-V estimates in longitudinal direction improved by about 4 percent on average for different crash configurations.

Various studies have shown that a high degree of variation exists in the stiffness characteristics of different vehicles. The results from this study also suggest that using the same stiffness coefficients for different vehicles with the same wheelbase may underestimate the WinSMASH delta-V. The results of this analysis suggest the advantage of the use of vehicle specific coefficients.

The WinSMASH was developed to utilize the vehicle specific stiffness coefficients. The main source of vehicle stiffness data is NHTSA's vehicle crash test database which contains detailed information on over 5000 crash tests involving primarily the vehicle models from year 1975 to current model year. The vehicle specific coefficients for front, side, and rear structure are computed for more than 2000 vehicle models from year 1975 to 2006. Additionally, since the main body structure of the vehicle model does not change every year, the same stiffness coefficients can

be used for the years during which the model structure has not changed. The stiffness coefficients for the tested vehicles can also be applied to its sister/clone models.

The frontal stiffness coefficients of 1395 vehicles, rear stiffness coefficients of 299 vehicles, and side stiffness coefficients of 600 vehicles have been computed. However, it represents only a fraction of the number of vehicles in the current fleet. There is a need to be able to reconstruct impacts involving vehicle models not tested by the agency.

Estimating d_0 and d_1 for vehicle not tested

In 1991, Prasad proposed a linear regression model based on the correlation between the vehicle parameters and stiffness coefficients of crash tested vehicles to estimate the stiffness coefficients of non-tested vehicles [6]. Since then the crash test data on more vehicles has become available in the NHTSA data base. The use of a statistical modeling scheme is examined to improve the estimates of the frontal stiffness coefficients for vehicles that are not crash-tested.

Twelve variables from 1300 frontal vehicle crash tests with computed d_0 and d_1, are used for this analysis. The variable chosen for this study are: Vehicle Age (w.r.t. model year 2006), body type (BT), distance between the side rails (E), engine displacement (ENGDSP), front overhang (F), C.G. (VEHCG), length (VEHLEN), width (VEHWID), weight (VEHWT), wheelbase (WHLBAS), d_0 and d_1.

An exploratory data analysis is performed by using scatter plots, correlation coefficients and descriptive statistics in SAS to see if there are any patterns, relationships, or trends the variables might hold. Then, a general linear model is fitted to predict d_0 and d_1. From the full model with all independent variables, statistically insignificant independent variables are removed one by one by using Multivariate Analysis of Variance until all independent variables are statistically significant in a fitted model. A final fitted general linear model is developed to predict d_0 and d_1 from predictor variables including vehicle age, length, weight, wheelbase, width, c.g., front overhang and body type. The body type is a categorical variable that divides the vehicles into four categories: passenger cars, pickup trucks, SUVs and vans.

For passenger cars the fitted general linear model for d_1 is:

$$d_1 = 14.4057 - 0.1307*AGE - .00001665*VEHLEN + 0.0018371*VEHWT - 0.0003816*WHLBAS - 0.0006609*VEHWID - 0.0010748*VEHCG - 0.0453959*F$$

The estimates produced by the fitted model are evaluated through simulation study. A sub-sample of 100 cases is randomly selected from the set of 1204 crash tested vehicles with known d_0 and d_1. Those 100 tests are treated as non-tested vehicles and are not used in the general linear model for the simulation study. The fitted model developed in the above analysis is used to predict the stiffness coefficients of selected cases. The actual values are compared with the model predicted coefficients and with the current wheelbase based categorical coefficients.

The average difference between the model based predicted and actual was 0.9 percent for d_0 and 13 percent for d_1. The average difference between the current categorical based and actual was 4 percent for d_0 and 17 percent for d_1. Figure 9 compares the actual d_1 with the d_1 predicted by the general linear model and d_1 from the wheelbase based category for passenger cars. The wheelbase based d_1 is shown by triangular symbols.

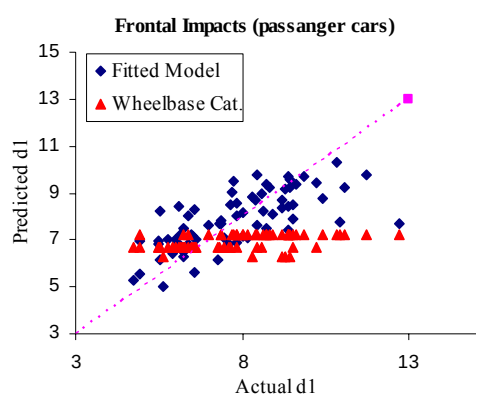

Figure 9. Comparison of d_1 predicted by general linear model and wheelbase base category.

A similar analysis is currently being carried out for side and rear stiffness coefficients. The details of the general linear models will be presented in a separate paper.

The analysis showed that the general linear model is a better predictor of the stiffness coefficients of non-tested vehicles than the average values used over a wheelbase category. In the current model for stiffness category, a wrong stiffness could be assigned to a vehicle if its wheelbase is close to the upper or lower end of the wheelbase range. The vehicle's other characteristics such as weight, length,

and front overhang could match with the cars in the next higher or lower size category. The new method considers four categories of vehicle body type namely, passenger car, pickups, SUVs, and vans. For each category, relevant vehicle parameters are used to compute the stiffness coefficients of the vehicle. It eliminates the errors associated with assigning a stiffness category to the vehicles that fall in the upper or lower range of wheelbase size. If all the vehicle parameters used in the general linear model are known, the model will give a better estimate of stiffness coefficients of a vehicle than the average stiffness coefficients obtained from wheelbase based categories.

A database of stiffness coefficients is currently under development and will be integrated into WinSMASH. An automated selection procedure based on the vehicle parameters such as make, model, year wheelbase and weight, is being implemented. The software will use the vehicle specific stiffness coefficients for damage analysis, if available. The modeling scheme briefly discussed in the paper will be used if the vehicle is not in the database. If the stiffness and vehicle parameters needed to either lookup or estimate the stiffness coefficients are unknown, then the updated wheelbase based categorical stiffness coefficients will be used.

CONCLUSIONS

The paper presented an overview of NHTSA's crash reconstruction program WinSMASH. The software replaced the CRASH3 program and has been used by NASS/CDS investigators since 1995 to compute the delta-V of vehicles involved in crashes. At present, some programming errors are being resolved and new features including an automated scheme to select the stiffness coefficients, and new graphics enhancements are being implemented. The new stiffness selection method entails:

1) Use of vehicle specific stiffness, if available.
2) If the search process in step 1 does not reveal any vehicle, sister/clone information will be used to obtain stiffness of a compatible vehicle.
3) Otherwise, use the general linear model to estimate stiffness coefficient.
4) Use wheelbase based categories, if 1, 2 and 3 above can not be used.

The software is currently being tested and will be made available to the public once all features are implemented.

As with CRASH3, NHTSA maintains that WinSMASH is intended as a statistical tool to identify and isolate problems in motor vehicle safety, not as a simulation program, and should be used accordingly.

REFERENCES

1. Campbell, K. , "Energy Basis for Collision Severity", SAE 740565; 1974.
2. "CRASH3 Technical Manual," Accident Investigation Division, NCSA, NHTSA, 1986.
3. Prasad, Aloke K., "Energy Dissipated in Vehicle Crush- A study using Repeated Test Technique," SAE Paper 90-0412 , 1990.
4. Prasad, Aloke K., "CRASH3 Damage Algorithm Reformulation for Front and Rear Collisions," SAE paper 900098, 1990
5. Prasad, Aloke K., "CRASH3 Damage Model Reformulation", Report No. VRTC-87-0053, Vol 1& II, November 1987.
6. Prasad, Aloke K., "Energy Absorbed by Vehicle Structures in Side-Impacts," SAE paper 910599, 1991
7. McHenry, Raymond R., and McHenry, Brian G., "McHenry Accident Reconstruction 2003", Training Seminar 2003.
8. Prasad, Aloke K., "Missing vehicle Algorithm (OLDMISS) Reformulation," SAE paper 910121, 1991.
9. Niehoff, P., Gabler, H.C., Brophy, J. Chidester, A., Hinch, J., and Ragland, C., "Evaluation of Event Data Recorders in Full System Crash Tests", Proceedings of the Nineteenth International Conference on Enhanced Safety of Vehicles, Paper No. 05-0271, Washington, DC (June 2005)
10. Chidester, A. "Chip", Hinch, J., Mercer, Thomas C., Schultz, Keith S., "Recording Automotive Crash Event Data", International Symposium on Transportation Recorders, Arlington, VA 1999.
11. Niehoff, P. and Gabler, H.C., "The Accuracy of WinSMASH Delta-V Estimates: The Influence of Vehicle Type, Stiffness, and Impact Mode", 50th Annual Proceedings of the Association for the Advancement of Automotive Medicine, Chicago, IL (October 2006).

OFFSET TEST DESIGN AND PRELIMINARY RESULTS

James Saunders, Allison Louden, Aloke Prasad
National Highway Traffic Safety Administration
07-0240

ABSTRACT

The National Highway Traffic Safety Administration (NHTSA) is conducting a research program to investigate the feasibility of a high speed frontal offset deformable barrier (ODB) crash test to improve frontal occupant crash protection. The focus of the program is to reduce debilitating lower extremity injuries in frontal offset collisions. This paper discusses three areas of research in this program: new seating procedure, preliminary results of the new crash test, and an analysis of frontal stiffness characteristics of redesigned vehicles and their ODB test procedure performance.

The new seating procedure uses Hybrid III male dummies fitted with Thor-LX/HIII legs (HIII50LX). A particularly challenging problem was the development of a test procedure with repeatable positioning of the Thor-LX/HIII feet with respect to the pedals in some vehicles. inversion/eversion was the primary failure mode of the ankle was. The kinematics and mechanism of this failure are examined.

Preliminary data are presented that compare the frontal stiffness characteristics of vehicle models that were redesigned and used in both NCAP and IIHS crashworthiness rating programs. The potential impact of this on the compatibility of the light vehicle fleet is discussed.

INTRODUCTION

In vehicle crashes lower limb injuries are the second most common site of AIS 2+ injuries (Thomas, 1995). These lower leg injuries also have been reported to be the cause of permanent disability and Impairment (Burgess et al., 1995). Kuppa et al., 2001a, showed that the foot and ankle AIS 2+ injuries are 33% of lower leg injuries and 41% of associated Functional Life-years Lost to injury.

NHTSA has focused on the development of performance tests not currently addressed by FMVSS No. 208, particularly high severity frontal offset crashes. These tests are planned to result in large occupant compartment intrusion that could compromise occupant survival space and thus increase the potential for lower leg injuries. The ODB test procedure is being evaluated for its potential to predict lower leg injuries.

Saunders et al., 2004 showed that a high speed ODB test procedure (combining 56, 60, and 64 km/h test) appeared to correctly predict the risk and proportion of below-the-knee injuries in severe real world offset crashes, especially the proportion of foot and ankle injuries. In these tests Saunders used the Thor-Lx/HIII retrofit advanced lower leg. The Thor-Lx has rotational potentiometers to measure dorsiflextion, inversion/eversion, and internal/external rotations of the foot. This gives the Thor-Lx the ability to predict ankle and foot injuries. The current lower leg of the HIII does not have the ability to predict these foot and ankle injuries.

University of Michigan Transportation Research Institute (UMTRI) has conducted studies documenting the seating positions used by various sized humans. They have developed a mathematical regression for locating the seat longitudinal position based on those studies. The Insurance Institute for Highway Safety (IIHS) has adopted this procedure in their ODB test and had petitioned the agency to do so as well.

NHTSA has been using dummy seating procedures based on seat mid-track position for frontal crash tests with the HIII 50th percentile male. UMTRI found that the average person does not position the seat at mid-track in its study. Therefore, NHTSA has been investigating different seating procedures that do not use the seat track position. NHTSA has investigated the IIHS seating procedure and found that this procedure may not always put the right foot in the neutral position on the accelerator pedal because the procedure was developed using regression analysis with scatter in the data.

The current effort has developed a dummy seating position built on a different paradigm. This seating procedure uses a step-by-step process that mimics the procedures used by humans, thus avoiding the errors introduced by regression and by evolving vehicle interior designs. The procedures are described in

sections below and listed in Appendix A.

Since the EU Directive 96/79 for frontal crash protection became effective in 1998, other countries and consumer rating programs have adopted the use of a fixed ODB crash test procedure. The Australian and European regulation requires an ODB crash test at 56 km/h while their consumer rating programs, Euro NCAP (European New Car Assessment Program), Australian NCAP, and IIHS conduct the ODB crash test at 64 km/h. IIHS has evaluated over 150 vehicle models using their 64 km/h ODB crash test procedure and indicated in a status report (September, 2001) that various vehicle models that had received a "poor" rating were redesigned and later obtained "good" or "marginal" rating in their ODB crash tests. According to IIHS, this improved performance in the redesigned vehicles was attributed to vehicle structure design that prevents major collapse of the occupant compartment. Nolan and Lund (2001) found that the majority of vehicles (mainly passenger cars) whose structural performance improved in the IIHS frontal offset crash tests after being redesigned did so without significant alteration to the stiffness of the vehicle for the first half-meter of deformation. However, General Motors Corporation (Verma, et al., 2003) indicated that the use of fixed barriers as a test device may lead to higher force levels for front ends of larger vehicles and could act to increase the incompatibility between large and small vehicles. Saunders (2005) reported on pairs of vehicle-to-vehicle crash tests in which the redesigned vehicle in each pair obtained a better rating in the IIHS ODB tests than its respective older model (the other vehicle in the pair). The redesigned vehicle models were found to be more aggressive in these crash tests than their older counterparts as demonstrated by the injury measures of the dummies in the target vehicle. However, Saunders could not establish a relationship between the increase in aggressivity of the redesigned vehicles and the corresponding increase in front end stiffness in the redesigned vehicle due to the confounding effects of the redesigned vehicle's mass and vehicle front end geometry.

This paper presents the preliminary results of NHTSA's research on a high speed (56 km/h) ODB test. First, a description is provided of the dummy-based seating procedure and the repeatability of this procedure is presented. This is followed by a discussion of the results of the ODB tests using this new seating procedure. Next, the Thor-Lx/HIII kinematics is analyzed from the rotational data recorded and a description of the mechanism that caused the ankle to rotate. And finally, the paper discusses the potential concerns of an ODB test procedure on the compatibility of the light vehicle fleet.

SEATING PROCEDURE

This section describes a seating procedure that mimics the procedures used by humans to position themselves in the vehicle. This procedure ensures the feet are in neutral position and the right foot is placed on the accelerator pedal, which provides proper dummy interaction with the vehicle interior to be able to predict lower leg injuries.

DESCRIPTION OF DUMMY-BASED SEATING PROCEDURE FOR HIII50LX DUMMY:

Driver:

A seating procedure was developed for the HIII50LX in the driver seat based on the assumption that the longitudinal position of the seat is determined by the proper placement of the right foot on the accelerator pedal. The seat was moved to the full-rear position and was placed in the full down position with the seat cushion at its mid angle position. The H-point tool (OSCAR) was used to get a predefined H-point location. The OSCAR was used to find a repeatable and consistent starting position for the dummy. The feet of the dummy were placed in neutral position (X and Z rotation of zero degrees and Y rotation of -15 degrees), which is the most stable position of the feet for the Thor Lx legs.

The seat was then moved forward to place the right foot on the accelerator pedal such that:

1. The foot was in neutral position.
2. The heel was resting on the floor pan (with carpeting but without floor mats). The floor mats were removed to avoid inconsistency caused by various after-market mats that might be provided as dealer options.
3. The heel was at the same lateral location as the accelerator pedal, as defined by the heel-point (intersection of the pedal line of symmetry and the floor pan).
4. The accelerator pedal was not depressed.
5. The thigh-leg-foot was in the same vertical plane.

Procedures were developed for two configurations of vehicle interior:

1. Vehicle with brake and clutch pedals either removed or permanently depressed
2. Vehicle with brake and clutch pedals in un-depressed position

In most instances, the brake/clutch pedals are rearward (closer to the seat) than the accelerator pedal. Thus, if the brake/clutch pedals are left in their un-depressed state, the left foot was unable to be positioned at the same longitudinal and symmetric position as the right foot. The left foot was then placed on the un-depressed brake/clutch pedal and the left knee was at an elevated position compared to the right knee.

In order to place the left foot laterally symmetric to the right foot and at the same longitudinal position as the right foot, the pedals were depressed artificially and held in that position by mechanical means. This was considered to be an alternative way of placing the left foot.

All repeatability data is based on the above procedure.

Subsequent discussions on avoiding the placement of the left foot on the brake or clutch pedals resulted in a variation of the seating procedure. This procedure moves the left foot to the left to avoid lateral overlap with the pedals before the seat is moved forward. This procedure is listed in Appendix A and was selected for use in these offset crash tests. The procedure in Appendix A is assumed to provide the same repeatability as the procedure with the pedals depressed artificially and held in that position by mechanical means.

Passenger:

The intent for the final position on the passenger side was to have the feet in the neutral position and as far forward as possible, preferably on the toe-pan. The initial seat position and dummy placement were the same as the driver. The feet were placed together to avoid early contact with the wheel-well and center tunnel projections. The toes were pushed down towards the floor (in extension, away from the neutral position) to avoid contact with ducts in the lower dashboard, and the seat was moved forward until the feet contacted the vehicle interior or the seat reached the full-forward position. The feet were then returned to neutral position and separated symmetrically to get the knee separation of 10.8 inches (like in the current FMVSS No. 208 procedure) or until contact was made with the vehicle interior.

TEST PROCEDURE DEVELOPMENT

Five vehicles were selected for use in developing this test procedure. These vehicles range in size from small passenger car to LTV.

The vehicles used were:

1. 2002 Ford Focus
2. 2005 Cadillac STS
3. 2005 VW Jetta
4. 2005 Honda Ridgeline
5. 2005 Honda Odyssey

Two teams of technicians were used to study the repeatability and reproducibility of the seating procedure. Each team repeated the seating procedure three times. An initial determination of the OSCAR H-point and pelvic angles (with the seat full rear and full down) was made once and used in all seating tests. A coordinate measuring tool (FARO) was used throughout to measure the seat position and the dummy's head, pelvis, knee, and ankle location.

DISCUSSION OF SEATING PROCEDURE TESTS:

The dummy-based procedure consistently placed the driver seat to the rear of the mid-track location used in FMVSS No. 208. Figures 1 shows the positions for the Ford Focus using the current mid-track seating procedure and using the dummy-based seating procedure. The dummy-based procedure placed the seat 3.1 inches rear of the mid-track position for the Focus.

For the passenger side, the forward progress of the dummy in the dummy-based procedure was determined by the layout of the lower dash and ducts. The positions for the Cadillac (which had the greatest difference from the mid-track position) using the current mid-track procedure and using the dummy-based seating procedure are shown in Figure 2.

Figure 1 Ford Focus Driver – (a) Mid-track Position, (b) Dummy-based Position.

Figure 2 Cadillac STS Passenger – (a) Mid-track Position, (b) Dummy-based Position

REPEATABILITY, REPRODUCIBILITY, AND COMPARISON OF THE PROCEDURES

Each team (Team 1 or Team 2) repeated the dummy-based procedure 3 times for each vehicle for the driver and for the passenger sides. Also, each team repeated the current FMVSS No. 208 procedure twice, except for Jetta.

Figure 3 and Figure 4 show the location of the driver's ankle, knee, H-Point, and head CG in the longitudinal-vertical plane (such as when looking at the dummy through the open doorway) for each of the vehicles for the dummy based and mid-track procedure, respectively. The results show that the repeat measurements taken by each team are within +/- 1 inch for the dummy based and mid-track procedure, respectively. The results also show that the average measurement between each team was within +/- 1 inch for both procedures. This demonstrates that the dummy based seating procedure is as repeatable and reproducible as the mid-track procedure. The results for the passenger were similar to the driver.

TEST RESULTS

This section summarizes results from the ODB crash test series run for NHTSA that was conducted using the procedure defined in FMVSS No. 208 (S18) with a modification to the seating procedure. In all tests, the HIII50LX was positioned according to the seating procedure presented above. The HIII50LX was instrumented to calculate the Injury Assessment Values (IAVs) as defined in the FMVSS No. 208 Advanced Air Bag Final Rule. The following is a list of FMVSS No. 208 IAVs used in this test series:

1. Head injury criteria with a time interval of 15 ms (HIC15).
2. IAVs for the neck includeing Nij, neck tension (N), and neck compression (N).
3. Chest acceleration whose cumulative acceleration is not more than 3 ms (Clip3ms).
4. Chest compression (mm).
5. Femur load (N).

The Thor-Lx/HIII was instrumented with upper and lower tibia load cells, three ankle rotational potentiometers, and tri-axial foot accelerometers. The polarities of the data channels were recorded according to SAE J211. The IAVs calculated for the Thor-Lx/HIII include the following:

1. Upper and lower tibia compressive force (N).
2. Upper and lower tibia index (TI) is calculated using the following equation:

$$TI=F/12000+M/240 \qquad (1)$$

Where: F=axial Force in N
M=the resultant moment (Nm) of the x and y tibia moments

3. Knee shear (mm)
4. Ankle rotation
   a. Dorsiflextion (degrees) is the maximum positive y rotation.
   b. Inversion/eversion (degrees) is the maximum of either the positive or negative x rotation.

The injury assessment reference values (IARVs) used to determine the probability of injury are listed in Table 1 (Kuppa, et. al. 2001a and 2001b).

Table 1
IARVs

Injury Criteria	IARV for HIII 50M
HIC15	700
Nij	1.0
Neck tension	4170 N
Neck compression	4000 N
Clip3ms	60
Chest compression	63 mm
Femur load	10008 N
knee shear	15 mm
Upper tibia axial force	5600 N
Lower tibia axial force	5200 N
Upper tibia index	0.91
Lower tibia index	0.91
Dorsiflexion	35 deg
Inversion/eversion	35 deg

ODB CRASH TESTS RESULTS

The crash tests showed that 1 of the 6 vehicles tested had all the IAVs below the IARVs (Table 2 and 3). The only time the HIC15 exceeded its IARV was when the dummy rebounded from the air bag and the dummy's head hit the b-pillar. All vehicles that exceeded at least one of the IARVs also exceeded the inversion/eversion IARV for either the left and/or right foot. The only vehicle that exceeded the TI IARV was the Dodge Stratus. Next, the kinematics of the dummy are compared to the inversion/eversion values that the Thor-Lx/HIII recorded.

The tests demonstrated that the kinematics of the Thor-Lx/HIII feet were similar to the angular output of the Thor-Lx/HIII. Figure 5 shows the kinematics of the feet compared to the output from the Thor-Lx/HIII for the Mitsibushi Galant, which is representative of the other vehicles. The left foot moved forward and started to rotate at 40 ms, and by 75 ms, the left foot had rotated over 25 degrees. The maximum rotation of 36 degrees occurred at 129 ms. The right foot did not start to rotate until 75 ms. Once the right foot started to rotate, it rotated 39 degrees in 30 ms. Since the rotational output from the Thor-Lx/HIII matches the kinematics of the feet, the next step was to try to

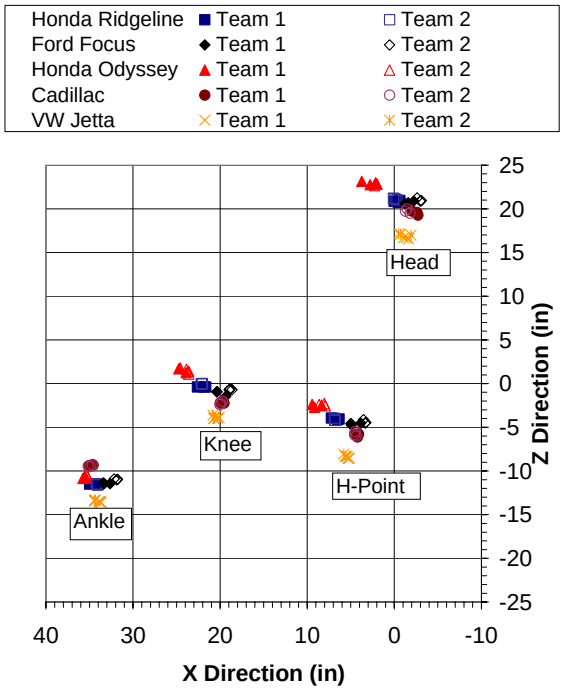

Figure 3. Dummy-based Procedure location of the driver's ankle, knee, H-Point, and head CG, with Pedals – Driver Side

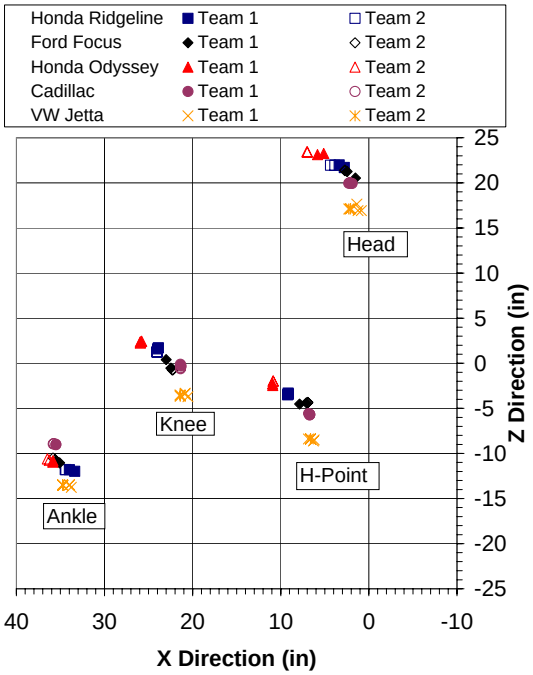

Figure 4. Mid-track procedure location of the driver's ankle, knee, H-Point, and head CG, with Pedals –Driver Side

Table 2
IAVs for FMVSS No. 208

TSTNO	MAKE	MODEL	YEAR	HIC15	HIC15 B-PILLAR	Neck Tension (N)	Neck Compression (N)	Nij	3ms Clip (Gs)	Chest Compression (mm)	Femur Left (N)	Femur Right (N)
				700	700	4170	4000	1.00	60	63	10008	10008
5654	DODGE	STRATUS	2006	114	213	717	725	0.25	31	22	2883	1028
5666	SUZUKI	VERONA	2006	187	2434	2174	222	0.34	33	24	3978	3589
5717	MITSUBISHI	GALANT	2006	157	NA	1008	715	0.29	31	23	108	133
5879	SUZUKI	FORENZA	2006	176	459	1063	790	0.37	34	26	714	482
5880	MAZDA	MAZDA6	2007	215	373	975	1792	0.56	27	18	112	77
5878	FORD	FIVE HUNDRED	2007	86	NA	1090	55	0.24	27	36	193	1

Table 3
IAVs for below the knee injuries and maximum x-dir toepan intrusion

TSTNO	MAKE	MODEL	YEAR	Left Knee Shear (mm)	Right Knee Shear (mm)	Left Tibia Force (N)	Right Tibia Force (N)	Tibia Index LL	Tibia Index LU	Tibia Index RL	Tibia Index RU	Left Ankle Rotation X (degrees)	Left Ankle Rotation Y (degrees)	Right Ankle Rotation X (degrees)	Right Ankle Rotation Y (degrees)	Max Toepan Intrusion (x-dir) (mm)
				15	15	5600	5600	0.91	0.91	0.91	0.91	35	35	35	35	
5654	DODGE	STRATUS	2006	1	1	3831	3636	0.44	0.44	1.05	0.81	14	30	38	5	111
5666	SUZUKI	VERONA	2006	18	1	3468	3907	0.60	0.64	0.65	0.73	41	33	31	14	133
5717	MITSUBISHI	GALANT	2006	25	1	1907	2405	0.27	0.37	0.67	0.53	36	11	39	0	68
5879	SUZUKI	FORENZA	2006	1	1	2078	1623	0.47	0.59	0.44	0.34	39	19	36	10	68
5880	MAZDA	MAZDA6	2007	0	1	1891	1475	0.27	0.51	0.31	0.51	36	5	22	0	24
5878	FORD	FIVE HUNDRED	2007	6	0	877	1172	0.28	0.31	0.24	0.25	30	0	32	0	27

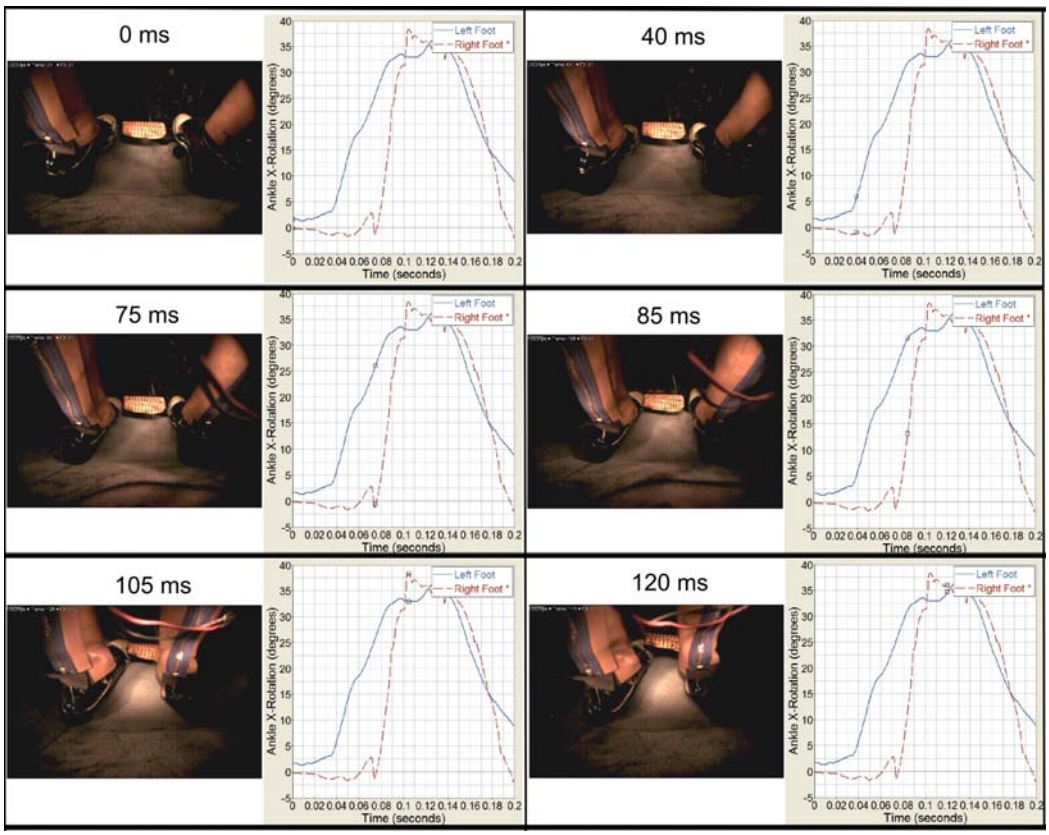

* The right foot rotation was flipped for graphical purposes.

Figure 5. Kinematics and Thor-Lx/HIII output of the Mitsibushi Galant

determine what caused these vehicles to exceed the IARVs for ankle rotation.

The injury mechanisms that could have caused the dummy to exceed the IARVs for ankle rotation are: 1) Toepan x-intrusion, 2) Toepan resultant acceleration, and 3) Toepan geometry. It was impossible to determine the exact mechanism that caused the dummy to exceed the IARVs because all the vehicles tested had a combination of all three injury mechanisms. The following will describe each of these injury mechanisms.

The inversion/eversion IARV was exceeded for high as well as low levels of toepan intrusions. The toepan intrusion points were measured pre and post test and Figure 6 graphically shows the location of these intrusion points. When the difference in the x-displacement of the toepan for the intrusion points around the right foot for the Dodge Stratus and Mitsibushi Galant are plotted, it is shown that inversion/eversion IARV was exceeded for a vehicle with maximum x intrusion of 111 mm and also with maximum x intrusion of 68 mm (Figure 7). The results also show that a vehicle could have a higher intrusion and not exceed the inversion/eversion IARV, whereas a vehicle with low intrusion can exceed the inversion/eversion. This was shown when the intrusion points around the left foot were plotted for the Stratus and the Galant (Figure 8). The Stratus had 94 mm of intrusion and only 14 degrees of inversion/eversion, whereas, the Galant had 49 mm of intrusion and 36 degrees of inversion/eversion.

The second mechanism, toepan resultant acceleration, can cause the dummy to exceed the inversion/eversion IARV even when the toepan resultant acceleration, velocity, and dynamic displacement are similar. For example, a tri-axial accelerometer was placed by the dummy's left foot in the Mazda6 and Ford 500 tests. Figures 9 and 10 show that the two vehicles had similar resultant toepan x-acceleration, velocity, and dynamic displacement, but the Mazda6 exceeded the IARV for inversion/eversion while the Ford 500 was below the IARV for inversion/eversion.

The last mechanism, toepan geometry, seems not correlate to dummy foot rotation since different inversion/eversion IAVs can occur even when the vehicles have similar toepan geometry. The Dodge Stratus and the Ford 500 have similar toepans (Figure 11), but the difference in inversion/eversion was 16 degrees. Also, the right foot was always placed on the accelerator pedal, which is a similar surface for all vehicles tested, but the inversion/eversion ranged from 22 degrees to 39 degrees.

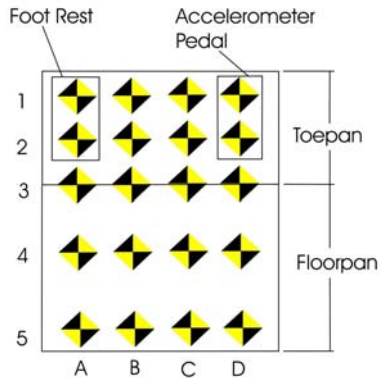

Figure 6. Intrusion points measured on the toepan and floorpan.

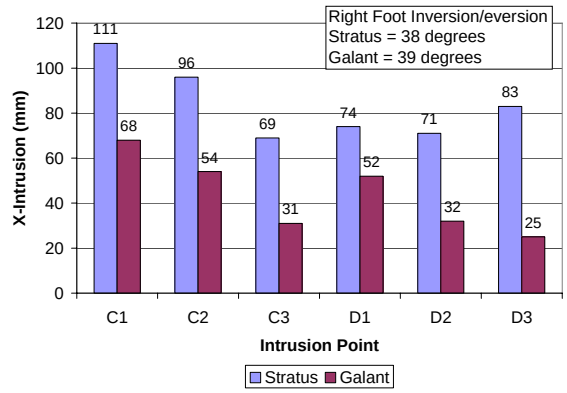

Figure 7. Comparison of x intrusion around the right foot of the HIII50LX for the Dodge Stratus and Mitsibushi Galant.

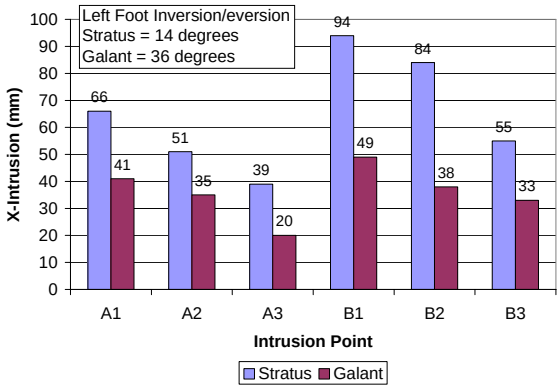

Figure 8. Comparison of x intrusion around the left foot of the HIII50LX for the Dodge Stratus and Mitsibushi Galant.

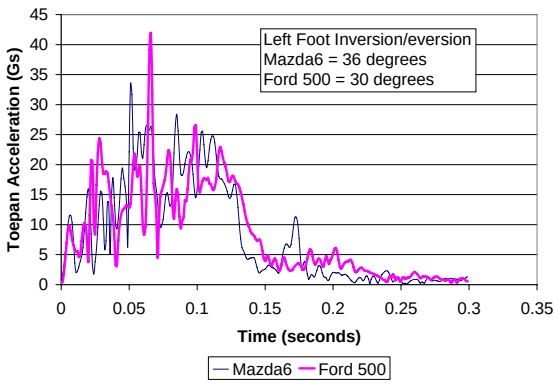

Figure 9. Footrest resultant acceleration for the Mazda6 and Ford 500.

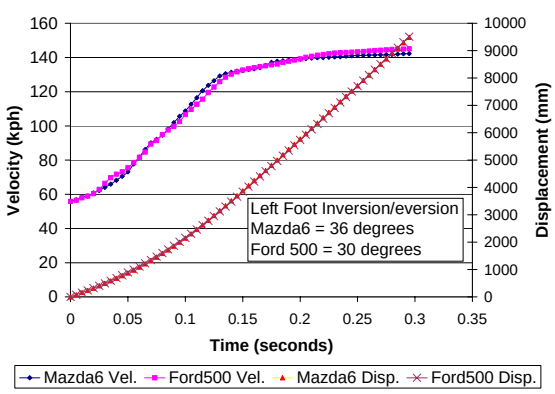

Figure 10. Resultant footrest velocity and displacement for the Mazda6 and Ford 500

Figure 11. Driver toepan pictures of (a) Dodge Stratus and (b) Ford 500

STIFFNESS CHANGES

Some concern exists that requiring all vehicles to meet the ODB test procedure might cause compatibility problems between vehicles in the fleet. This section discusses this concern.

For offset performance, the IIHS ODB test was used, which rates a vehicle using a 64 kph ODB crash test. IIHS provides a rating for a vehicle in the following categories: 1) Overall, 2) Structure and safety cage, 3) Injury measures, and 4) Restraints and dummy kinematics. Each category is given one of the following ratings: good (G), acceptable (A), marginal (M), and poor (P). IIHS also provides the model year range for which their ratings are valid. The structure and safety cage category was the most likely rating to change vehicle structures; therefore, it was the rating used for this analysis.

One metric being researched for compatibility performance is the amount of energy absorbed in the first 25 mm to 400 mm of crush in a 35 mph rigid wall test, which is symbolized as E400 (Smith, 2006). The equation for E400 is,

Initial crush energy = E400 = $F\left(X_f - X_i\right)$ (2)

Where F is the average total force exerted on the wall over the 25 to 400 mm crush interval, Xi is the initial crush (25 mm), and Xf is the final crush (400 mm). E400 was calculated using load cell wall data collected in conjunction with NHTSA's NCAP 56 kph full frontal rigid wall crash tests.

To compare the effects of offset design and compatibility, NHTSA's crash test database was searched for offset-redesigned vehicles tested by NCAP and were also rated by IIHS. In this analysis there was no effort to ensure that the NCAP vehicle tested matched exactly the vehicle tested by IIHS (i.e.

engine size, body style, and options), but only that it fell into the IIHS applicable range of model years. If there was more than one vehicle tested by NCAP in the valid model year range, then the average weight and average E400 was used. Finally, for comparison purposes, each vehicle was grouped into a different class and weight category. The weight classes for Passenger Cars (PCs) were as defined in Swanson, et al, (2003) with Sport Utility Vehicles (SUVs), Pickups (PUs), and Vans divided according to Table 4.

Figures 12 through 16 show the E400 and IIHS structure and safety cage rating for the offset redesigned vehicles. These bar charts note the weight class of the vehicle tested through a suitable suffix to the model name, including all subsequent redesigns (R1, R2, etc.). To demonstrate the relative changes in energy absorption between vehicles, these charts include an arbitrarily defined upper and lower zone for energy compatibility matching of the vehicle fleet as assumed by Saunders, et. al, (2007). At this time it is assumed that the most desirable condition is when all vehicles move into this zone and thus are able to properly share crash energy. But more research is needed to demonstrate the energy compatibility matching does not have a negative effect on self-protection and if it is the optimal metric to use for compatibility.

Table 4. Definition of vehicle classes.

	Class	Test Weight (Kg)
PCs	Mini	≤1065
	Light (Lt)	1065<w≤1292
	Compact (Com)	1292<w≤1519
	Medium (Med)	1519<w≤1746
	Heavy	>1746
Minivans	Vans	All
Pickups	PU Small	<2268
	PU Heavy	≥2268
Utility Vehicles	UV Small	≤1814
	UV Mid	1814<w≤2268
	UV Heavy	>2268

The general trend for PCs was to increase E400 and get stiffer when the structure and safety cage rating was increased for offset performance but PCs generally converged into the energy matching zone (Figures 12 and 13).

About half of the SUVs and about half of the vans tested increased E400 for the redesigned vehicles with an increase in structure and safety cage rating (Figures 14 and 15, respectively). SUVs were generally higher than the energy matching zone, and Vans were scattered all around. All PUs tested showed an increase in E400 when the structure and safety cage rating was increased (Figure 16). Small PUs were slightly higher than the matching zone, but heavy PUs are higher and moving away from the energy matching zone. It should be noted that before redesign all the heavy PUs were classified as small PUs.

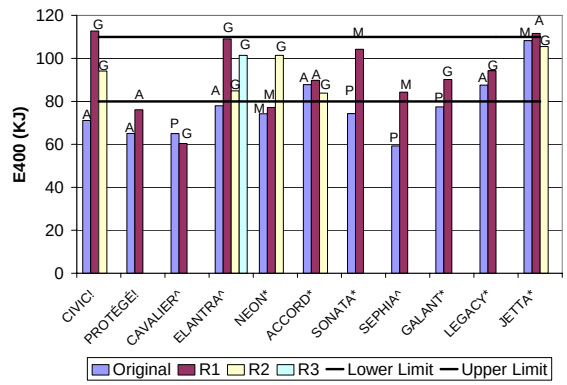

Figure 12. E400 and IIHS structure rating for smaller passenger cars. Name suffixes: !=Lt to Com, ^=Com, *=Com to Med.

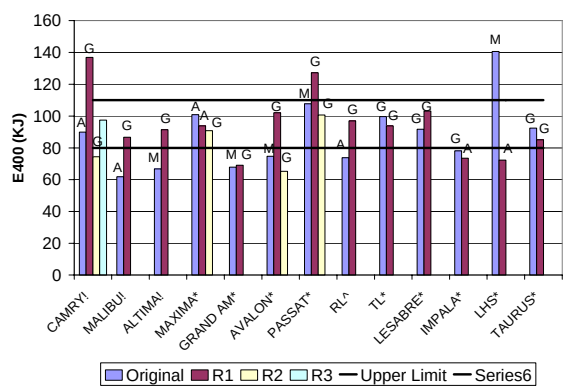

Figure 13. E400 and IIHS structure rating for larger passenger cars. Name suffixes: !=Med, *=Med to Heavy.

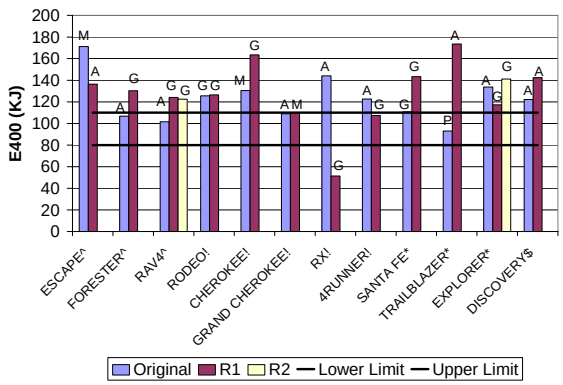

Figure 14. E400 and IIHS structure rating for SUVs. Name suffixes: ^=UV Small, != UV Mid, * UV Mid to UV Heavy, $ UV Heavy

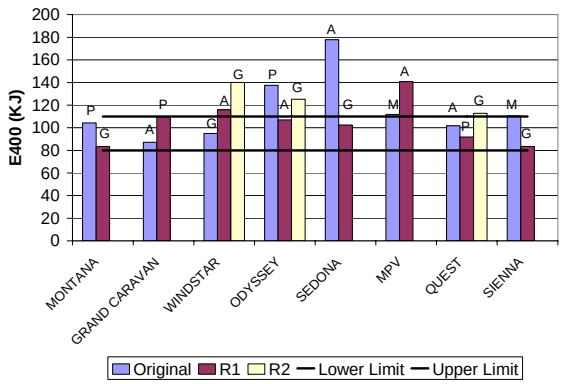

Figure 15. E400 and IIHS structure rating for Vans.

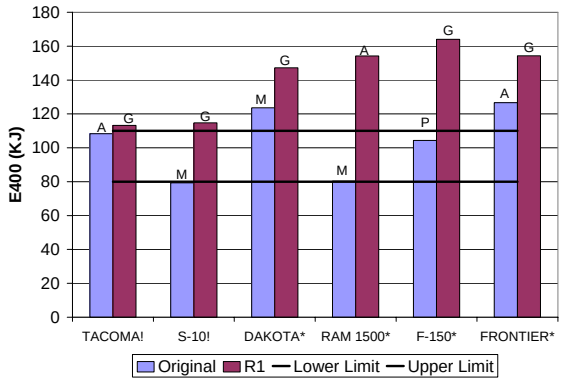

Figure 16. E400 and IIHS structure rating for PUs. Name suffixes: !=PU Small, *=PU Small to PU Heavy

FUTURE RESEARCH

The areas of research that still need to be investigated include:

1. Develop a dummy-based seating procedure for the HIII 5th percentile female with Thor-FLx retrofit legs.
2. Evaluate the repeatability of the ODB crash test procedure.
3. Continue performing crash tests to be able to calculate the benefits of the ODB test procedure.
4. Perform crash tests and simulations to explore the relationship between offset performance and compatibility performance.

CONCLUSIONS

The following conclusions can be drawn about the dummy-based seating procedure:

1. Seating procedures are available for the 50th percentile Hybrid III dummy with Thor lower legs with the seat in dummy-based or in mid-track positions.
2. The repeatability of dummy-based or mid-track procedures is similar. The foot angles at the ankle are not near neutral for the mid-track procedures. The mid-track procedure generally places the foot in dorsiflexion.
3. The final position of the ankle is similar in the longitudinal-vertical plane, for the dummy-based position with or without brake/clutch pedals.
4. The position of the head CG is controlled by the procedures for determining seat back angles.

The crash tests showed that inversion/eversion IARVs were exceeded in 5 of the 6 tests. Also, the kinematics of the Thor-Lx/HIII feet were similar to the rotational output recorded. It was impossible to determine the exact mechanism that caused the feet to exceed eversion/inversion because there was always more than one mechanism observed in the crash test.

All Pickups tested that achieved a higher rating for their structure and safety cage rating for the new design or replacement of the earlier vehicle increased its E400. Also, Pickups over 2268 kgs moved away from and higher than the energy matching zone. All other classes of vehicles had some vehicles that increased, stayed the same, or decreased for E400.

REFERENCES

Durgess, et al., “Lower Extremity Injuries in Drivers of Airbag-Equipped Automobiles- Clinical and Crash Reconstruction Correlations, “ Journal of Trauma, 1995, Vol. 38, pp. 509-516.

Kuppa, S., Wang, J., Haffner, M., Eppinger, R., "Lower Extremity Injuries and Associated Injury Criteria," 17th International Technical Conference on the Enhanced Safety of Vehicles, Amsterdam, The Netherlands, June 4-7, 2001a.

Kuppa, S., Haffner, M., Eppinger, R., Saunders, J., "Lower Extremity Response and Trauma Assessment using the Thor-Lx/HIIIr and the Denton leg in Frontal Offset Vehicle Crashes," 17th International Technical Conference on the Enhanced Safety of Vehicles, Amsterdam, The Netherlands, June 4-7, 2001b.

J. Nolan, Lund, A., "Frontal Offset Deformable Barrier Crash Testing and its Effect on Vehicle Stiffness," 17th International Technical Conference on the Enhanced Safety of Vehicles, Amsterdam, The Netherlands, June 4-7, 2001

Saunders, J.W, Prasad, A., "NHTSA's Frontal Offset Research Program," Proceedings of the 19th Experimental Safety Vehicles, Paper 05-0206, Washington, DC 2005.

Saunders, J. et al., "NHTSA's Frontal Offset Research Program, " Paper 2004-01-1169, Society of Automotive Engineers, March 2004.

Saunders, J, Smith, D, Barsan, A, "Restraint Robustness in Frontal Crashes", Paper 2007-01-1181, Society of Automotive Engineers, April 2007.

Smith, D.L., NHTSA Compatibility Research Update, SAE Government Industry Meeting, May 2006.

Swanson, J, Rockwell, T, Beuse, N, summers, L, Summers, S, and Park, B, "Evaluation of Stiffness Measures from the U.S. New Car Assessment Program," Proceedings of the 18th Experimental Safety Vehicles, Paper 527, Nagoya, Japan 2003.

Thomas, P. et al., "Lower Limb Injuries – The Effect of Intrusion, Crash Sverity and the Pedals on Injury Risk and Injury Type in Frontal Collisions, " Proceedings of the Thirty-Ninth Stapp Car Crash Conference, SAE Paper No. 952728, 1995.

Verma, M., Lange R., Levelle J., "Relationships of Crash Test Procedures to Vehicle Compatibility," Paper 2003-01-0900, Society of Automotive Engineers, March 2003

APPENDIX A

Dummy Based Seating Procedure

Driver side positioning procedure:

Place the seat at full rear, full down, and seat cushion at mid-angle, with seat back at nominal angle specified by the manufacturer.

__1. Place adjustable pedals in the full forward position (towards the front of the vehicle.)
__N/A – the pedals are not adjustable.

__2 Locate and mark the right heel point (RHP) on the carpet.
Flat accelerator pedals: Extend a line through the axis of symmetry (that is closest to the vertical plane) of the accelerator pedal. The RHP is the intersection of that line with the floor pan.
Curved accelerator pedals: Construct a line in the side view tangent to the accelerator pedal such that the distance from the contact point on the pedal to the floor pan, along the tangent line, is 200 mm. The RHP is at the intersection of this tangent line and the floor pan

__3 Locate a longitudinal line L1 and a transverse line T1 on the floor pan through the RHP. Locate a Left Heel Point (LHP) point on the line T1 that is to the left of the seat centerline at the same distance from the seat centerline as the RHP. Locate a longitudinal line L2 through the LHP.

__4. Set the steering wheel hub at the geometric center of the full range of driving positions including any telescoping positions as determined in data sheet 14.3.

__5. Verify that the seat is in the rearmost seat track position and full down height adjustment with the seat cushion at the mid-angle with the seat back at the manufacturer's nominal seat back angle.

__6 With the seat in the rearmost, full down, mid-angle position, determine the H-point using SAE J826 and the FMVSS No. 208 leg and thigh dimensions.

__7. With the seat in the rearmost, full down, mid-angle position, place the dummy in the seat such that the midsagittal plane is coincident with the longitudinal seat cushion markings and the upper torso resting against the seat back.

__8. Rest the thighs on the seat cushion.

__9. Set the distance between the outboard knee clevis flange surfaces at 10.6 inches.
__measured distance (10.6 inches)

__10. Set the heels of the feet on the floor pan.

__11. Position the H-point of the dummy within 0.5 inch of the vertical dimension and 0.5 inch of the horizontal dimension of a point 0.25 inch below the H-point determined in step 6.
Then measure the pelvic angle with respect to the horizontal using the pelvic angle gage. Adjust the dummy position until these three measurements are within the specifications.
____horizontal inches from the point 0.25 below the determined H-point (0.5 inch max.)
____vertical inches from the point 0.25 below the determined H-point (0.5 inch max.)
____pelvic angle (20° to 25°)
The H-point and pelvic angle are not adjusted after this step.

__12. Set the left and right feet in the neutral position (longitudinal centerline of foot in the same plane as the lower leg/thigh, foot at -15 degrees +/- 2 degrees to lower leg), as determined by the output of the potentiometers at the ankle.

__13. Without moving the seat, and while keeping the right thigh and leg in the same vertical plane, set the right foot heel on Line L1. If the vehicle interior prevents the heel from reaching L1, place the heel as close to L1 as possible, while maintaining a clearance of 0.25" from the vehicle interior.

__14. Without moving the seat, and while keeping the left thigh and leg in the same vertical plane, move the left foot laterally to the left until the right edge of the foot is clear of the brake or clutch pedal by 0.25” laterally. Stop the leftward movement of the left foot if the left heel reaches on Line L2 or if the left edge of the shoe contacts the vehicle interior.

__15. Place a 25 lbs (110 N +/- 5N) weight (e.g. 110 N lead shot bag), no larger than 4” x 4”, on each knee-thigh area. The weight should be centered on the assembly-hole on the top of the knee.

__16. Raise the heels off the floor pan so that the seat can be moved forward.

__17. Using only the control that primarily moves the seat in the fore-aft direction, move the seat forward and rest the rearmost point of the right foot heel on the floor pan such that:

- the heel is on the line L1 and
- the foot is in the same plane as the lower leg/thigh, foot at -15 degrees +/- 2 degrees (about the Y- axis) to lower leg and
- foot is contacting the accelerator pedal and
- the thighs are resting on the seat cushion and
- the thigh, leg and foot are in the same vertical plane.

Note: If the heel is unable to reach line L1 because the foot contacts the vehicle interior, place the foot as close to the line L1 as possible while maintaining a gap of no more than 5 mm between the shoe and the vehicle interior.

Note: If the left foot contacts the brake or clutch pedals or the vehicle interior, then stop the forward movement of the left foot, raising the left knee off the seat cushion if needed. The pedals should not be depressed. Keep moving the seat forward until the right foot contacts the accelerator pedal.

Note: Stop the forward movement of the seat if the seat reaches its full-forward seat track position, or if the dummy contacts the steering wheel or vehicle interior like the knee bolsters.

__18. If the right foot does not reach the accelerator pedal, move the adjustable pedal until it contacts the foot. Locate a new heel point. Repeat steps 7 – 17 to re-position the seat. If the pedals are not adjustable, place the heel at the point closest to the pedal, in the same longitudinal vertical plane as the line L1.

__N/A – the accelerator pedal is not adjustable

__N/A – the accelerator pedal did not need to be moved.

__19. Remove the leg weights.

__20. Verify that the left thigh and leg are in a vertical longitudinal plane, the foot in the neutral position (longitudinal centerline of foot in the same plane as the lower leg/thigh, foot at -15 degrees +/- 2 degrees (Y-axis) to lower leg), the heel on the floor pan. Place the heel on the line L2, unless the left edge of the shoe contacts the vehicle, preventing the heel from reaching Line L2.

__21. Verify that the right foot is in the neutral position, at the lateral location determined in step 17, and is contacting the accelerator pedal. If the foot is not contacting the accelerator pedal, move the seat forward to rest the right foot on the accelerator pedal, keeping the foot in the neutral position

__22. While holding the thighs in place, push with a 50 lb force on a 3 inch diameter area of the chest that is centered 5" (127mm) vertically below the chin on the midsaggital plane of the dummy.

__23 Fasten the seat belt around the dummy.

__24 Remove all slack from the lap belt portion.

__25 Pull the upper torso webbing out of the retractor and allow it to retract; repeat this four times.

__26 Apply a 2 to 4 pound tension load to the lap belt.

____pound load applied

__27 Is the belt system equipped with a tension-relieving device?

__Yes, continue

__No, go to 29

__28 Introduce the maximum amount of slack into the upper torso belt that is recommended by the vehicle manufacturer in the vehicle owner’s manual.

__29. Place the upper arms adjacent to the torso with the centerline as close to a vertical plane as possible.

__30. Adjust the head level within ± 0.5 degrees using the seat back adjustment. Check the head angle after pushing on the chest with a 50 lb force on a 3 inch diameter area of the chest that is centered 5" (127mm) vertically below the chin on the midsaggital plane of the dummy, while holding the thighs in place, and releasing.

__31 No seat back adjustment. Adjust the neck bracket to achieve head level within ± 0.5 degrees Record neck bracket setting. _____

__32. Maintaining the head alignment as determined above, place the right hand with the palm in contact with the steering wheel at the rim's horizontal centerline and with the thumb over the steering wheel.

__33. Maintaining the head alignment as determined above place the left hand with the palm in contact with the steering wheel at the rim's horizontal centerline and with the thumb over the steering wheel.

__34. If the hands don't reach the steering wheel at the horizontal centerline, maintaining the head alignment place them at symmetric location on the wheel, below the horizontal centerline.

__35. Tape the thumb of each hand to the steering wheel by using masking tape with a width of 0.25 inch. The length of the tape shall only be enough to go around the thumb and steering wheel one time.

__36 Verify that the feet are in the neutral position (+/- 2 deg), and at lateral locations determined in step 17 (right foot) and step 20 (left foot), and the head is level (+/- 0.5 deg). Adjust and repeat until the feet position and angles and head angles are within this range.

Passenger side seating procedure:

__1. Verify that the seat is in the rearmost seat track position and full down height adjustment with the seat cushion at the mid-angle, the seat back is at the manufacturer's nominal design position for the 50th male.

__2 With the seat in the rearmost, full down, mid-angle position, seat back at the manufacturer's nominal design position for the 50th male, determine the H-point using SAE J826 and the FMVSS No. 208 leg and thigh dimensions.

__3. Place the dummy in the seat such that the midsagittal plane is coincident with the longitudinal seat cushion markings and the upper torso resting against the seat back.

__4. Rest the thighs on the seat cushion.

__5. Set the distance between the outboard knee clevis flange surfaces at 9 ¼ inches, with the leg-knee-thigh in the same vertical plane.
__measured distance

__6. Set the heels of the feet on the floor pan.

__7. Position the H-point of the dummy within 0.5 inch of the vertical dimension and 0.5 inch of the horizontal dimension of a point 0.25 inch below the H-point determined in step 2.
Then measure the pelvic angle with respect to the horizontal using the pelvic angle gage. Adjust the dummy position until these three measurements are within the specifications.
____horizontal inches from the point 0.25 below the determined H-point (0.5 inch max.)
____vertical inches from the point 0.25 below the determined H-point (0.5 inch max.)
____pelvic angle (20° to 25°)
The H-point and pelvic angle are not adjusted again after this step.

__8. Place a 25 lbs (110 N +/- 5 N) weight (e.g. 110 N lead shot bag), no larger than 4" x 4", on each knee-thigh area. The weight should be centered on the assembly-hole on the top of the knee.

__9. Set the left and right feet such that the following conditions are met after the feet are placed:
__ The foot is in neutral position.
__ The leg and thigh are in the same plane.
__ The thighs are resting on the seat cushion.
__ The heel is in contact with the floor pan.

__10 Lift the feet off the floor and set the toe towards the floor pan (Y angle = -25 +/- 2 deg). Using controls that move the seat fore-aft, move the seat forward until either foot contacts vehicle interior. Position the feet at that seat location with the heels on the floor and the feet in neutral position. If the vehicle interior prevents the feet from reaching the neutral position, place the feet as close as possible to the neutral position while maintaining a distance of 5 mm from the vehicle interior.

__11 Move the seat forward while maintaining the foot orientations (+/-2 deg) until either foot contacts the vehicle interior.

__12 Keeping the thigh-leg in the same vertical plane, move the feet apart symmetrically about the dummy midsaggital plane until the either foot contacts the vehicle interior or the knee spacing of 10.6 inches is attained, whichever comes first. Place the feet in neutral position unless contact with the vehicle interior prevents the feet from reaching the neutral position.

Check all that applies:
__ The right foot contacted a flat part of the toe board.
__ The right foot contacted the right side of vehicle interior.
__ The right foot contacted is at neutral position
__ The left foot contacted a flat part of the toe board.
__ The left foot contacted the left side if the vehicle interior.
__ The left foot contacted is at neutral position

__13. Remove the leg weights. Verify that the thighs and legs are in the same vertical longitudinal plane.

__14. While holding the thighs in place, push with a 50 lb force on a 3 inch diameter area of the chest that is centered 5" (127mm) vertically below the chin on the midsaggital plane of the dummy.

__15. Seat belt

__16 Fasten the seat belt around the dummy.

__17 Remove all slack from the lap belt portion.

__18 Pull the upper torso webbing out of the retractor and allow it to retract; repeat this four times.

__19 Apply a 2 to 4 pound tension load to the lap belt.
____pound load applied

__20 Is the belt system equipped with a tension-relieving device?
__Yes, continue
__No, go to 22

__21 Introduce the maximum amount of slack into the upper torso bet that is recommended by the vehicle manufacturer in the vehicle owner's manual.

__22. Place the upper arms adjacent to the torso with the centerline as close to a vertical plane as possible.

__23. Place the right upper arm in contact with the seat back and side of the torso. (S10.2.2)

__24. Place the left hand palm in contact with the outside of the left thigh and the little finger in contact with the seat cushion.

__25. Place the right hand palm in contact with the outside of the right thigh and the little finger in contact with the seat cushion.

__26. Adjust the head level within ± 0.5 degrees using the seat back adjustment. Check the head angle after pushing on the chest with a 50 lb force on a 3 inch diameter area of the chest that is centered 5" (127mm) vertically below the chin on the midsaggital plane of the dummy, while holding the thighs in place, and releasing.

__27 No seat back adjustment. Adjust the neck bracket to achieve head level within ± 0.5 degrees
Record neck bracket setting. _____

AXIAL COLLAPSE OF SQUARE TUBES WITH SHORT LENGTH

Shigeru Ogawa, Noriaki Ito, Michinari Watanabe, Arihiro Furumoto, Masatoki Kito
Mazda Motor Corporation
Japan
Daiheng Chen
Tokyo University of Science
Japan
Shigeyuki Haruyama
Fukuoka Industrial Technology Center
Japan
Paper Number 07-0259

ABSTRACT

In order to reduce high impact load occurring in axial collapse of a crush can, which is installed in the front part of car, the elastoplastic nonlinear behavior of short thin-walled frusta with square cross-section subjected to statically axial compression is studied by using finite element method. The square tubes 1.8mm in thickness, with upper cross-section of 85mm x 90mm and lower cross-section of 130mm x 135 mm, have different lengths ranging from 135mm to 225mm. A typical tensile stress-strain curve for aluminum is modeled as 2 straight-line hardening relationship.

The FEM code MSC.Marc is used to simulate the axial compression of thin-walled frusta of square cross-section. The load-displacement curves of frusta are obtained from the numerical analyses. It is found from the curves that in the axial collapse process of the frusta there are two peaks of the load, corresponding to the initial buckling and formation of the second wrinkle. Unlike the axial collapse of long tubes, however, the load due to the second wrinkle is higher in magnitude than the initial buckling load. The reason for high second peak load is that the frusta are too short to form the 2nd wrinkle.

The second peak load is very sensitive to the boundary condition on the lower end. Usually, high load occurs in a strong restraint.

Also, it is found the effects of holes in side plate of frusta on the second peak load are very complex. If the holes were located exactly right on the folding lobes, the second peak load could be reduced. The other methods to reduce the second peak load were also investigated. It seems that the most effective method for lowering load is shortening the wavelength of wrinkles.

INTRODUCTION

In the development of vehicle crashworthiness, crush can, which is located in bumper, must strike a balance between high energy absorption to secure reparability in low-speed crash and frame resistance in high-speed crash. In particular, in order to satisfy reparability while maintaining good styling, crush can should be as short as possible while being able to absorb energy efficiently. In this paper, influence of length and restraint condition on crush characteristics was studied using a base geometry simulating crush can. Besides, geometry variations were also studied to absorb energy efficiently.

Method and Model of Analysis

In this analysis, generic FEM analysis software MSC.Marc was used to analyze the axial compression of an analytical model (Figure 1) representing the aforementioned simplified model. A square tube was modeled with 3D quadrilateral shells and its bottom was completely fixed to a rigid wall. The square tube was compressed by pressing the rigid body against its top with displacement control, taking into consideration the friction coefficient between the rigid body and the top of square tube. The dimensions of base model are shown in Figure 1. The model is 1.8mm in thickness and made of 440Mpa steel plate.

The characteristics of the simplified model were studied by changing the length of square tube, restraint conditions, etc. from the base model. Though the crush behavior of square tube also relates to the impact speed, quasi-static crush was studied since the characteristics at low speed are similar to quasi-static crush and the characteristics at low speed are also related to quasi-static crush.

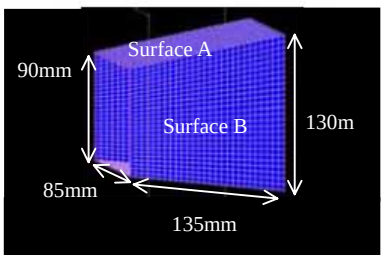

Figure 1. Analytical model

A homogeneous isotropic elasto-plastic body conforming to Von Mises yield criterion was used for the analysis so that stress σ and strain ε can be approximated by 2 straight-line hardening relationship. σ_y, E, and E_h represent yield stress, longitudinal elastic modulus, and work hardening respectively. In this study, material Poisson's ratio ν = 0.3, longitudinal elastic modulus E = 70.6 (GPa), and yield stress σ_y = E/1000 and work hardening characteristics E_h is used for the influence of material characteristics. Though actual material may not be approximated by 2 straight-line hardening relationship, the influence of magnitude of work hardening on the crush characteristics can be represented by the effect of work hardening characteristics E_h obtained here.

Analysis Results of Base Model

Figure 2 and 3 show the relationship between compressive load and axial displacement of base model in axial compression and its deflection. In Figure 2 and 3, after high peak load was generated, deformation progressed with fluctuation of load. Once the first wrinkle collapsed, the second wrinkle was generated. At that time, a load generated by the second wrinkle was higher than the first peak load.
At the early phase of deflection, the load fluctuated due to the influence of contact condition between rigid body and component.

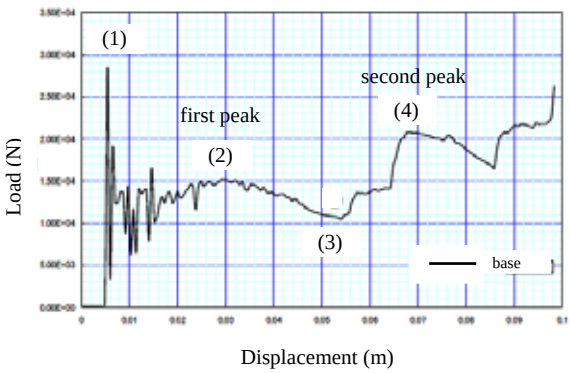

Figure 2. Load-deflection curve of base model

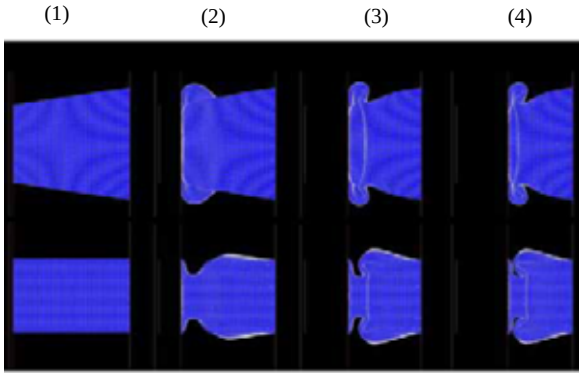

Figure 3. Deflection of base model

Study on the Length of Model

The length of model was changed to 180mm and 225mm from base model with its angle fixed ($\theta=\tan^{-1}(20/135)$).

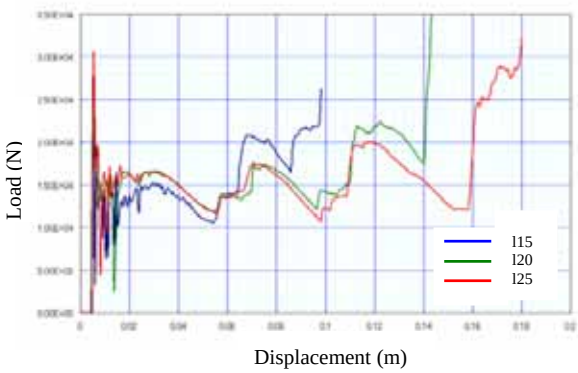

Figure 4. Load-deflection curve of model length changed

Figure 4 shows the relationship between compressive load and axial displacement in axial compression of a square tube extended. Table 1 shows the length of first wrinkle.

As shown in this table, with longer component such as model l20 (L=180mm) and model l25 (225mm), the wrinkle and amplitude of load-deflection curve become longer.

Table 1. Length of first wrinkle

Model	Wrinkle Length(mm)
l15	65
l20	70
l25	70

Based on the results, remaining length of component is predicted as shown in table 2. Since model l20 and model l25 have a length enough to generate the second wrinkle, the similar load-amplitude curve is obtained for the first and

second wrinkle. In case of base model, with remaining length of 5mm, the second wrinkle was not made like the first one since its end was restrained. As a conclusion, its length is not enough to generate the second wrinkle. Therefore, in case of base model, the second peak load rose significantly since collapse margin is insufficient to generate a wrinkle and its bottom restraint hinders deflection that leads to wrinkle. This is also obvious from the difference in the third load amplitude between model l20 and model l25.

Table 2. Length of the first wrinkle

Model	Wrinkle Length(mm)	Remaining Length(mm)
l15	65	5
l20	70	40
l25	70	85

The axial compression of square tube can be categorized into three types depending on its length in axial direction.

(1) A square tube long enough to generate more than three wrinkles
In this case, with less influence of bottom restrain, wrinkles are generated one after another with its length controlled automatically; thus, the load does not rise due to the last wrinkle generation.

(2) A short square tube that cannot generate a wrinkle
In this case, the deflection is similar to that of a plate as circumferential wrinkle is be made.

(3) A square tube with one or two wrinkles
Without a length enough to generate the second wrinkle, load generated by wrinkle becomes high with great influence of restraint.

Since the base model falls within category (3), it is subject to the influence of restraint; thus, it is very important to adjust the length of wrinkle.

Study on Influence of Restrain Condition

The results of study on the influence of restraint condition are described in this section. Figure 5 shows respective restraint conditions that were studied.

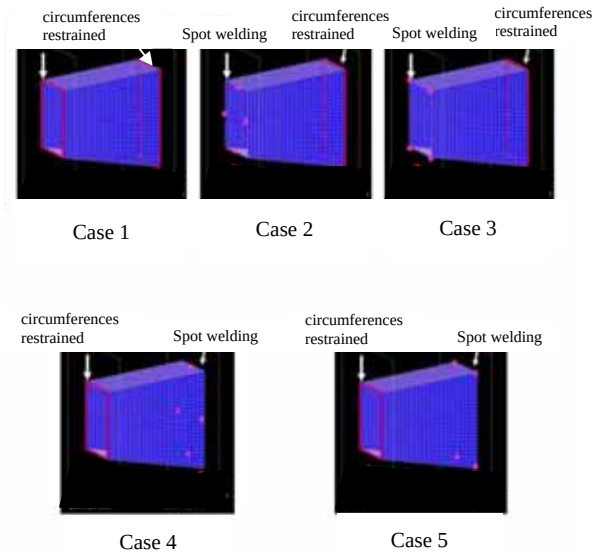

Figure 5. Restraint condition

Table 3 shows the measurement results of length of wrinkle generated in cases 1 through 5. Figure 6 shows the measurement positions of individual wrinkles. Figure 7 shows load-deflection curve of cases 1 through 3. Figure 8 shows load-deflection curve of case 1, case 4, and case 5.

Table 3. Length of first wrinkle

Model	Wrinkle Length(mm)
1 (Top & bottom circumferences restrained)	65
2 (Top center restrained)	80
3 (Top corner restrained)	80
4 (Bottom center restrained)	67.5
5 (Bottom corner restrained)	65

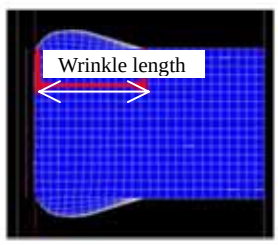

Figure 6. Measurement position of wrinkle length

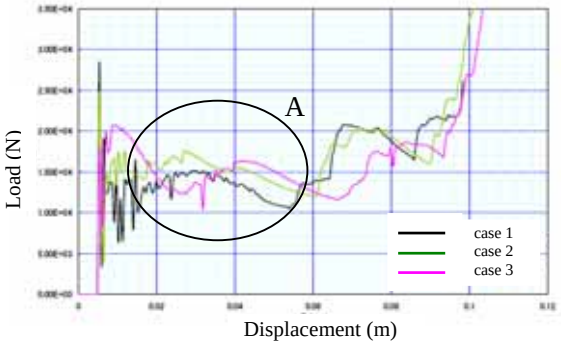

Figure 7. Load-deflection curve of model with restraint condition of contact surface varied

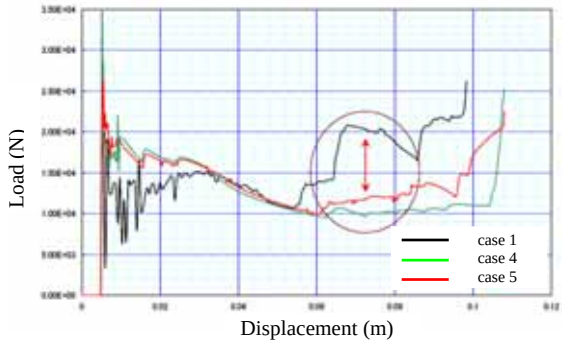

Figure 8. Load-deflection curve of model with different restraint conditions of restrain surface varied

The analysis results show:

(1) The influence of restraint condition is complicated since the length is short.

(2) The behavior of first wrinkle generation depends on the restrain around starting point.

(3) As shown in portion A in Figure 7, the weaker the restrain is, the longer the first wrinkle becomes. Consequently, load of the second wrinkle varies. (Case 3 does not have the second peak load since it does not have length enough to generate the second wrinkle.
As shown in portion B in Figure 8, the restraint at the end has a great influence on last load increase at the end of compression. Generally, the load decreases as strain becomes weaker.

A Model with Holes Locally

In order to reduce the peak load, holes (10mm X 10mm square holes in the center of surfaces A and B) were made around wrinkle peak in base model as shown in Figure 9.

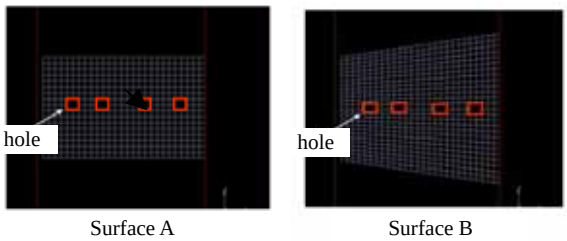

Figure 9. Geometry of analytical model with holes

Figure 10 shows the analysis result. Figure 11 shows the deflection. Points (1) through (4) shown in Figure 10 correspond to numbers shown in Figure 11. These figures indicate that, by making local holes, the second peak load can be reduced. The effect of local holes, however, is only limited to the case where the location of wrinkle is predictable. It is still not sure whether the same effect is expected in a complicated load input or oblique impact. If the number of holes is increased, it may intentionally reduce the energy absorption area.

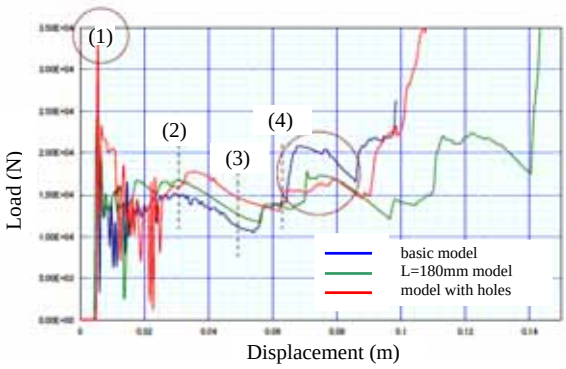

Figure 10. Load-deflection curve of model with holes

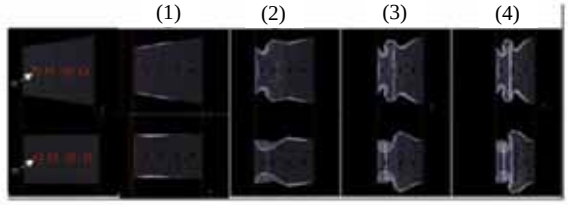

Figure 11. Deflection of model with holes

Model with Corrugation in Axial Direction

Chen [2006] elucidated the following three deflection modes of a square tube:

(1) N mode: a mode where no deflection is generated along corrugation

(2) S mode (Simultaneous Crush): a deflection mode along corrugation where a load monotonically increases.

(3) P mode (Progressive Crush): a deflection mode along corrugation with load amplitude

S mode is favorable since no peak load is generated at initial phase. The load monotonously increases in compression with small load amplitude, and so on. Though corrugation may decrease energy absorption rate compared with the conventional square tube, it has been proven out that by optimizing the geometry, the equivalent effect as the conventional one can be obtained.

Therefore, a study was made to figure out whether the corrugate square tube is applicable as a refinement of the base model.

Three geometries were studied with regular corrugation of wave amplitude of 2a and a sin functional curve of y=asin (2πλ), where a, λ is amplitude and wavelength respectively. Figure 12 shows load-deflection curve of individual models, and Figure 13, 14, and 15 show their deflection.

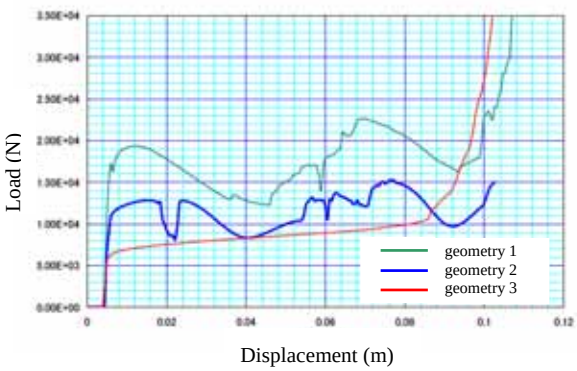

Figure 12. Load-deflection curve of geometry 1, 2 and 3

Figure 13. Deflection of geometry 1

Figure 14. Deflection of geometry 2

Figure 15. Deflection of geometry 3

As is indicated in load-deflection curve in Figure 12 and deflection in Figure 13 though 15, geometry 3 resulted in S mode. As was mentioned, however, geometry 3 resulted in the lowest average load among those 3 geometries. Though this geometry with corrugation is able to obtain S mode, the design must be optimized in order to control deflection mode and to have high energy absorption rate.

CONCLUSION

The following conclusions have been obtained from analytical results.

(1) Length of component
As a short square tube, the base model does not have enough length to generate the second wrinkle; thus, the second peak load rises. Control is required so that the second wrinkle can be generated.

(2) Influence of restraint condition
With short overall length of square tube, the influence of restraint condition is complicated; thus, it is difficult to cope with the issue by changing restraint condition.

(3) Study on geometry change
-A model with holes locally
The second peal load is decreased by having holes. However, it is not desirable solution since this is only applicable to the case where wrinkle position can be predicted and this may lead to the initial peak load increase.
-A model with corrugation in axial direction
By having corrugation, such a deflection mode is obtained that the load monotonously increases without initial peak load. It is, however, difficult to apply the geometry studied as it is. The fact that wrinkle length can be controlled with the corrugation could be a clue for the improvement of component.

REFERENCES

[1] Tokyo University of Science, Deiheng Chen and Takeshi Hiratsuka. 2006. "Study of Axially Crushed Cylindrical Tubes with Corrugated Surface Based on Numerical Analysis", Transactions of the Japan Society of Mechanical Engineers, Series A, Vol.72, No.722 (2006), pp.1464-1471.

DEVELOPMENT OF NEW GENERATION MOBILE DEFORMABLE BARRIER

Masanori Ueno
Japan Automobile Research Institute
Keiji Hatano
Naomi Fukushima
Japan Automobile Manufacturers Association, Inc.
Yoshihisa Tsuburai
Japan Automobile Standards Internationalization Center
Japan
Paper Number 07-0299

ABSTRACT

The barrier face that using the current regulation of Japan and EU was developed in the stiffness of ’70s vehicles[1]. Therefore, the stiffness of this barrier is different from the current vehicles that adapts to the frontal impact tests and considering of compatibility. Then, we did the development of the new barrier face that the stiffness of the current vehicles including the small sized sports utility vehicles was reproduced.
First, we investigated the stiffness of the front-end of the vehicle for ’98MY in IHRA-SIWG[2],[3]. Next, we started the development of the barrier face in based on the results of this investigation. In the same time, they started the development of new barrier face in Europe[4]. So, we cooperated with their development for harmonization.
The developed barrier face named the advanced European mobile deformable barrier (AE-MDB) is the almost matched to the stiffness of investigated results of current vehicles. However, the deformation mode was different between the car-to-car test and the MDB-to-car test. Therefore, we did more improvement in the barrier face. The improvement items were the addition of the beam element and the tuning of the stiffness of lower row. The beam element is reproduced the bumper reinforcement of the actual vehicle. In these improvements, we completed the development of the new barrier face that matched to the stiffness of the current vehicle, and the same deformation mode between the car-to-car (CTC) test and the MDB-to-car test.
We hope that this barrier face is adopted in the new regulations for side impact.

INTRODUCTION

Japan adopts the side impact test procedure equal to EU. The barrier face used for this test procedure reproduced the stiffness of the vehicle in the ’70s. The stiffness of current vehicles are different from ’70s vehicles, because they are adapting to various safety regulations for example the frontal impact test, the compatibility and so on. Therefore, the stiffness of the barrier face is different from the stiffness of current vehicles. As for this, the results of the investigations in IHRA-SIWG are clear[5],[6],[7]. Then, the development of the barrier face that reproduced the stiffness of the current vehicles was necessary. They started the development of the various type of the new barrier face in IHRA-SIWG and EEVC WG13 etc. Japan also started the development of new barrier face called J-MDB. However, Japan did join the development in Europe from the viewpoint of the international harmonization, because the same regulation is adopted in Europe, and they were doing development with the same concept as Japan. The developed barrier face in this group was called AE-MDB V2[8]. However, this barrier face had some problems.

THE DEVELOPMENT OF BARRIER FACE

The Problems of AE-MDB V2

The deformation modes were different when the results of the tests using AE-MDB V2 and the CTC tests were compared.
In the struck vehicles, as shown in Figure 1, the deformation of the AE-MDB tests was larger than the CTC tests in door-height (thorax and H-point level)

section, but it's the contrary trend in the side-sill-height section. In the door-height section, the deformation of the door was larger in the AE-MDB tests than the CTC tests, and the deformation of the B-pillar was smaller than that.

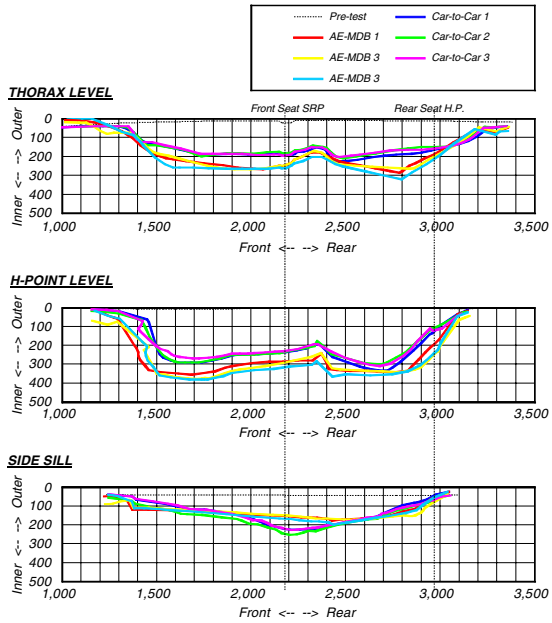

Figure 1. The comparison of deformation of the struck vehicle between the AE-MDB V2 tests and the car-to-car tests.

In the striking vehicles, as shown in Figure 2, the deformation mode was different between the AE-MDB tests and the CTC tests. The deformation of the center area of the AE-MDB was very big in comparison with the deformation of the actual car.

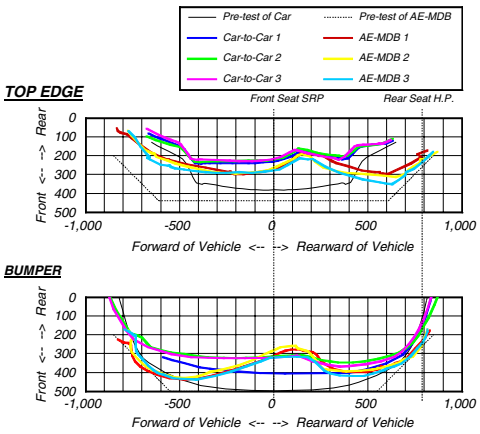

Figure 2. The comparison of deformation of the striking vehicle between the AE-MDB V2 tests and the car-to-car tests.

Therefore, we investigated the cause that the deformations were different between AE-MDB tests and CTC tests. In the AE-MDB, that is made of the individual six blocks which are covered the face plate of 0.5mm thickness, same as ECE Reg.95 barrier face. In the actual car, that is the structure that the left and right longitudinal members are connected with the bumper beam. And, the bumper beam will be stiffer year by year for compatibility.

So that, as shown in Figure 3, we suggested adding the independent bumper on AE-MDB for reproduced bumper-beam, to fit the deformation mode of AE-MDB test to the car-to-car tests.

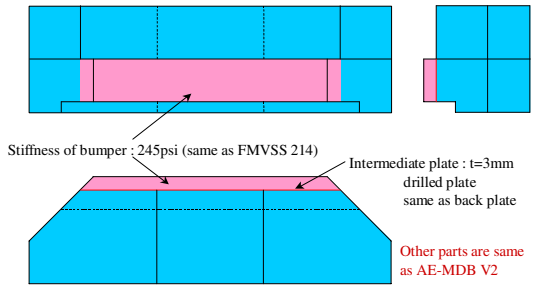

Figure 3. The modification proposal of the AE-MDB.

Development of the 'Modified AE-MDB'

We developed the 'Modified AE-MDB' to solve the problem of AE-MDB V2 that deformation mode was different from the CTC test. As shown in Figure 4, the lower row was changed with the 'Modified AE-MDB' from the AE-MDB V2. The modified points were follows.

- Cut off the bumper section.
- Add the independent bumper with drilled plate on the main-body of the lower row.
- Covered by face plate of original barrier face.

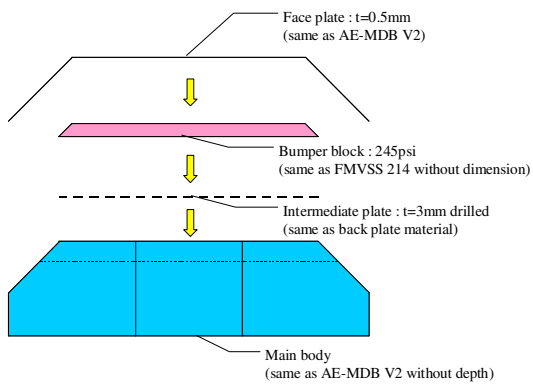

Figure 4. The lower row structure of the 'Modified AE-MDB'.

However, the stiffness of main-body was not changed from the AE-MDB V2.

Load Cell Wall Test - We carried out the load cell wall test to confirm the stiffness of the developed the 'Modified AE-MDB'. The test procedure for the 'Modified AE-MDB' is same as the barrier calibration test of ECE Reg.95 without the mass of trolley. The mass of trolley was 1500kg required in the AE-MDB specification. The collision velocity of the LCW test of the 'Modified AE-MDB' was 35km/h.

The force-deflection curves of the 'Modified AE-MDB' are shown in Figure 5. The upper row blocks, Block A, Block B and Block C, which were not changed from the AE-MDB V2, were within the required corridor. However, the lower row blocks especially Block E was without the required corridor to stiffer side. The both side blocks of the lower row, Block D and Block F, were upper limit of the required corridor in the initial part of the displacement. Also, the whole barrier face stiffness, Total, was almost at upper limit of the required corridor.

This is because; the 'Modified AE-MDB' was cut off the softer part of the lower row from original AE-MDB V2. Then, the stiffer independent bumper than the main body was added there. Because of that, the blocks of the lower row become stiffer. Furthermore, it can think that the load value of the Block E was increased by the load exchange with the stiffer blocks of the both side.

Using this 'Modified AE-MDB' to confirm the influence of bumper-beam though this was not matched for the required corridor carried out the full-scale test.

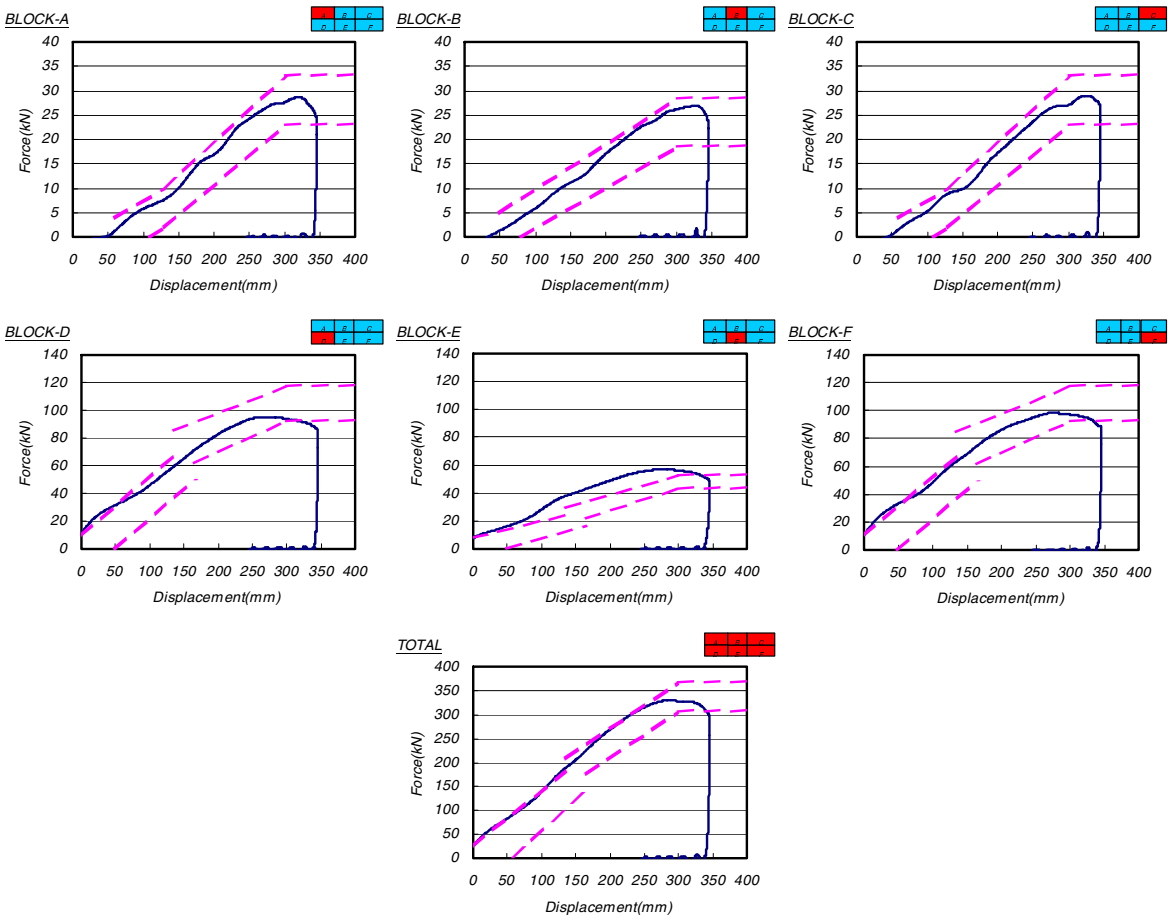

Figure 5. The force-displacement curve of the 'Modified AE-MDB'.

Full-Scale Test - We carried out the full-scale side impact test using the 'Modified AE-MDB'. The test condition of this test was same as ECE Reg.95. The impact point was put on the position where the centerline of the MDB corresponded to the seating reference point of the struck vehicle. And, the impact velocity was 50km/h.

In the struck vehicles, as shown in Figure 6, at the thorax level were almost similar between the AE-MDB V2 and the 'Modified AE-MDB'. This is because; the upper row of the 'Modified AE-MDB' was not changed from the AE-MDB V2. At the H-point level in the B-pillar position, 2,300 to 2,400 in lateral axis, the 'modified AE-MDB' was larger than the AE-MDB V2. And, it almost corresponds with the deformation mode of the 'Modified AE-MDB' test when it increases the deformation mode of the CTC test 80mm. The deformation by the 'Modified AE-MDB' was larger than the deformation by the AE-MDB V2 in side sill level.

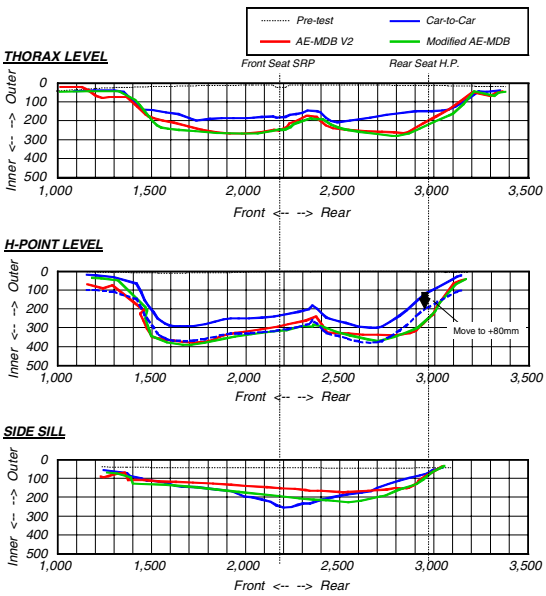

Figure 6. The comparison of deformation of the struck vehicle between the AE-MDB tests and the car-to-car test.

In the striking vehicles, as shown in Figure 7, in the bumper level, the deformation of the 'Modified AE-MDB' was smaller than for the AE-MDB V2. And, it almost corresponds with the deformation mode of the 'Modified AE-MDB' and the deformation mode of the bumper beam of actual vehicle.

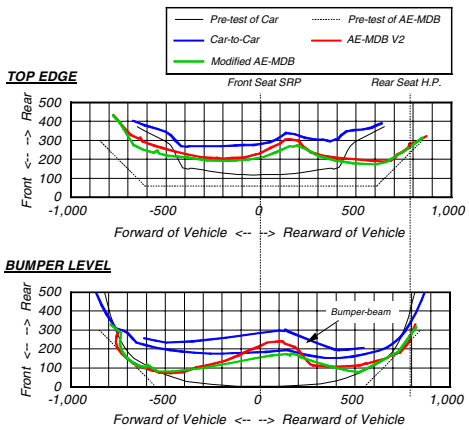

Figure 7. The comparison of deformation of the striking vehicle between the AE-MDB tests and the car-to-car test.

The 'Modified AE-MDB' improved the deformation mode of the door section of the struck vehicle and the bumper of the striking vehicle. And, more improvement of the lower row will be necessary.

The Problems of the 'Modified AE-MDB' - The force-displacement curves of the blocks of the lower row were without the required corridor to stiffer side. Therefore, the deformation of the full-scale side impact test using the 'Modified AE-MDB' was larger than the CTC test and the AE-MDB V2 test. And, the face plate of the 'Modified AE-MDB' was split due to the collision. Then, the development of the new barrier face to conform to the required corridor was started.

Development of AE-MDB V3.1J

We developed the new barrier face that matched completely in the required corridor of the AE-MDB. We called that the AE-MDB V3.1J. The structure of the lower row of this barrier face is shown in Figure 8. The point that this barrier face is changed from the 'Modified AE-MDB' to is shown in the following.

- Add the front plate between the face plate and the bumper to prevent the face plate from splitting.
- Tuning the stiffness of the main-body of the lower row for matching to the required corridor.

Other parts of the barrier face were not changed in this improvement.

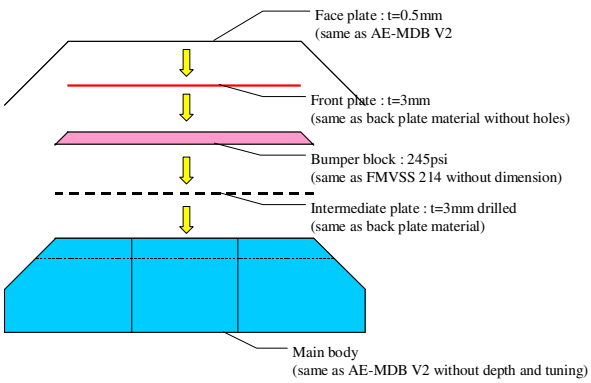

Figure 8. The lower row structure of the AE-MDB V3.1J.

<u>Load Cell Wall Test</u> - Again, we carried out the load cell wall test to confirm the stiffness of the developed the AE-MDB V3.1J. The test procedure for this barrier face is same as the previous LCW test. So, the mass of the trolley was 1500kg, and the velocity of the trolley was 35km/h.

The comparison of the force-displacement curves of the AE-MDB V3.1J and the 'Modified AE-MDB' are shown in Figure 9. The force-displacement curves of the upper row of the AE-MDB V3.1J were almost similar to the 'Modified AE-MDB' within the required corridor. Because, there were no changed from the 'Modified AE-MDB'. In the force-displacement curves of the AE-MDB V3.1J, the both side of the lower row were within the center of the required corridor even in the initial part of the displacement. In the force-displacement curve of the AE-MDB V3.1J, the lower center block was different from 'Modified AE-MDB', and it's within the required corridor clearly. These splendid results could obtain by tuning the main body of the lower row of the AE-MDB V3.1J. And then, the whole barrier face stiffness of the AE-MDB V3.1J was within the required corridor clearly, too.

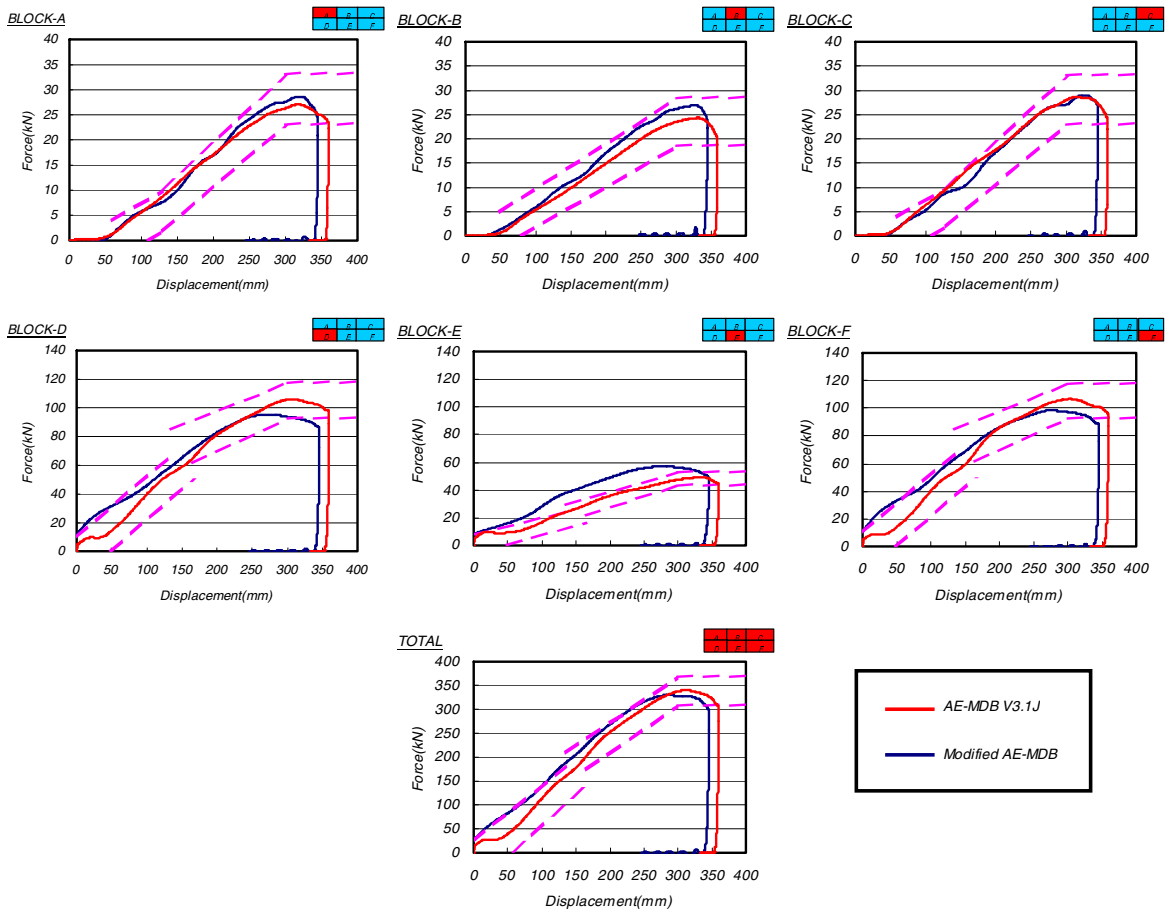

Figure 9. The force-displacement curve of the AE-MDB V3.1J.

Full-Scale Test - We carried out the full-scale side impact test using the AE-MDB V3.1J, too. And, the CTC test was carried out for the comparison. These test configurations are shown in Figure 10.

In the MDB-to-car test, the test condition was different from the test of the 'Modified AE-MDB', and that is same as the test procedure of AE-MDB proposed by EEVC WG13. The impact point was put on the position where the centerline of the MDB corresponded to the 250mm rearward of the seating reference point of the struck vehicle. And, the impact velocity was 50km/h. And, the ES-2 dummies were put on the front and the rear seat in struck side.

In the CTC test, that was carried out on both moving conditions. The impact point was put on the position where the centerline of the striking vehicle corresponded to the seating reference point of the struck vehicle. Then, the velocity of the striking vehicle was 48km/h and the velocity of the struck vehicle was 24km/h. Also, the ES-2 dummies were put on the front and the rear seat in struck side.

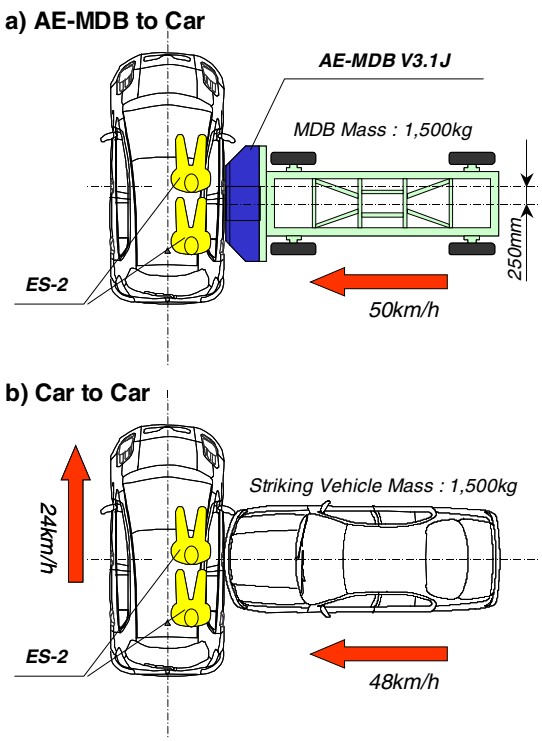

Figure 10. The test configuration.

In the struck vehicle, the deformations after the test were shown in Figure 11. At the thorax level and the side sill were almost similar between the AE-MDB V3.1J and the CTC test. At the H-point level, the results of both tests were not the deformation mode that the door was greatly deformed in comparison with the B-pillar like the previous test series but the passenger compartment area was homogeneously deformed. However, the deformation of the AE-MDB V3.1J was larger than the CTC test in rear seat H-point area. This difference of deformation is supposed an influence by the difference in a position of an initial collision.

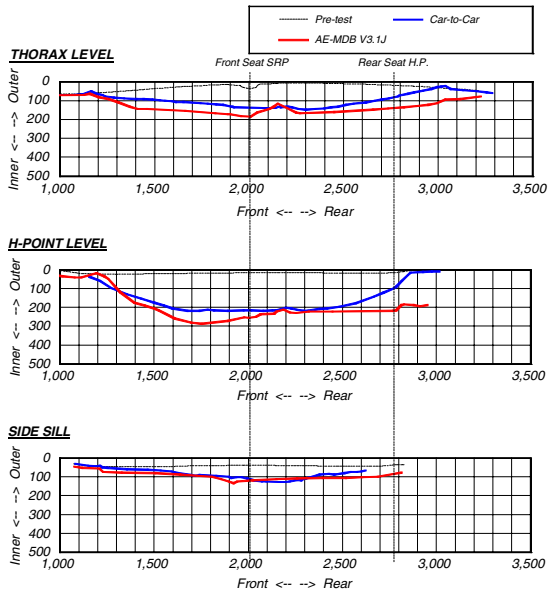

Figure 11. The comparison of deformation of the struck vehicle between the AE-MDB V3.1J test and the car-to-car test.

In the striking vehicle, the deformations after the test were shown in Figure 12. The radiator-core support was measured with the CTC test as the top edge. Also, the bumper-beam was measured as the bumper. In the CTC test, the post-test deformation lines were offset for left side in this figure. As for this, there was dragged on the right direction in front-end of the striking vehicle because the CTC test was both moving condition.

The deformation of the top edge of the AE-MDB V3.1J was larger in the equivalent part to B-pillar of struck vehicle. And, the deformation of the CTC test was homogeneously. Also, the deformation of the bumper section was homogeneously in the both tests.

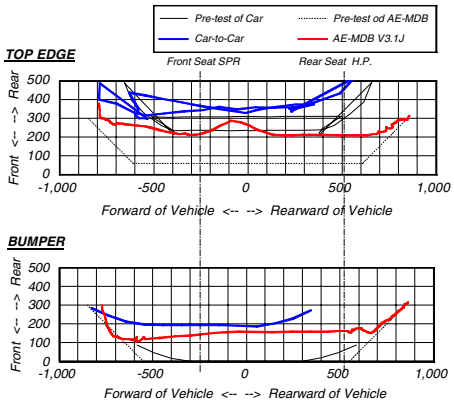

Figure 12. The comparison of deformation of the striking vehicle between the AE-MDB V3.1J test and the car-to-car test.

The injury values of the dummies were shown in Table 1 to compare with the JNCAP results of the same vehicle. Though the velocity of the striking vehicle of AE-MDB V3.1J was 50km/h, the CTC test was 48km/h and the JNCAP test was 55km/h. And, the test vehicles using the AE-MDB V3.1J and the CTC were equipped the SAB (side air-bag) and CAB (curtain air-bag) systems. But, the test vehicle of the JNCAP was not equipped these restraint systems. The injury values of the AE-MDB V3.1J test were larger than the CTC test and the JNCAP test in each region. And the injury values of the rear seat dummy were larger than the front seat dummy.

Table 1.
The injury values of the dummies.

	AE-MDB V3.1 to Car Front : ES-2 Test Velocity : 50km/h	AE-MDB V3.1 to Car Rear : ES-2 Test Velocity : 50km/h	Car to Car Both Moving Front : ES-2 Test Velocity : 48km/h vs 28km/h	Car to Car Both Moving Rear : ES-2 Test Velocity : 48km/h vs 28km/h	Reference : JNCAP Reg.95 Multi Front : EuroSID-1 Test Velocity : 55km/h	Proposed Limits ECE Reg.95
HPC	152	245	43	111	213	1000
Thorax U.Rib Defl. (mm)	-14.4	-23.5	-10.5	-20.3		
Thorax M.Rib Defl. (mm)	-21.8	-22.7	-18.6	-13.6	-19.4	42.0
Thorax L.Rib Defl. (mm)	-25.7	-25.7	-22.5	-6.9		
Thorax U.Rib V*C (m/s)	-0.08	-0.18	-0.04	-0.11		
Thorax M.Rib V*C (m/s)	-0.12	-0.18	-0.13	-0.07	-	1.00
Thorax L.Rib V*C (m/s)	-0.14	-0.27	-0.17	-0.02		
Abdominal Force (kN)	-0.99	-1.84	-0.48	-0.74	-0.96	2.5
Pubic Force (kN)	-2.92	-3.45	-1.38	-1.04	-2.51	6.0

The injury values of the dummies in the AE-MDB test, the CTC test and the JNCAP test were shown in Figure 13. This is shown in the percentage of injury value to proposal limit of current regulation.

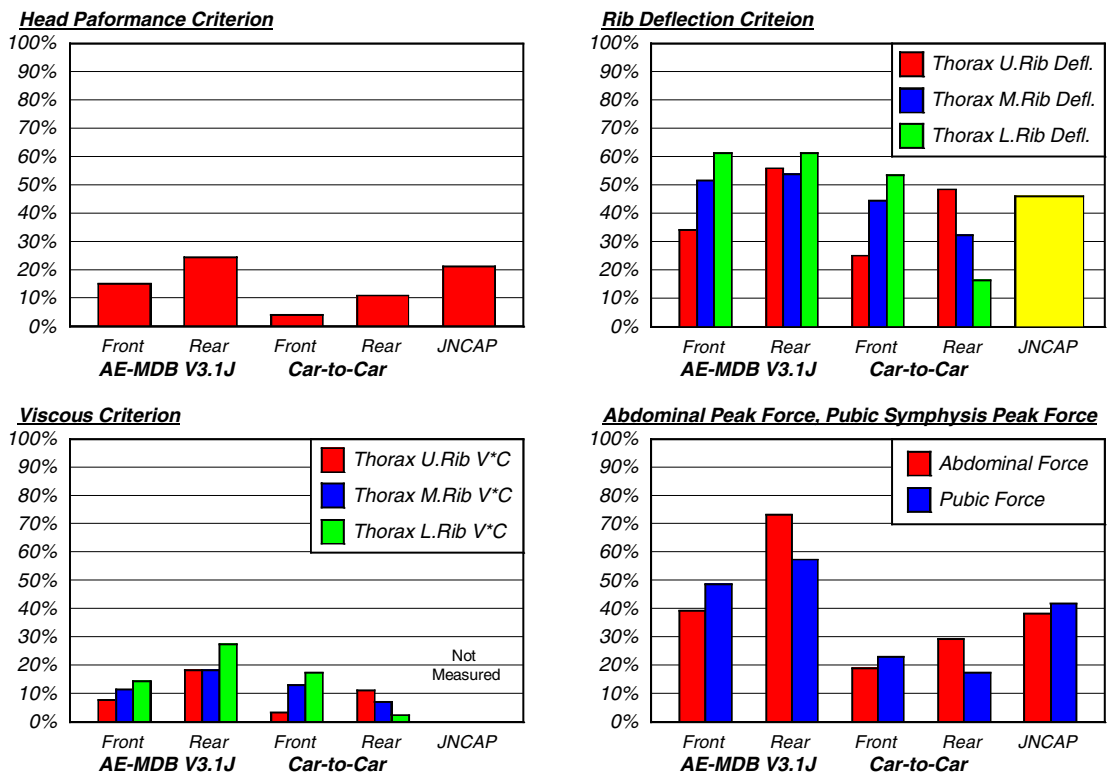

Figure 13. The comparison of injury values between the AE-MDB test, car-to-car test and JNCAP test.

In the head performance criterion (HPC), each result, especially CTC test, was very low value under 30% to the proposal limit. The rear dummies were larger than the front dummies, because the head of the rear dummies without the cover area of the CAB system.

In the rib deflection criterion, the maximum value of each rib deflection is used for the evaluation in the regulation. Therefore, in this case, the lower rib deflection is used for the RDC in the both dummies of the AE-MDB test and the front dummy of the car-to-car test. And, the upper rib deflection is used in the rear dummy of the CTC test. The results of the AE-MDB test were larger by about 30% than the JNCAP test with both dummies of the front seat and the rear seat, though the vehicle of the AE-MDB test was equipped with SAB system in front seat. Also, the results of the CTC test were larger by about 5-15% than the JNCAP test. The rear dummy of the CTC test was different trend from other dummies. In this dummy, the rib deflection was increasing to the upside. But other dummies, the rib deflection was increasing to the downside. This difference of trend is supposed an influence by the vehicle deformation in the rear seat position of the CTC test was smaller than the AE-MDB V3.1J test.

In the rib viscous criterion (V*C), also the maximum value is used for the evaluation in the regulation. The V*C cannot compared with the JNCAP test, because it was not measured in the JNCAP test. The V*C values were very small value under 30% to the proposal limit with both tests of the AE-MDB V3.1J test and the CTC test. The V*C values depended on the RDC values. Therefore a tendency of the V*C values were different only in the rear dummy of the CTC test.

In the abdominal peak force (APF), the result of the front seat dummy of the AE-MDB V3.1J test was almost same value to the result of the JNCAP test, though the vehicle of the AE-MDB test was equipped with the SAB system in the front seat. On the other hand, the result of the front seat dummy of the CTC test was almost half value of the other tests. In the rear seat dummy, though the AE-MDB V3.1J test was almost 2 times of the JNCAP test, the CTC test was small by about 30% than the JNCAP test. The APF values of the rear seat dummies were larger than the front seat dummies in both tests.

In the pubic symphysis peak force (PSPF), though the front dummy of the AE-MDB test was larger about 15% than the JNCAP test, the CTC test was smaller about 45% than the JNCAP test. Also in the rear dummy, though the AE-MDB test was larger about 40% than the JNCAP test, the CTC test was smaller about 60% than the JNCAP test. As for this, the AE-MDB test was larger than the JNCAP test, but the CTC test was smaller than the JNCAP test. Therefore, the results of the AE-MDB were about 2-3 times of the results of the CTC test.

The injury values of the rear seat dummy were larger than the front seat dummy in each region. One of the reasons, the SAB system was equipped only in the front seat.

The injury values of the AE-MDB test were larger than the CTC test in each region. One of the reasons, the lateral element of the velocity for struck vehicle of the AE-MDB test was higher than the CTC test of both moving condition.

CONCLUSIONS

We carried out this study to develop the new barrier face to reproduce the stiffness of the current vehicle including the small sized sports utility vehicles. The force-deflection corridor was not changed from the original AE-MDB that decided by the stiffness of the ’98MY vehicles. The independent bumper was added in front of barrier face without change the shape of whole barrier face with a purpose of fitting the deformation mode to the actual vehicle. Then, the tuning by chemical etching was done to fit the original corridor of the AE-MDB in the main body of the lower row of new barrier face, because the stiffness of new barrier face changed by adding the independent bumper.

We succeeded in the development of the new barrier face as a result of such process. And this new barrier face was within the required corridor of the AE-MDB completely.

After that, we carried out the full-scale side impact test to confirm the deformation mode when the new barrier face was used. The deformation mode of the full-scale test was the homogeneously like the CTC test. The injury values were compared with the results of the CTC test and the JNCAP test of same vehicle. The results of the full-scale test using this new barrier face were severe than the results of the other tests. One of the purposes of the development of this barrier face is reproduce the stiffness including the small sized sports utility vehicles. Therefore, it was presumed that the injury values of

the test using this new barrier face were severe than the CTC test.
The next step, we plan the validation test using another vehicles, and/or using another dummies.
The review of the barrier face is necessary for about every ten years, because the stiffness and the dimension of the vehicles will be changing year by year to improve safety.

ACKNOWLEDGEMENTS

The support of the JAMA-SIWG members, JASIC and Showa Aircraft Industry Co., Ltd. is gratefully. JAMA and JASIC members had precious advice on the occasion of the development of this barrier face. Showa Aircraft Industry Co., Ltd. was produced this barrier face for our research.

REFERENCES

[1] ECE Regulation No.95 – Uniform provisions concerning the approval of vehicles with regard to the protection of the occupants in the event of a lateral collision.

[2] Hisajima,K., et al, "A consideration on barrier face specification of side impact MDB", 17th ESV, Paper number 221, 2001.

[3] Yonezawa,H., et al, "Japanese research activity on future side impact test procedures", 17th ESV, Paper number 267, 2001.

[4] Roberts,A.K., et al, "Progress on the Development of the Advanced European Mobile Deformable Barrier face (AE-MDB)", 18th ESV, Paper number 126, 2003.

[5] Seyer,K., "International Harmonized Research Activities Side Impact Working Group", 17th ESV, Paper number 151, 2001

[6] Seyer,K., "International Harmonized Research Activities Side Impact Working Group Status Report", 18th ESV, Paper number 579, 2003.

[7] Newland,C., "International Harmonized Research Activities Side Impact Working Group Status Report", 19th ESV, Paper number 05-0460, 2005.

[8] Ellway,J.D., "The Development of an Advanced European Mobile Deformable Barrier face (AE-MDB)", 19th ESV, Paper number 05-0239, 2005.

application of the presented advanced airbag simulation methodology.

3. The accuracy and robustness of constitutive material models for engineering plastics and polymeric foams under high strain rate and large deformations for airbag door modelling as well as for robust response of local airbag dummy interactions (improvement of dummy model robustness).

4. In order to investigate the effects of design parameter variations, a vast amount of computing resources are needed.

CONCLUSION

The presented advanced initially chambered driver airbag performs in reality and virtually far below the injury value limits required by FMVSS 208. The advanced CFD airbag simulation methodology allows a deep insight into better understanding the physical problems. Therefore it is a helpful and powerful tool for pushing the future development of new airbag technologies. For instance by changing the cushion geometry – here the inner control volume of the presented chambered airbag – the effect on risk performance can be studied with numerical simulation. In mathematical terms, an approximation of the inner control volume size to the airbag volume itself leads to a conventional airbag. But shrinking with parallel application of new materials (to avoid burning) could lead to the next generation of advanced airbags designed for the low risk deployment target. Further, the CFD integrated simulation allows investigation into the effectiveness of different folding patterns in order to evaluate the consequences for the gas jet path and for the ensuing dummy injury values. The challenge of solving the airbag risk and protection compromise tells its own tale that further investment into the advanced airbag simulation methodology, as presented in this paper, will be a technically profitable task for the future.

REFERENCES

1. *Driver fatalities in 1985-1994 air bag cars*. Ferguson S.A., Lund A.K., Greene M.A., Insurance Institute for Highway Safety, Arlington, USA, 1995.
2. *Risk of death among child passengers in front and rear seating positions*. Braver E.R., Whitfield R.A., Fergusson S.A., Child Occupant Protection 2nd Symposium Proceedings (P-316), SAE, pp 25-34.
3. *Crash investigation reports*. U.S. NHTSA Department of Transportation, Washington DC, USA, 1998.
4. *5th Percentile Driver Out of Position Computer simulation.* R. Roychoudhury, D. Sun, M. Hamid, C. Hanson, SAE Paper 2000-01-1006.
5. *Driver Fatalities in Frontal Crashes of Airbag Equipped Vehicles: A Review of 1989-1996 NASS Cases, Accident Research and Analysis.* Cammisa X.C., Ferguson S.A., Lund A.K., SAE Paper 2000-01-1003.
6. *Assessment of Airbag Deployment Loads*. Horsch J., Lau I., Miller G., SAE Paper 902324.
7. *Dual-Stage Inflators and OoP Occupants - A Performance Study.* Malczyk A., Franke D., Adomeit H.-P., SAE Paper 982325.
8. *Ringairbag – Smart Driver Airbag Concept.* Krönes W., Schmidt W., 6th International Symposium and Exhibition on Sophisticated Car Occupant Safety Systems, Karlsruhe Germany, December 2002.
9. *Influence of Air Bag Folding Pattern on OOP-injury Potential.* Mao Y., Appel H., SAE Paper 2001-01-0164.
10. *A Math-Based CAE High-Speed Punch Methodology for Polymer Airbag Cover Design*. Lee M.C., Novak G.E., SAE Paper 2006-01-1187.
11. *Out of Position Simulation – Possibilities and Limitations with Conventional Methods.* Beesten B., Hagen S., Rabe M., 6th International Symposium and Exhibition on Sophisticated Car Occupant Safety Systems, Karlsruhe Germany, December 2002.
12. *Development of a Benchmark Problem Set for Assessing Out-of-Position Simulation Capabilities*. Wenyu Lian, SAE Paper 2004-01-1628.
13. *Numerical Simulation of Fully Folded Airbags and Their Interaction with Occupants with Pam-Safe.* Lasry D., Hoffmann R., Protard J.-B., SAE Paper 910150.

14. *Airbag modelling for Out-of-Position: Numerical approach and advanced airbag testing*. Rekveldt M., Swartjes F., Steenbrink S., Madymo User Conference, Como, Italy, October 2002.
15. *Advanced Airbag Fluid Structure Coupled Simulations Applied to Out-of-Position Simulations*. Ullrich P., Tramecon A., Kuhnert J., ESI Distributions, 2000.
16. *Simulation of Airbag Deployment Using a Coupled Fluid-Structure Approach*. Souli M., Olovsson L., Do I., 7th International LS-DYNA Users Conference, 2002.
17. *Evaluation and Comparison of CFD Integrated Airbag Models in LS-DYNA, MADYMO and PAM-CRASH*. Zhang H., Raman S., Gopal M. Han T., SAE Paper 2004-01-1627.
18. *OOP-Simulation – A Tool to Design Airbags? Current Capabilities in Numerical Simulation.* Beesten B., Hirth A., Reilink R., Remensperger R., Rieger D., Seer G., 7th International Symposium and Exhibition on Sophisticated Car Occupant Safety Systems, Karlsruhe Germany, November 2004.
19. *Madymo 6.3.1 Reference / Theory Manual*. TNO Madymo BV. Delft, The Netherlands. August 2006.
20. *Fully Multidimensional Flux-Corrected Transport Algorithms for Fluids.* Zalesak S.T., Journal of Computational Physics Vol. 31, pp 335-362, 1979.
21. *Solution of Continuity Equations by the Method of Flux-Corrected Transport*. Boris J.P., Book D.L., Methods in Computational Physics Vol. 16, Academic Press, 1976.
22. *Numerical Modelling of the Inflation Procedure of an Airbag and the Thermo-Chemical Process in the Gas Generator*. Rieger Doris, Institute of Aeronautics, Technical University Munich, October 2005.
23. *A Simulation Approach for the Early Phase of a Driver Airbag Deployment to Investigate OoP Scenarios.* Mahangare M., Trepess D., Blundell M.V., Freisinger M., Hoffmann J., Smith S., European Madymo User Conference, Cambridge, UK, September 2005.
24. *A Methodology for the Simulation of Out-of-Position Driver Airbag Deployment.* Mahangare M., Trepess D., Blundell M., Freisinger M., Hoffmann J., Smith S., International Journal of Crashworthiness, pp 511-517, November 2006.
25. *Investigation of an Advanced Driver Airbag Out-of-Position (OoP) Injury Prediction with Madymo Gasflow Simulations.* Freisinger M., Hoffmann J., Blundell M., Mahangare M., Smith S., International Madymo User Conference, Detroit, USA, November 2006.
26. *Advances in Airbag Inflator Modelling.* Bosio A.C., Lupker H.A., 4th International MADYMO Users Meeting, Eindhoven, The Netherlands, 1993.
27. *The Development and Validation of the Material Model Fabric_Shear for Modelling Advanced Woven Fabrics*. U. Stein, G. Weissenbach, M. Schlenger, M. Tyler-Street, P. Ritmeijer. 10th International Users Meeting. Amsterdam, The Netherlands. October 2004.
28. *A Study on the Modelling Technique of Airbag Cushion Fabric.* Hong S., Park S., Kim C., 9th International MADYMO Users Meeting, 2002.
29. *An Integrated Testing and CAE Application Methodology for Curtain Airbag Development.* Narayanasamy N., Hamid M., Ma D., Suarez V., SAE Paper 2005-01-0289.
30. *Airbag Fabric Picture Frame Test Manual. Version 1.0*, TNO MADYMO BV, 2005.
31. *Madymo Folder - Folding Airbag Models Version 9.0*. Oasys Limited. London, UK. November 2003.
32. *Capability of Simplified Folded Airbag Models in Gasflow Simulations.* Doris Rieger. 4th European Madymo User Conference. Brussels, Belgium. October 2004.
33. *Airbag Modelling Using Initial Metric Methodology*. Tanavde A., Khandelwal H., Lasry D., Ni X., Haug E., Schlosser J., Balakrishnan P., SAE Paper 950875.
34. *Analytical Design of Cockpit Modules for Safety and Comfort*. Lin J.Z., Pitrof S.M., SAE Paper 2004-02-1481.
35. *Validation/Verification of Hidden Airbag Door Loads and Kinematics*. Coulton J., CAD-FEM Users Meeting – International Congress on FEM Technology, Friedrichshafen, Germany, 2002.
36. *Use of MADYMO CFD for Driver Out of Position Simulation*. Lee W., SAE Paper 2006-01-0825.
37. *Digital Prototypes: Another Milestone for the Improvement of Processes and Cooperation in Vehicle Development.* Breitling T., Dragon L., Grossmann T., International VDI Symposium of Numerical Analysis and Simulation in Vehicle Engineering, Würzburg, Germany, 2006.
38. *Data Management, Process Support and CAx Integration of Engineering at Audi.* Reicheneder J., Gruber K., Wirch, W., Mayer S., International VDI Symposium of Numerical Analysis and Simulation in Vehicle Engineering, Würzburg, Germany, 2006.

INFLUENCE OF HIII 5% DUMMY TOLERANCES ON POSITIONING AND TEST RESULTS IN OUT-OF-POSITION LOAD CASES ACCORDING TO THE FMVSS 208

Steffen Sohr
Heiko Hofmann
Sascha Kutschenreuter
Heiko Ruck
TAKATA-PETRI
Germany
Paper Number 07-0340

ABSTRACT

With the introduction of the FMVSS 208 Final Rule, the requirements for occupant protection systems in frontal crashes have significantly increased. Especially the requirements regarding the airbag aggressiveness for "Low Risk Deployment" pose new challenges for both automobile manufacturers and suppliers.

The testing procedure detailed in § S26 of the FMVSS 208 is commonly referred to as "Out-of-Position" (OoP). This procedure considers the HIII 5% dummy on the driver side for two different positions (position 1: "Chin on Module", position 2: "Chin on Rim").

With the applied testing method, the test setup allows tolerances regarding the dummy positioning relative to the vehicle environment.

A comprehensive analysis of the influence of the dummy positioning has shown that particularly the head angle can vary among dummy manufacturers and may result in different OoP load characteristics.

Beside In addition to tolerances caused by the airbag module and the steering wheel design itself, the dummy's head angle is a significant factor for a variation of the OoP test results.

Out-of-position tests with identical module design have shown that the dummy positioning resulting from the head angle can lead to a misinterpretation of the test results. Depending on the dummy position, the OoP results range from far below the legal limits to a value exceeding them.

During the module development process, this scope of interpretations dramatically affects the assessment of the OoP performance and may lead to wrong conclusions.

INTRODUCTION

Recent years saw a number of developments for innovative occupant protection systems aimed to fulfil the increased requirements related to frontal and side protection. Specifically, the introduction of frontal and side airbags resulted in considerable improvements in automotive safety.

Although there are obvious positive effects of an improved protection potential for vehicle occupants, there are other aspects, mainly tracing back to airbag aggressiveness during its deployment phase.

The resulting features and requirements to the airbag design are commonly summarized under the term „Out-of-Position"-performance and address airbag-induced injuries mainly occurring in low speed areas.

Basing on the findings from real world accidents, the new „low risk deployment" requirements for frontal airbags have been included in the US legislation „49 CFR 571.208 (FMVSS 208): Occupant Crash Protection" in order to minimize the injury risk caused by airbag-supported restraint systems (See Appendix B).

On the driver side test with HIII 5%-dummy in two positions are required: Position 1: "Chin on Module" (See Figure 1) and Position 2: "Chin on Rim" (See Figure 2)

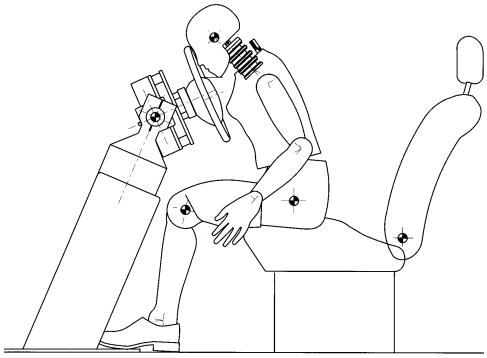

Figure 1. OoP-Test Configuration Position 1.

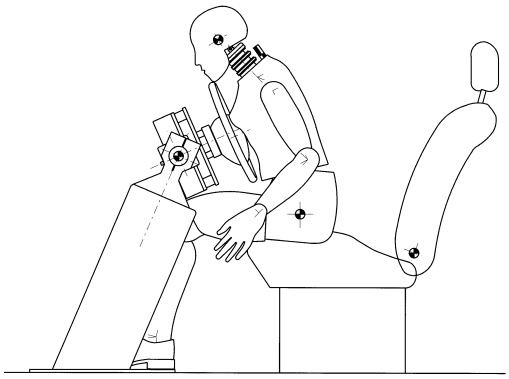

Figure 2. OoP-Test Configuration Position 2.

The applied test procedure to be used for the verification of OoP-Performance has to consider tolerances which are generally influenced by the following parameters:

1) Interpretation of seating regulation for dummy positioning in position 2
2) Specific vehicle characteristics
3) Airbag module characteristics
4) Specific differences in dummies

Following these tolerances and their influence on the assessment of OoP-performance will be described in further detail:

What kind of Tolerances exists?

<u>Tolerances due to legal text on positioning</u>

For Position 2, there is a difference between the description in FMVSS 208 S26.3 on positioning and the Test Procedure Protocol Data Sheet.

FMVS208 allows using the steering wheel adjustment to adjust the Chin Point on the Steering Wheel Point if possible. The Test Procedure Data Protocol Sheet already ends at that point where the Chin Point is within 10 mm +/3 mm of the Steering Wheel Point and switches straight to the airbag deployment preparation.

The interpretation of the Test Procedure Protocol may lead to a lower Chin Point position regarding the Steering Wheel Point. That means a harder interaction between chin and airbag which leads to a higher neck tension force Fz+.

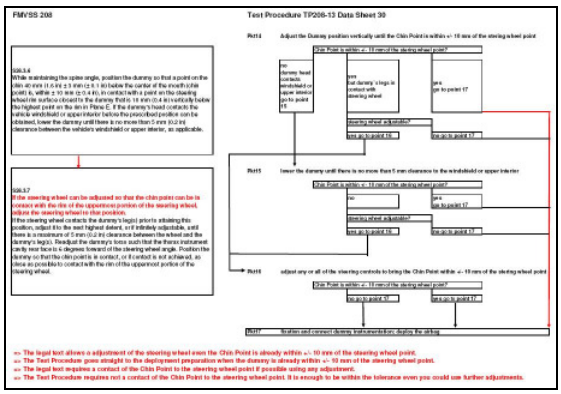

Figure 3. Differences between the positioning description in FMVSS 208 S26.3 and the Test Procedure Protocol Data Sheet; Pos. 2. [1;2] (see also appendix A).

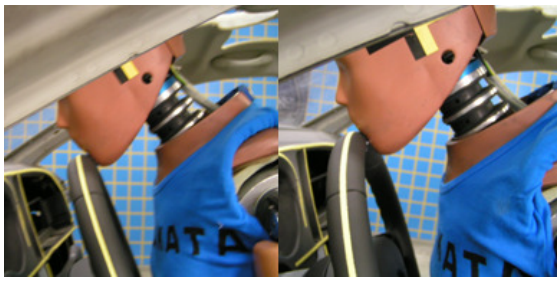

Figure 4. Example for different interpretation of FMVSS 208 S26.3 and the Test Procedure Protocol Data Sheet; Pos. 2.

The different chin position consequently results in a different position of the sternum to the airbag module in x- and z- direction, too.

<u>Tolerances on vehicle side</u>

Differences in the whole ergonomic tolerance chain may lead, for example, to different distances between the dashboard, steering wheel and windscreen.

Further tolerances are known for the steering column deformation force. A delayed deformation or a deformation on a high force level during the time may result in higher dummy measurement values because the dummy has to absorb more energy when the steering column is not running.

<u>Tolerances on airbag module</u>

Tolerances such as inflator pressure, airbag folding or gaps and expansions generated during the deployment are known. Especially the dynamical expansions during the deployment can lead to

different contact situations and variation of the lever arms in case a cover should contact the dummy.
The inflator performance is another parameter which might have influence on the variation of OoP results.
When using a robust module design the parameter variation does not play an important role. It is even possible to use serial modules with single stage inflators.

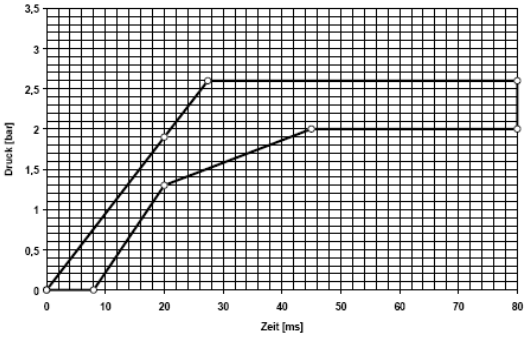

Figure 5. Example for an inflator tolerance +22°C. [3]

Tolerances on Dummy

There are two leading manufacturers for the H-III female. It is commonly known, however, that their dummy models are not really identical.

Even 2 dummies from one producer may differ in size (distances centre of gravity pelvis – centre of gravity chest – centre of gravity head).
Even differences in relative angles between head and chest are not unknown and may result in different chin distances to module in Position 1 and, furthermore, to different chest distances to the module cover and to different Chin Point positions to steering wheel point in position 2. That provokes different chest values and different neck forces and neck bending moments as well.
Beside the differences described above, the biggest difference between the two dummy manufacturers is the chest jacket they use. They differ both in design and stiffness. These differences lead to a different chest distance to the airbag module (esp. Position 2) and different chest deflection.

Calibration specifications produce additional tolerances. Corridors regarding hysteresis are defined for chest deflection, neck forces and neck moments.
Therefore, the OoP results for different dummies also vary.
There is also an interrelation between chest rip stiffness and neck values. The stiffer the dummy chest the higher is the axial neck force and neck bending moment, too, as to be seen in the graphs 6 to 9. They show the curves for 3 different dummies which are within the thorax calibration tolerances.

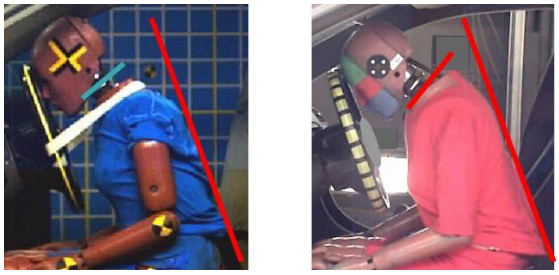

Figure 6. Example for different head angle by same thorax angle in same vehicle; Pos. 1.

Figure 7. Example for different distance to module in same vehicle by same thorax angle due to different chin point to steering wheel point caused by different head angles; Pos. 2.

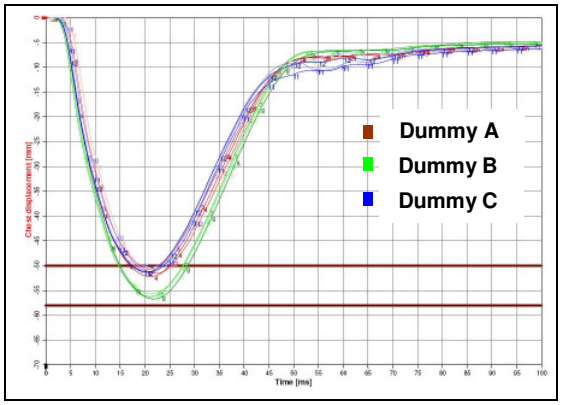

Figure 8. Chest deflection vs. time for thorax calibration for 3 different dummies; dummy B with softer rip set.

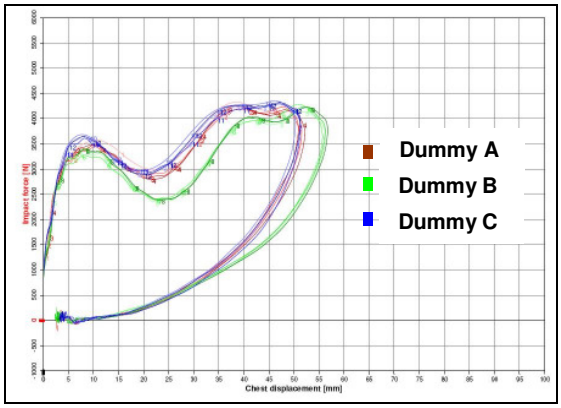

Figure 9. Impact force vs. chest deflection for thorax calibration for 3 different dummies; dummy B with softer rip set.

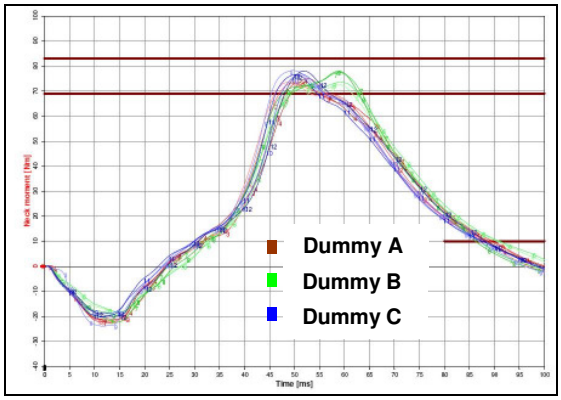

Figure 10. Thorax calibration: Neck moment My vs. time for 3 different dummies; dummy B with softer rip set.

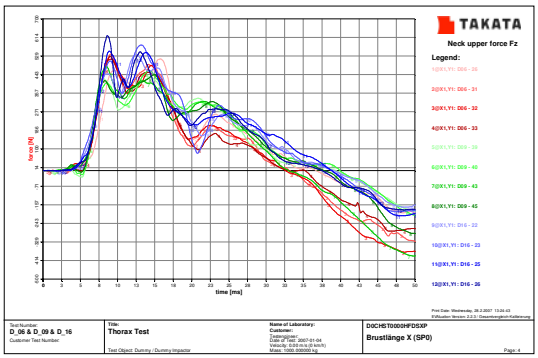

Figure 11. Thorax calibration test: Neck force Fz vs. time for 3 different dummies; dummy B (green curves) with softer rip set.

Considering the tolerances described before the question arises how to deal with them. To reduce all of them will not only produce costs which cannot be defended, but seems even to be impossible. Moreover, complicated mechanical mechanisms do not allow for a general solution.

The future will show whether it will be necessary to change vent position and cover opening geometry. Today, FMVSS 208 requires showing robustness whereas the low risk has to come from the airbag deployment.

What are the consequences of the Tolerances?

<u>Tolerances due to legal positioning text</u>

The interpretation of the test procedure protocol could lead into a lower dummy positioning of approximately 10mm in comparison to the FMVSS 208 legal text (See Figure 12). In general higher neck values (e.g. Nte) in Pos. 2 result from a lower chin position (See Figure 13).

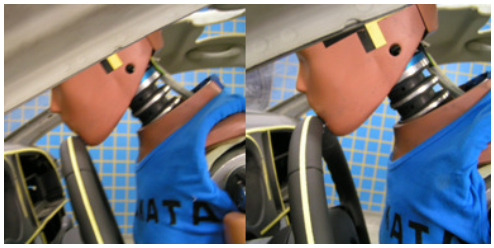

Figure 12. Interpretation of legal text vs. interpretation of test procedure protocol (chin point ca. 10 mm lower than steering wheel point).

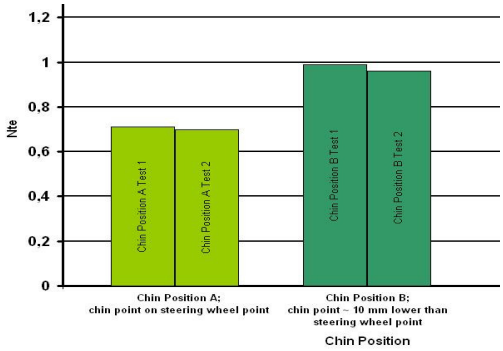

Figure 13. Influence of chin position on Neck value (Nte) in pos. 2.

The measurements show that the values are higher when the chin position is lower, as there is more interaction between chin and airbag in this position.

Tolerances on Dummy side

<u>Example for different head angle relative to chest Position 1</u>

As already shown, different head angles for different dummies are possible.
The diagram below shows the neck moment My time histories for 4 different dummies with different neck angles. The tests Position 1 were conducted with a comparable airbag module in the same car environment. Steering wheel angle and chest angle were always the same.

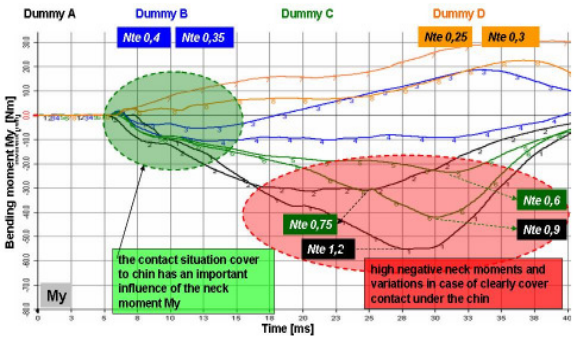

Figure 14. Neck bending moment vs. time depending on 4 different dummies; OoP Pos. 1. [4]

The graphs show a big variation in the neck bending moment maxima. The negative extension (-my) maxima are the higher the more the cover hits under the chin. The contact situation itself depends on the head angle, i.e. on the chin distance to the airbag module.

It is also possible to change completely the bending moment characteristic. This makes it possible to induce a flexion moment (dummy B and D) or to induce an extension moment (dummy A and C) just by varying the dummy.

The next diagram displays the head angles of the 4 dummies relative to the thorax angle. Moreover, it is shown in which way the Nte depends on the difference between angle head – thorax. All tests had exactly the same testing conditions. The Nte is the higher the lower the relative angle head to thorax is.

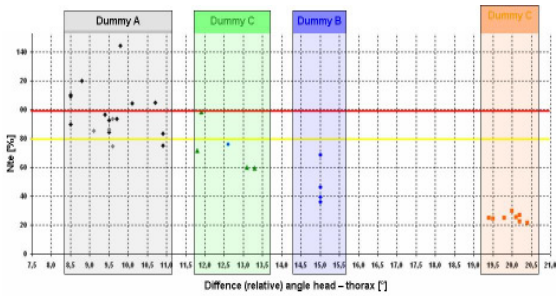

Figure 15. Neck load (Nte) vs. head angle for 4 different dummies; OoP Pos. 1. [4]

Chapter 4 describes which effects occur and what consequences result for a robust module design.

Especially for dummy A, it will not be possible to find a robust solution. Airbag folding optimizing is not the solution, as the resultant force will always be applied in z-direction. Hence, the dummy will always react with axial neck tension force and neck bending extension. As a result the Nte will always be dominant with high maxima. All further system tolerances, especially inflator variation, will be reflected in the Nte value.

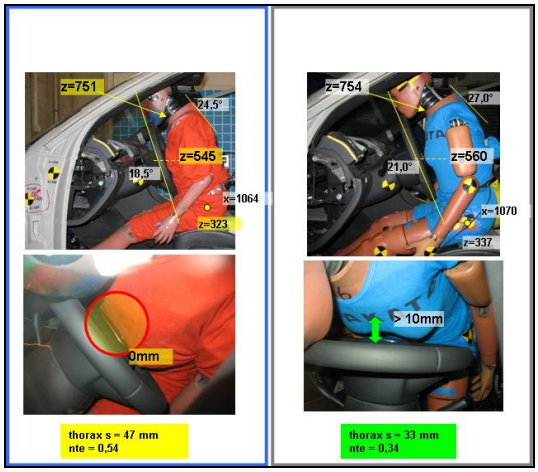

Figure 16. Example for different chin and sternum positions due to different dummy geometries; OoP Pos. 2.

Example for further Tolerances

The following graphs show the Nte and neck force Fz vs. the steering wheel column deformation. The tendency reveals that the dummy neck values increase with lower steering column deformation.

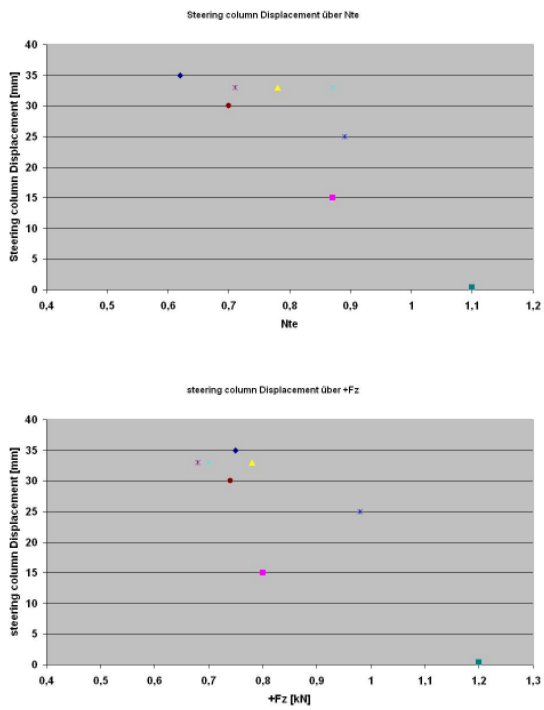

Figure 17. Neck tension force and Nte depending on steering column deformation; OoP Pos. 2. [5]

WHAT ARE THE REASONS FOR DIFFERENCES IN OOP LOADS?

The relative position of the dummy in front of the module leads to typical loads in its neck. The proximity of the dummy to the module makes it very complicated to identify the applied forces on the dummy. Numerical simulation offers the possibility to define forces acting on the dummy in a determined direction. Doing so, the measured forces and torques (reactions of the dummy) can be allocated to the impact forces, and, hence, the interrelationship between action and reaction can be recognized and understood.

Impact force in the x direction of the dummy head

In an OoP test, it is very important to affect the forces acting on the head of the dummy. The only possibility to evoke a flexion moment in the neck of the dummy during an OoP-Test is to impact the chin in x direction.

A lane from the module to the face of the occupant is necessary to let the airbag act on the described direction.

This is the reason why Dummy B and Dummy D react with a flexion moment (See Figure 11). Due to different chin positions, the airbag deploys in front of the chin. The resultant airbag force is impacting the chin in x direction.

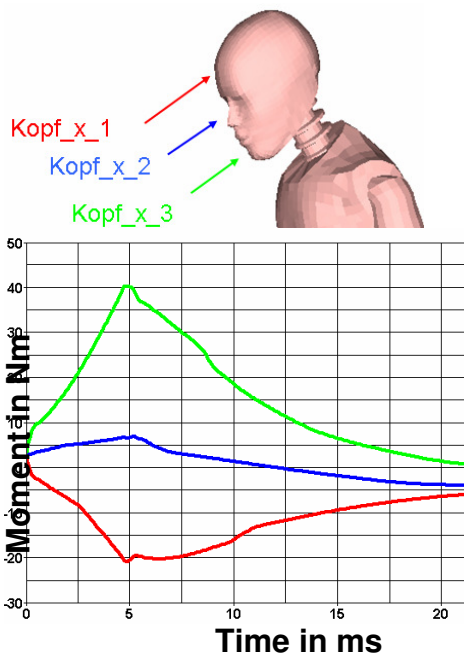

Figure 18: neck bending moment over time; lever variation for impact force 1200 kN [6]

Impact force in the z direction of the dummy head

This is the most uncontrollably direction of the impact forces. An impact force acting in this direction always causes a negative neck bending moment. The maximum of this moment depends on the lever between the impact force and the revolute joint of the neck.

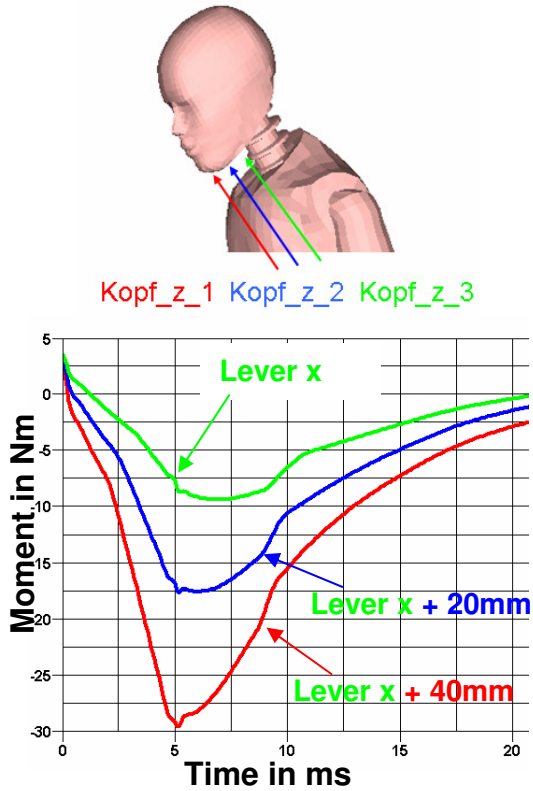

Figure 19: neck bending moment over time; lever variation for impact force 1200 kN [6]

The lever difference of the shown curves is only 40 mm. In addition to the high extension moment, the impact load causes a tension force in the neck. The combination of this force and the moment leads to serious N_{TE}. This relationship is responsible for the described differences of dummy A and dummy C for the OoP test setup "chin on module" (See Figure 11). For this reason it is absolutely necessary to avoid forces acting in this direction.

Impact force in the x direction of the dummy thorax

That load condition is typical for the OoP Position 2. An impact load working in x direction on the thorax of the occupant causes a chest deflection. The maximum of this deflection depends on the position where the load attacks.

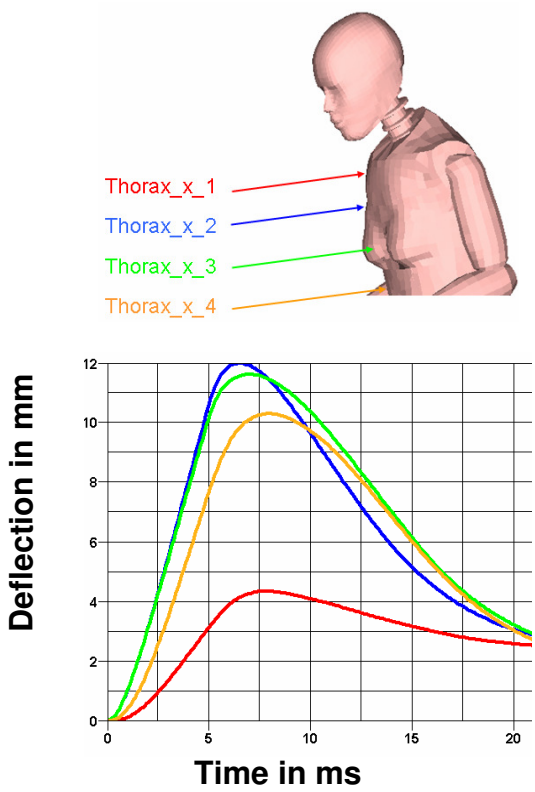

Figure 20: chest deflection over time; lever variation for impact force 1200 kN [6]

Furthermore, an impact load on the thorax in the described direction always causes an extension moment. This becomes especially true in the OoP test "chin on rim".

The occupant is jeopardized as an extension moment combined with a chest deflection will always occur. An example for this can be found in Figure 20.

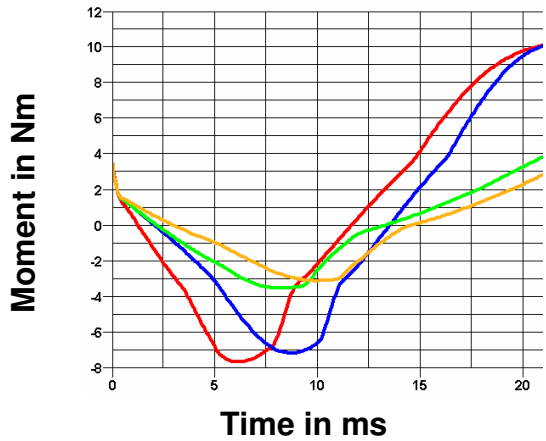

Figure 21: neck bending moment over time; lever variation for impact force 1200 kN [6]

The neck extension moment is less when the resultant airbag force is applied in a lower thorax or abdominal area.

Without a module designed for the OoP loading conditions, it is extremely difficult to fulfil the requirements of the OoP-test "chin on rim". During the deployment of the airbag cushion it is necessary to avoid contact between the airbag or parts of the module with the dummy chin because this might result in an impact force in z direction to the head of the dummy. This force causes an additional extension moment which superposes the moment caused by the thorax impact force.

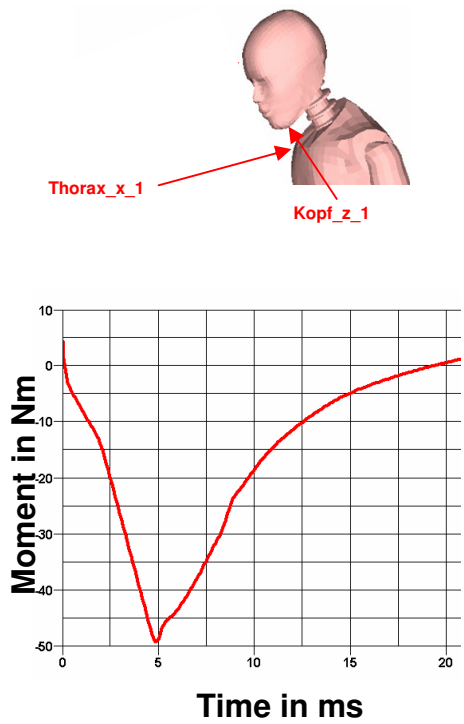

Figure 22: resultant neck bending moment over time caused by force thorax x and force head z (1200 N each) [6]

The loads on the dummy during an OoP test can be controlled if it is possible to apply the impact loads on determined regions of the dummy.

The only possibility to achieve a flexion moment is to apply a force in x direction on the chin.
Impact loads acting in z direction on the head always lead to extension moments with a high maximum.

Loads on the thorax cause an extension moment, too.

With a module designed for the loading conditions of an OoP test the described relations can be benefited.

LOAD MECHANISMS IN OUT-OF-POSITION SITUATIONS

Impulse-like force application

An impulse-like force application on the dummy under OoP conditions mainly results from:

- High inner pressure at the beginning of the airbag deployment as a result of inflator ignition; shortly after opening of the airbag cover the gas output hits the dummy that is still bearing the accumulated pressure („punch-out"-effect)
  Temporarily, there are high forces, specially in the head and thorax area.
- The opening airbag cover is accelerated by the airbag and produces an impulse on the dummy, the results are peaks in head and thorax area and high tensile neck forces.
- Parts of the folded fabric which are ejected as a concentrated mass out of the airbag module produce shock-like loads on the dummy

Loads caused by airbag membrane forces

OoP loads as a result of airbag membrane forces are mainly caused by:

- Loads during the airbag interaction phase which are only caused by the pressure-loaded airbag and generally lead to high neck forces and neck moments as well as to head and chest accelerations
- Loads during the airbag interaction phase induced by the airbag itself and in connection with the cover contact; the cover segments adjacent to the dummy (e.g., at the chin) increase the lever effect of the deploying airbag.
- Interaction with the airbag during the entire deployment phase, dummy loads result from the impact on the seat rest or other rear structures

CONCLUSIONS

There are a number of tolerances that influence the results of OoP tests. These tolerances result from the interpretation of the dummy seating procedure, from the airbag module and from the dummies themselves. Here, small changes sometimes might have big effects.

It is common knowledge that it is not the amount of energy application caused by the airbag which becomes the decisive parameter.

The simplified presentation of the load mechanisms shows which forces in positions 1 and 2 should be applied controlled by a robust and OoP-optimized airbag module design.

REFERENCES

[1] USA/Federal: 49 CFR 571.208 (FMVSS 208). 2005.

[2] Data Sheet 30 Test Procedure TP208-13 – Low Risk Deployment Test Using an Unbelted 5th Percentile Female Dummy

[3] Example for tank pressure field (ambient) based on the MTG 5, AK - LV 03. 2005

[4] Internal project documents. 2007. (not published)

[5] Internal project documents. 2006. (not published)

[6] Kutschenreuter, S. 2006. "Analytical Investigation on phenomenon of Out-of-Position load cases on driver side." Diploma theses (not published)

APPENDIX A

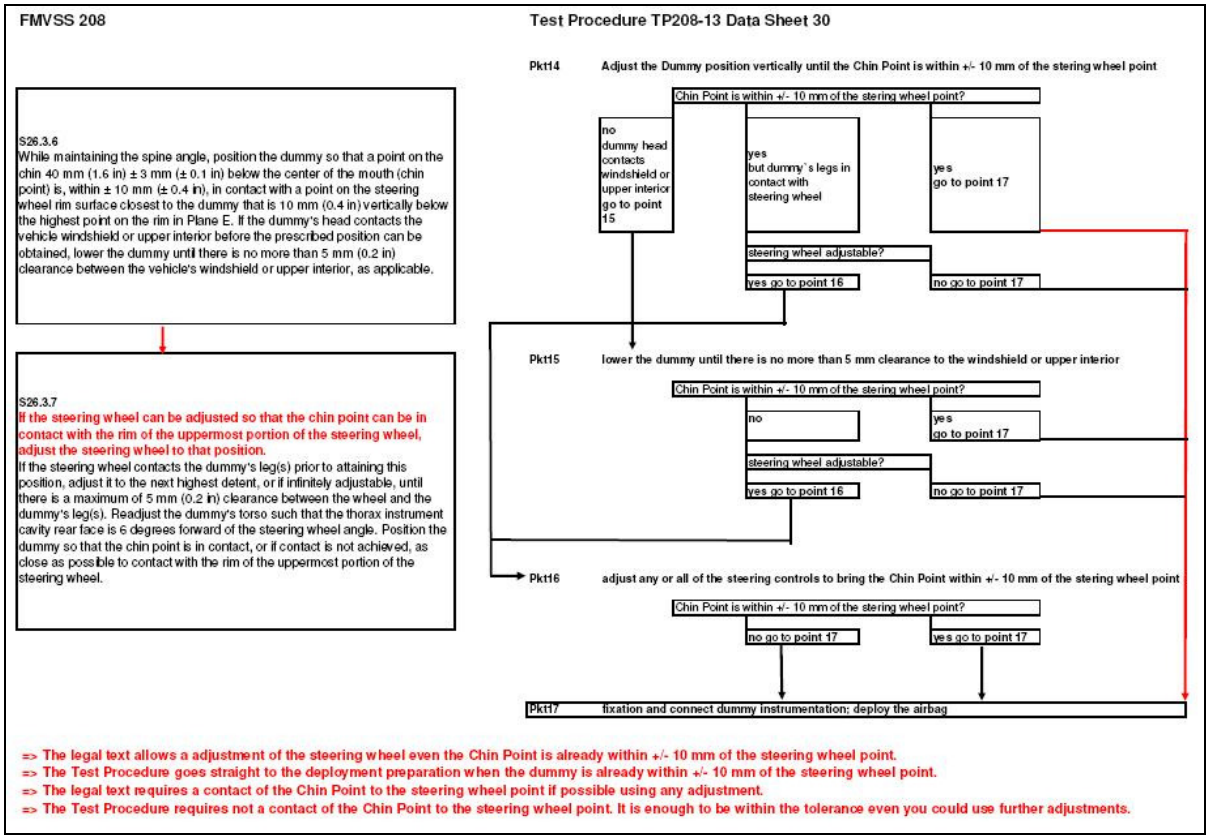

Figure A1. Differences between the positioning description in FMVSS 208 S26.3 and the Test Procedure Protocol Data Sheet; Pos. 2. [1;2]

APPENDIX B

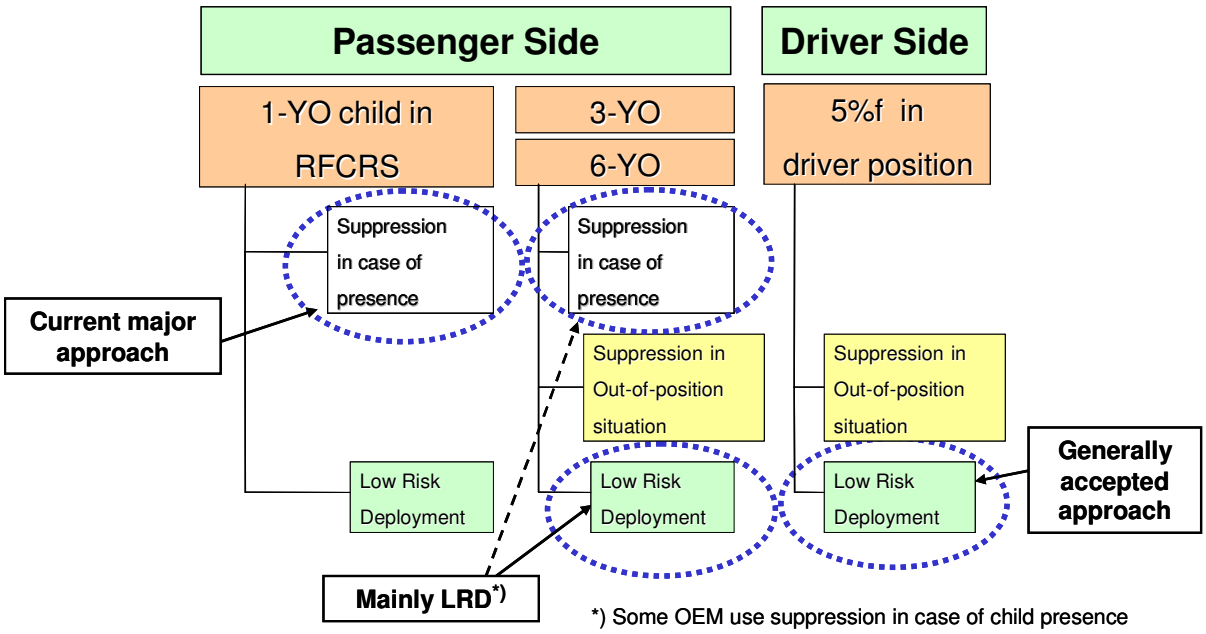

Figure B1. „Out-of-position“ requirements according to the Federal Regulation 49 CFR 571.208 (FMVSS 208).

ADAPTIVE SIDE IMPACT RESTRAINTS USING INTRUSION BASED CRASH SENSING AND DISCRIMINATION

Len Cech
Henk Helleman
Dr. Markus Schiefele
Dr. Jialou Hu
Debby Rice
TK Holdings Inc.
United States
Benedikt Heudorfer
Michael Kraft
Takata-Petri AG
Germany
Paper Number 07-0368

ABSTRACT

State of the art frontal airbag systems provide adaptive features such as multi-stage deployment and active or passive venting based on occupant position, stature, crash mode and severity. Research was done to understand the potential of reducing injuries and fatalities by applying a similar methodology to side impact protection.

Adaptive restraints have been proposed for side impact protection, however, the sensors and discrimination methods available for side crash detection, have, in general, not provided sufficient time and information to effectively apply these adaptations. However, recent analysis of an alternative magnetic field based crash sensor (MSI) has shown that this sensing concept provides crash mode and severity at very fast times which could allow a second triggering event for situation adapted protection. Using CAE tools it is shown how the improved triggering times can be employed and how much potential protection benefit can be gained by using various active adaptive restraint concepts.

To demonstrate the concept, MSI sensor data was analyzed for a series of crash and abuse tests to determine estimates of crash severity and mode at practical airbag deployment times for several deployment situations. The paper reviews the techniques used to process the MSI Data. The derived deployment times, along with severity and mode estimates, are used to demonstrate the effectiveness of several candidate active adaptive restraints compared with standard restraints.

In conclusion it is seen that adaptive side protection is worth consideration, and not only because the future requirements are expected to become more complex and demanding. However, these improvements do not come free of cost and therefore the pro and cons will have to be balanced very well.

INTRODUCTION

Frontal occupant restraints have evolved steadily in time, as new restraint and sensing innovations have been introduced. This evolution has directly benefited car occupants through improved safety, despite increasing traffic volume, compatibility issues and increased speeds. New and useful crash sensor, occupant classification and vehicle status information is often available on cars which can be used to optimize occupant protection for classes of occupants, crash modes and impact severity. For example, dual frontal crash detection sensors are often mounted on cars to quickly detect impact location, mode and severity; weight based classification systems discriminate occupant class, and multi-stage or variable stage airbag inflation or venting systems can be controlled. Often, safety benefit can be obtained with minor system adaptations. Such improvements have been slowly and steadily introduced in the market, resulting in continuing reductions in death and injury [1,2,3]; this is the primary motivation for improved frontal protection through adaptation. However, an important secondary factor must also be considered. As car buyers increasingly use safety performance as a key factor in model selection, and regulatory agencies evolve test standards to match real-world trends, in parallel, OEMs and suppliers must continue to study cost effective ways to improve and distinguish frontal occupant protection.

Side impact adaptive restraints have also been considered. Lessons learned in frontal protection can be directly applied to designing improved side systems. However, the long and complex mechanical side structure and close proximity of occupants to impact barriers, makes it more difficult to quickly and accurately discriminate crash mode and severity. Due to the very fast door intrusion times experienced in side impacts, the algorithms and methods available to improve protection through adaptation have been limited.

This paper attempts to revisit the topic of improved side impact protection through airbag adaptation using an alternative sensor which discriminates side impact crashes through door intrusion in proximity to the occupant. The Magnetic Side Impact (MSI) sensor is described fully in [4]. Subsequent testing and CAE analysis has shown the potential of the MSI

to provide faster average crash detection for deploying restraints than conventional accelerometer based crash detection systems. Because MSI senses average intrusion and not acceleration, CAE can be reliably used for analyzing not only the effectiveness of restraints, but also to derive the sensor signal early in the crash. To date, the effectiveness of CAE modeling of accelerometer data has been very limited, particularly in side impacts where even minor structural variations influence the detected signals early in the crash.

Additional analysis of actual crash data has shown that the MSI sensor provides information on crash mode and severity sufficiently soon after impact to consider side thorax airbag adaptation. CAE analysis was used to estimate the potential benefits of several basic forms of airbag adaptation including faster deployment, increased airbag volume and two stage inflation. Other forms of adaptation can be based on occupant classification, variable inflation, timed venting and variable venting. These are also discussed, but not yet supported through CAE analysis. In a similar way, adaptations could be considered for other forms of restraint such as belt pre-tensioners, side curtain airbags or reversible restraints (e.g. Motorized Seat Belts); however these topics fall outside the scope of this paper.

For completeness it should also be mentioned that there are passive methods to adjust restraint properties. In such cases, the settings are controlled by the variables that exist during the deployment of the airbag and progress of the crash and occupant. For example, an airbag may have a vent which is affected by the size and or stature of an occupant through direct or indirect interaction. In the case of passive adaptation, no additional sensors, signal processing or restraint actuators would be needed.

Figure 1 shows that the fatality rate per million vehicles that had been gradually decreasing over time has leveled off. This suggests that the current generation of restraint systems have reached the limits of their capabilities. At the same time demands for side impact protection are on the rise. New devices such as the Magnetic Side Impact (MSI) sensor allow for a breakthrough that can bring side impact protection to the next level. The earlier crash event detection and crash severity assessment offered by this sensor allow for more sophisticated and adaptable side restraint devices to be deployed. This will facilitate energy absorption at higher severity levels, providing better protection to more occupants in regulatory and consumer program testing as well as in real world accidents.

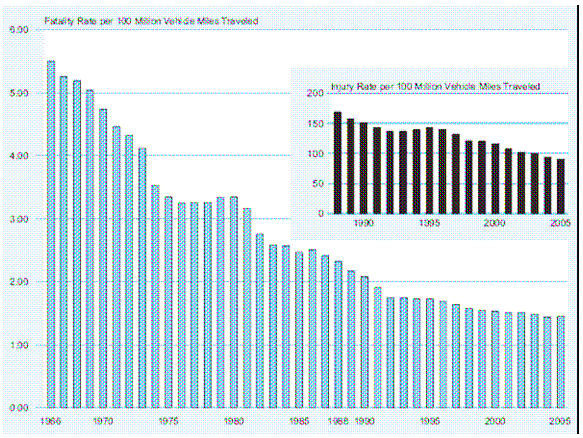

Figure 1. Fatality Rate per 100 Million Vehicle Miles Traveled, 1966-2005 [5]

REGULATORY FACTORS

Currently, the criterion for side protection varies globally. While harmonization is being pursued, it is not expected to take effect in the near future. Figure 2 depicts the wide range of requirements and priorities for regulatory tests in the future. Restraint designers must try to provide systems that function optimally for this wide range of tests and all classes of occupants. This can result in contradictory requirements, leading to different restraint systems for each global region. Selective adaptation provides a possible solution to achieve adequate protection over the widest range of tests and occupants with the same or similar system components.

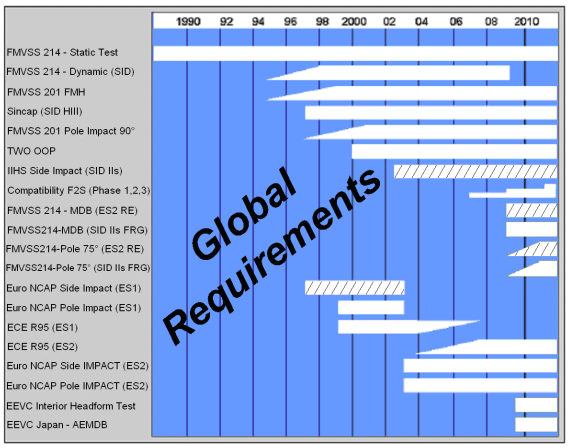

Figure 2. Plurality of global side crash requirement and new proposals [6]

As a first step in trying to meet this goal, a comprehensive investigation of the cooperation between adaptive restraints and side crash sensors using CAE is necessary. Crash simulations tend to be very time consuming, so the number of cases must be

selected in a systematic approach, to provide representative results in the end.
While other papers are available, which compare the benefits of different restraint systems for frontal crashes [7,8], this paper focuses strictly on side impacts.

The crash matrix considered in this paper is formed along two variables. The first variable is crash mode:

- 50km/h IIHS (90° IIHS MDB)
- 54 km/h FMVSS 214 MDB (27° crab)
- 50km/h ECE R95 (90° ECE R95 MDB)
- 32km/h FMVSS 214 NPRM pole (75°, 10 inch pole)

The crash modes from the above list are hashed in Figure 2, to allow an overview of which part of the global requirements is subject to investigation in this paper. The second variable combines sensor and protection type:

- standard airbag with accelerometer
- standard airbag with MSI
- enlarged airbag with MSI
- adaptive airbag with MSI (2nd stage)

DEFINITION OF TERMS

When talking about adaptive restraints, it is important to clearly define the key times in the sequence starting from first contact of the impacting barrier through deployment of the airbag and any adaptive components.

Time "0"

In a side impact it is the first contact of the impacting object with the vehicle (e.g. the falling edge of the trigger switch mounted on the vehicle door). This defines the origin for all subsequent times.

TTF1 (Time To Fire)

The time, when any crash detection system, detects a crash and deploys a protective restraint (airbag). Since this time can depend significantly on the kind of crash detection system, all deployment times originating from an accelerometer are labeled with the index A ($TTF1_A$), while all deployment times originating from the MSI sensor are labeled with the index M ($TTF1_M$). Any kind of restraint initiates at TTF1, a conventional restraint will be completely deployed, while an adaptive restraint will be deployed at its first stage.

TTS (Time To Severity)

This is the time when the MSI sensor can classify the crash mode (pole/barrier type) and estimate crash severity. For this paper, only the MSI is considered to provide this estimation.

TTF2

This is the time when a second stage of an adaptive restraint is deployed. Since knowledge about crash severity is important for the deployment of the second stage, the relation **TTF2 ≥ TTS** must hold. For lower speed crashes, a second restraint stage may not be needed, i.e. TTF2 → ∞. There is no index necessary for TTF2, because in the scope of this paper, only MSI provides a TTF2.

Crash Severity

Side impact crashes are often categorized into severity levels. In fact, many crash sensor discrimination algorithms simply classify impacts as ON (restraints are deployed) or OFF (restraints are suppressed). To consider adaptive restraints, a more precise crash severity measure is required. For side impact crashes, the intruding door or impacting object poses the biggest injury threat to the occupant. MSI is a door intrusion sensor [4]. While regulatory barrier and pole tests are carried out to evaluate restraint performance because they are repeatable, it is useful to have a method to relate the intrusion (severity) of any real-world crash to that of a regulatory test. For this paper, the term ***equivalent speed*** will be used to define crash severity. It is defined as the speed that a standard regulatory reference test must be run to duplicate the intrusion profile that occurs in any crash. For example, if the severity of a real world car-to-car crash is rated with an ***equivalent speed*** of 50 km/h, then the intrusion profile (in the sensing timeframe) could be similarly reproduced in a FMVSS 214 MDB regulatory test at an impact speed of 50km/h. While any regulatory tests could be considered as a reference, for this paper, the FMVSS 214 MDB crash mode is the reference for barrier type crashes and the FMVSS 214 NPRM pole test is the reference for pole type crashes.

ESTIMATING TTF AND TTS

The MSI coil measures the distance to conducting material in its proximity. In a crash, as the outer door skin starts to move relative to the sensor, the MSI signal increases. Figure 3 shows the normalized MSI signal and slope response for a regulatory ECE R95

crash. Since the MSI coil measures average door intrusion, the slope of the MSI signal is a good indicator of crash severity (intrusion speed).

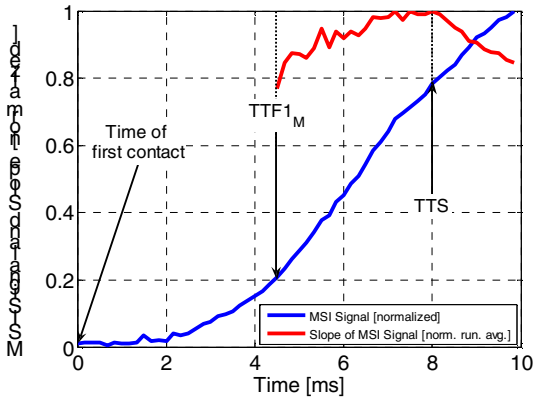

Figure 3. MSI Signal and Slope for an ECE R95 Crash Mode

The calculation of the slope starts right at TTF1 and is averaged over the ongoing signal. The calculation of the slope terminates at the derived TTS, if one of the following conditions is met:

1. The variance of the averaged slope is lower than a pre-determined, platform dependant threshold.

2. Time is greater than (TTF1 + 5ms)

3. A short term average of the slope decreases to zero. In this case the last 1ms of the signal is ignored for the final result, to make sure the result is not influenced by the plateau.

Table 1.
TTF1 and TTS for All Crash Modes Considered

Crash mode	$TTF1_M$	$TTF1_A$	TTS	equiv. speed
MDB Crashes:				
50km/h IIHS	3.0ms	5.8ms	7ms	50km/h
54km/h FMVSS 214 MDB	2.8ms	7.4ms	6ms	54km/h
50km/h ECE R95	4.5ms	7.0ms	8ms	34km/h
Pole crashes:				
32km/h FMVSS 214 NPRM pole	6.0ms	11.4ms	10ms	32km/h

Table 1 shows a compilation of TTF1 and TTS for sensors and crash modes considered in this paper. The table also shows the derived ***equivalent speed*** for each mode. All MSI slope calculations were terminated by the variation criteria (Condition 1). The TTF1 values in the table above were derived from full calibrations (crash and abuse tests included); the times were averaged over several crash series using mid-size sedans. The actual restraint deployment times that can be achieved on any specific platform must be derived through a full crash and abuse test set, where target TTF1 requirements vary by OEM and platform. The numbers used here are representative.
Further analysis of MSI signals shows the potential for classification of crash events into pole and barrier types, with unique ***equivalent speeds*** resulting from the dynamic differences in intrusion for poles and barriers. In practice, different adaptive restraint measures could be taken to reduce injury risk for each type.

CAE MODELS AND METHODOLOGY

A model of a typical mid size sedan, developed and validated for side impact studies in the research domain, was used for this study. The vehicle model comprises approximately 80,000 elements, providing a reasonable compromise between accuracy and computational efficiency.

Figure 4. Vehicle Model in Pole Impact

Individually validated barrier models, representative of the FMVSS 214 MDB, IIHS MDB and ECE R95 MDB were utilized as well as a model of the rigid pole of the FMVSS 214 NPRM dynamic oblique pole impact. The CAE analysis further incorporates dummy models representative of the Mid Size Adult Male (50th percentile) and Small Adult Female (5th percentile). While regulatory tests specify the size and type of dummy to be used, this study uses the

same dummy models throughout for ease of comparing results.

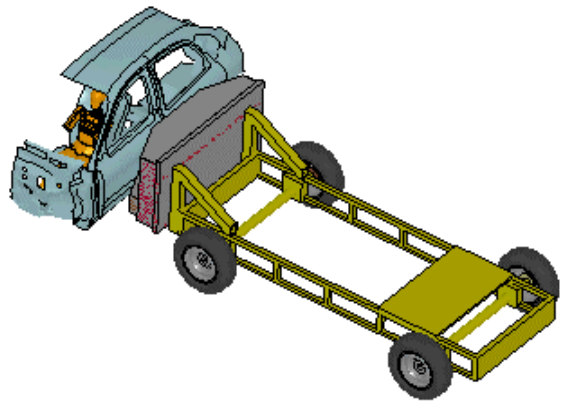

Figure 5. IIHS MDB Model

For Out of Position (OOP) injury risk assessments a model of the 3-year old Hybrid III dummy was used in ISO-2 position. The side airbag model used for this study is a typical single chamber airbag, typical for that used in vehicles of this class.

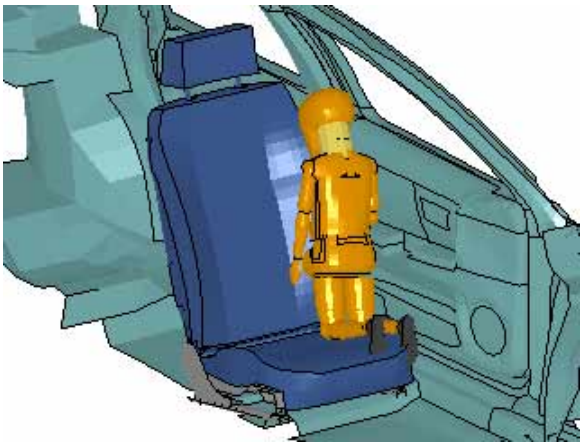

Figure 6. 3-Year Old Dummy in ISO-2 OOP

The airbag and inflator used in this study was designed to meet European regulatory MDB test standards and will not protect optimally in IIHS or the FMVSS 214 NPRM pole tests. For any airbag system, there is always a crash severity and/or occupant load where airbag protection potential is maximized. However, through active adaptation, the balance of internal pressure and venting can be controlled to best dissipate the impact energy.

The combination of two sensor types, four impact scenarios, and two adult dummy models allows for 16 permutations. Different restraint configurations and crash severity modes made for a total of 144 unique analysis models. To perform this study the LS-Dyna solver and an 8-node Linux cluster was utilized.

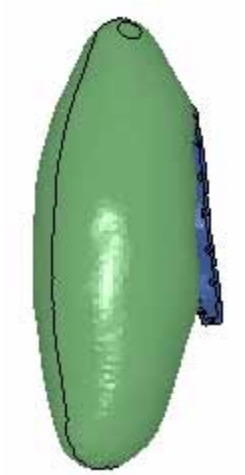

Figure 7. Baseline Side Airbag Model

CAE ANALYSIS

A first baseline CAE simulation set was performed to evaluate the possible benefits of the MSI sensor compared to an inertial sensor (accelerometer), using a standard airbag. Subsequent cases can be compared against the previous result to measure any level of incremental improvement. While many injury criteria are available to evaluate restraint effectiveness, rib deflection was chosen as the primary measure for this analysis. This measure is often the most critical for the vehicle size used in this analysis. A reduction in rib deflection represents an improvement in occupant protection. Note that in all subsequent figures, a value of one represents the peak rib deflection occurring on the Mid Size Adult Male dummy in the FMVSS 214 NPRM pole test. All other deflections are normalized to this level. Since this is a generic car, airbag and dummy model, absolute deflection levels cannot be cross validated against actual crash tests. Accordingly, normalization allows for a simple relative comparison of rib deflection levels across the crash, dummy and adaptation variables.

MSI Sensor and Accelerometer Comparison

The first question addressed in the CAE analysis was: would the faster MSI deployment times improve or degrade the performance of an airbag system designed for an inertial sensor? Keeping all other variables the same, the baseline airbag was deployed at $TTF1_A$ and $TTF1_M$ respectively.

Figure 8 and Figure 9 show the rib deflection measures, for Mid Size Male and Small Female

respectively. Figure 8 shows that the earlier MSI deployment times reduce peak rib deflection for the less severe ECE R95 and FMVSS 214 MDB crash modes, while the values for the more severe IIHS and FMVSS 214 NPRM pole crash modes are almost identical. The bag has been optimized for all current global requirements which are less severe than the IIHS test, so faster deployment shows little benefit for the IIHS and FMVSS NPRM pole crash. Figure 9 shows the deflection situation for a Small Female and the faster MSI deployment times show some measurable benefit. However, for the lower severity crash modes the deflection results are nearly identical.

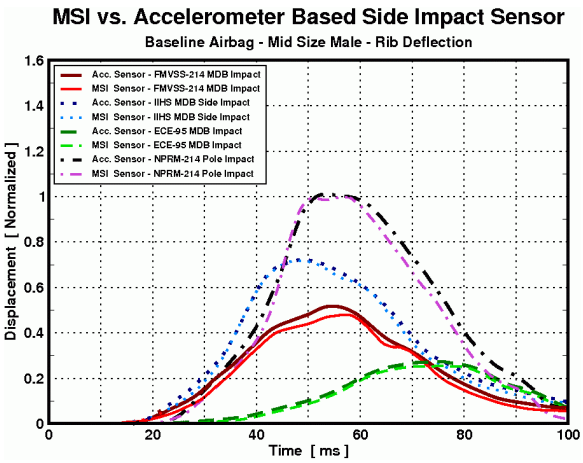

Figure 8. MSI vs. Inertial Sensor - Mid Size Male

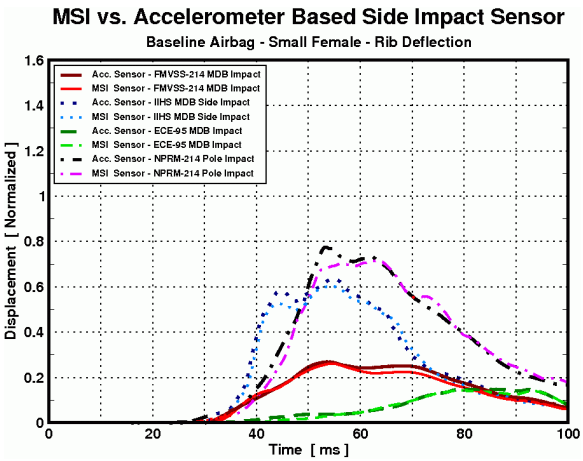

Figure 9. MSI vs. Inertial Sensor - Small Female

In no case analyzed, did a faster deployment result in higher peak rib deflections. This result suggests that the MSI could be effectively exchanged with an accelerometer in a conventional airbag system with no degradation in performance, and some measurable gains in reducing peak rib deflections.

Enlarged Bag Triggered by MSI

The second question addressed in the analysis is: Can a larger airbag deployed at the faster MSI TTF1 improve rib deflection? To simplify the analysis, only the width of the cushion was increased. Figure 10 shows the baseline cushion in red and the enlarged cushion in green. The resulting volume increase was 25%. Enlarging the cushion volume, while keeping the inflator constant results in a lower initial inflation pressure, and possibly less venting losses. With the larger contact area it was hypothesized that the overall contact forces of the higher volume airbag would be effectively the same as the original.

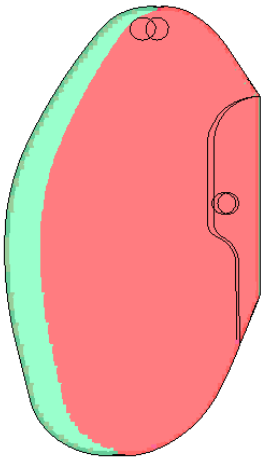

Figure 10. Baseline and Enlarged Cushions

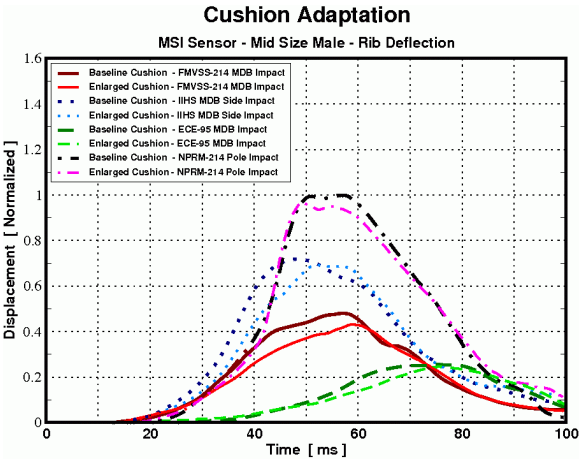

Figure 11. Cushion Adaptation - Mid Size Male

Figure 11 shows a comparison of dummy injury measures for the baseline cushion and enlarged cushion, both using MSI sensor trigger timing. A bigger bag is beneficial for all crash modes, except the low severity ECE R95 crash mode, where results are almost identical.

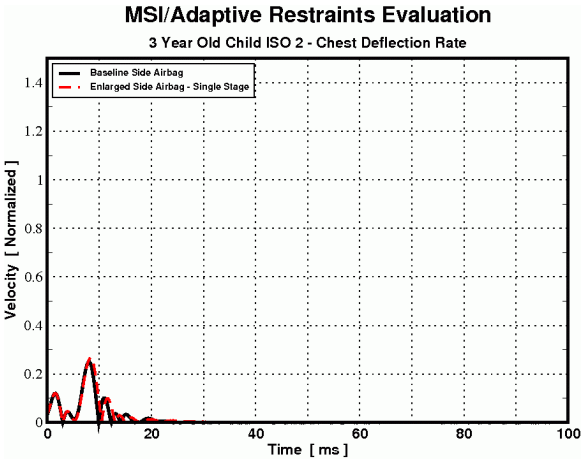

Figure 12. OOP Chest Deflection Comparison

One potential risk in simply enlarging the airbag cushion was how it would affect OOP performance. Therefore, a comparison was made, using the 3 year old child dummy in ISO-2 position. Figure 12 and Figure 13 show the comparative risk in terms of induced chest and head injury. In both figures, the solid black signal trace (Baseline Side Airbag) represents a known acceptable OOP performance. The dotted line represents the larger airbag.

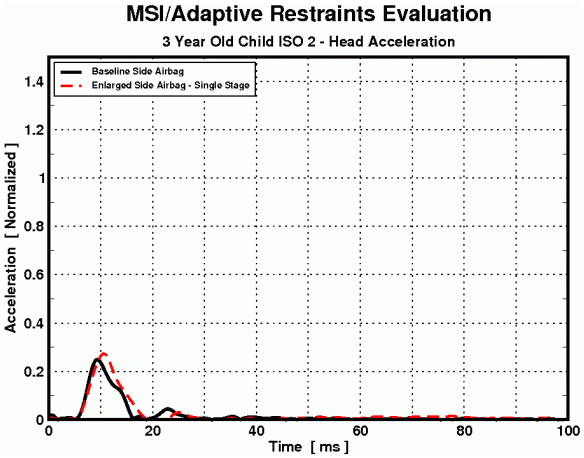

Figure 13. OOP Head Acceleration Comparison

Based on these figures, the effects of a larger airbag on OOP performance are minor and well within acceptable limits.

Enhanced Protection

Having established that the performance of the enlarged cushion is at least on-par with the baseline cushion, we next looked at further benefiting the occupants under high severity side impact conditions by adapting the restraints to the severity predicted by the MSI. Following the trends established for frontal impact restraints, the first adaptation considered here was the inclusion of a second inflation stage. This approach brings many possible variables, including peak inflation level, stage delay, and active venting; where any or all of these are valid options for optimizing restraint effectiveness. As a first step, this study simply considered enhancing inflation through a second stage load at a level of 25% of the primary stage.

Figure 14 shows the rib injury measures for the Mid Size Male for the enlarged airbag cushions that were inflated by either the primary stage only or the primary and secondary stages. The secondary stage is deployed at the time the MSI has established crash type and severity. (i.e. TTF2 equals TTS) as shown in Table 1.

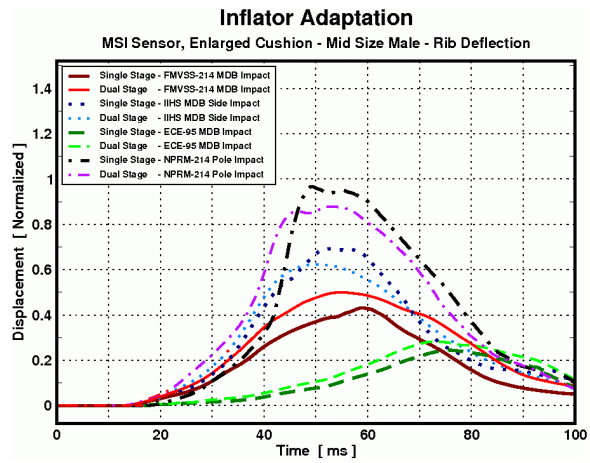

Figure 14. Inflator Adaptation - Mid Size Male

Clearly, the dual stage inflator shows a benefit for the higher severity cases (Pole and IIHS), while there is no perceived benefit for the lower severity cases. It is clear from Figure 14, that the threshold severity where a second stage should be deployed is somewhere between the severity of the FMVSS 214 MDB and the IIHS crash mode.

Aggravated and Real World Conditions

As discussed in [9,10], real world side impact severity on average may be considerably higher than current test conditions represent. We therefore explored the possibilities of the dual stage side airbag system under aggravated impact conditions. These comprise impacts with the same set of barrier objects but increased impact severity. Table 2 shows a compilation of the base line and aggravated speeds used in this paper.

Table 2.
Base Line and Aggravated Conditions

Base Crash Mode	Base Line Speed	Aggravated Speed
MDB Crashes:		
IIHS	50km/h	55km/h
FMVSS 214 MDB	54km/h	63km/h (SINCAP)
ECE R95	50km/h	55km/h
Pole crashes:		
FMVSS 214 NPRM pole	32km/h	35km/h

Figure 15 compares the rib deflections of the Mid Size Male for single and dual stage side airbags under these aggravated conditions. The figure shows that the second stage can be effectively used to improve protection in the three most severe tests.

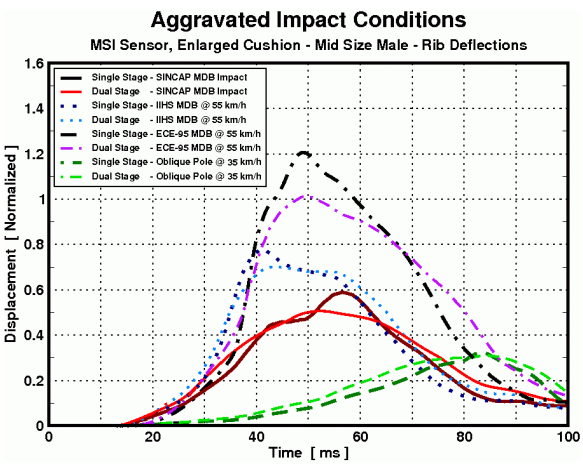

Figure 15. Aggravated Impact - Mid Size Male

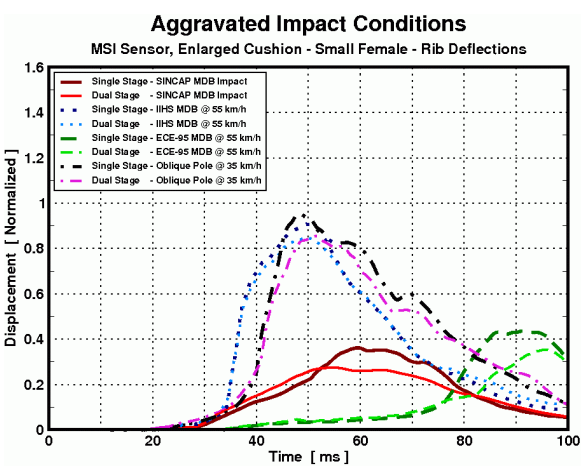

Figure 16. Aggravated Impact – Small Female

More benefit is obtained from the dual stage side airbag under more severe conditions, with little or no adverse effects on the performance for the lower severity tests. The peak rib deflection was reduced by 20% in the pole test with the use of the dual stage inflation. Figure 16 shows the results for the small female dummy under the increased speed impacts, which illustrate that the second stage improves the protection moderately for all tests.

DISCUSSION

The CAE analysis presented thus far intends to provide a basic starting point for the consideration of the potential benefits of adaptation in side impact protection. The results indicate that further analysis would be beneficial in order to optimize a second stage inflator by analyzing the tradeoffs for peak inflation levels in each stage, airbag volume, vent rate and other influencing factors. The achieved system must also show an improved benefit/cost ratio.

The MSI signal was used to estimate crash severity to derive a 2nd stage inflation decision and TTF2, from Table 1. From inspection of the results from figure 13-15, deployment of a second stage can be effective in reducing rib deflections in severe crash impacts. However, the severity threshold for deciding to deploy or not deploy the second stage must be carefully analyzed for each platform. For example, the MSI sensor location is chosen to balance fast TTF response over all regulatory tests. Inspection of Table 1 shows that the MSI effectively estimated severity for the FMVSS 214 MDB and the ECE R95 crash modes. The FMVSS 214 MDB (54km/h ***equivalent speed***) crash mode is rated slightly less than two thirds as severe as the ECE R95 crash mode (34km/h ***equivalent speed***). This same ratio is also approximately maintained in the peak values of the rib deflection values in those crashes. However, the MSI rates the FMVSS 214 MDB crash mode (63km/h ***equivalent speed***) more severe than the IIHS crash mode (50km/h ***equivalent speed***), but the IIHS crash mode produce more rib deflection. The reason for this is that the impact location of the IIHS barrier and the FMVSS 214 MDB are different. In the early phases of the crash, the IIHS barrier produces about the same average intrusion in proximity to the MSI sensor as the FMVSS 214 MDB. Therefore the IIHS ***equivalent speed*** is the same as the actual IIHS impact speed. This behavior can be tuned by optimal sensor placement to detect intrusion in the crash modes causing the worst injuries. This is an elegant way to allow the most protection for the most vulnerable point of the vehicle structure.

Real World Considerations

This analysis utilized a side airbag with greater width, which allows for a wider cover of the rib cage. This may provide additional benefits under real world impact conditions. For example, whereas the FMVSS 214 NPRM pole standard utilized an oblique impact angle of 75 degrees, recent NASS and FARS statistics on side impact suggest that the average "real world" impact incident angle for car-to-pole and car-to-car is approximately 63 degrees. The better thorax coverage of the enlarged airbag may afford additional benefits under such angled impact conditions. Not investigated in this study, but of equal perceived benefit is that the earlier trigger time afforded by the MSI sensor may allow for a more effective utilization of the side curtain restraints.

As shown in this paper the MSI can determine quickly whether a severe impact occurs. This information can be used to set various possibilities of adaptable restraints. For this paper, only a two-staged inflation of the side bag was considered. This was done to keep the number of simulation runs at an acceptable level. The ability of the MSI to detect and evaluate crash severity could be used for additional methods of restraint adaptation. Generally, adaptation of side restraints can be achieved by changing the properties of any of the following.

- **Bag shape variation** in x- or y- direction would adapt the cushion either to more absorption depth by the same deployment pattern compared to a side bag with a smaller depth or would improve the performance for oblique pole impacts. A challenging issue is to maintain the pressure at a balanced level during and after the extra expansion of the cushion shape.

- **Inflation method** by either having a 2-(or more) stage inflator or through by-passing a certain amount of gas generated from an "over-dimensioned" inflator can change the bag characteristics dramatically. This approach would cause differences in pressure level dependant on the demand necessary for a specific situation.

- **Active venting** on / off or even changing the size of the vent hole would generate a drastic improvement depending on the situation. It would have to be determined if an analog way or just a digital on/off function is sufficient. To optimize the restraint force-deflection characteristics an active adjustment of the vent hole seams to be most promising. [11]

Another potential method to improve side impact protection is by using information from occupant classification sensors in the car. As an example, seat weight classification systems can be used by the side protection system to selectively deploy or not deploy adaptive restraint functions. In the future, more sophisticated sensors can provide occupant position and stature information in real-time to continuously adapt the restraint optimally to the current conditions. Ultimately, fast deployment times and crash severity measures derived from MSI will be integrated as a key element in a holistic system safety approach.

CONCLUSIONS

In the introduction of this paper, a supporting case was made to consider new concepts for side impact crash protection. This paper has shown that the MSI provides fast restraint deployment as well as crash severity which can be used in improved protection adaptive side restraints.

This paper has also shown that there is still significant potential, for transferring more information from the crash sensor to the restraint system (e.g. crash severity) and by optimizing the restraint to make full use of the possibilities offered by the crash sensor (e.g. bigger cushion if faster TTF's are available).

If the crash sensor can also provide crash severity, adaptive restraints for side crashes are a first new path to follow, to further decrease fatalities and injuries, particularly in the case of more severe impact conditions which are expected to be reflected in future regulatory test standards.

REFERENCES

[1] Bauer et. al. 2005. "Adaptive depth airbag ", US Patent 20060249943.

[2] Fujimura et. al. 2001. "Airbag device with position adjusting mechanism", US Patent 6250677.

[3] Yokota et. al. 2005. "Side Airbag", US Patent 6976702.

[4] Cech et. al. 2005. "Active Magnetic Field Based Sensing System for Improved Detection and Discrimination of Side Impact Crashes", 19th ESV Conference, Washington DC, 2005.

[5] US Department of Transportation. "Traffic Safety Facts 2005", http://www-nrd.nhtsa.dot.gov/pdf/nrd-30/NCSA/TSFAnn/TSF2005.pdf, Washington DC, 2005

[6] McNeill et. al. 2005. "Current Worldwide Side Impact Activities – Divergence versus Harmonization and the Possible Effect on Future Car Design", 19th ESV Conference, Washington DC, 2005.

[7] Neale et. al. 2005. "A Numerical Investigation into the Effectiveness of "Smart" Restraint Systems in Mitigating Injury Risk Under "Real World" Accident Conditions", 19th ESV Conference, Washington DC, 2005.

[8] Holding et. al. 2001. "An Evaluation of the Benefits of Active Restraint Systems in Frontal Impacts through Computer Modeling and Dynamic Testing", 17th ESV Conference, Amsterdam, 2001.

[9] Arbelaez et. al. 2005. "Delta vs for IIHS Side Impact Crash Tests and Their Relationship to Real-World Crash Severity", 19th ESV Conference, Washington DC, 2005.

[10] US Department of Transportation 2007. "The New Car Assessment Program Suggested Approaches for Future Program Enhancements", National Highway Traffic Safety Administration, 2007.

[11] Gonter et. al. 2005, "System Requirements and Potential of adaptive Occupant Protection" , VDI-Berichte Nr. 1911, 2005

SIDE IMPACT INJURY PREDICTION WITH FE SIMULATIONS OF THE NEW ADVANCED WORLD SID FE DUMMY MODELS

Yi Liu, Fuchun Zhu, Zhenwen Wang and Michiel van Ratingen
First Technology Safety Systems, Inc
47460 Galleon Drive
Plymouth, MI 48170
United States
Paper Number 07-0372

ABSTRACT

Two new World SID (50th and 5th) FE models were developed for providing virtual tools of predicting occupant injuries during vehicle side collisions. The virtual dummy models have been verified with their physical counterparts in aspects of lab certification tests, bio-fidelity and sled tests. Many new techniques have been utilized in the model development including advanced testing and material modeling which guaranteed the high fidelity between the virtual models and the physical dummies. The good model-to-test correlations of various loading configurations have shown that the new FE models could be used as new tools in virtual simulations of vehicle side impact crash worthiness studies as options to other side impact dummies to predict better occupant injury due to superior bio-fidelity performances of the World SID dummies. The new dummy models were also tested under vehicle FMVSS214 impact conditions. A comparison of occupant injury parameters extracted from the models between the World SID 5th and SID-IIs dummy were also made using the load case.

INTRODUCTION

In recent years, developments of internationally harmonized Anthropomorphic Test Devices (ATDs) have been initiated by the International Organization for Standardization (ISO). These efforts have lead to the birth of two new side impact dummies, i.e. the World SID 50th and 5th (representing a 50th percentile male and a 5th percentile female), aiming to replace the existing worldwide regulatory and research side impact dummies.

The World SID 50th dummy has been evaluated by organizations around the world such as the US OSRP, NHTSA, APROSYS (the European funded program) and others against the current 50th percentile male side impact dummies such as DOT-SID, EuroSID-1 and EuroSID-2, and BioSID to compare the bio-fidelity ratings. As shown in Table 1, the World SID 50th (revised prototype) achieved the best overall dummy rating and also the best single body region ratings for the head, thorax, abdomen and pelvis. [1] It can be seen that according to Table 1, the World SID 50th new dummy exhibits a more human-like response in the specified crash events and has the highest bio-fidelity rating of any existing side impact crash test dummies in the world.

Table 1. Bio-fidelity comparison of side impact dummies

	World SID 50th	BioSID	EuroSID-2	EuroSID-1	DOT SID
Head	**10.0**	**6.7**	**5.0**	**5.0**	**0.0**
Neck	**5.2**	**6.7**	**4.4**	**7.8**	**2.5**
Shoulder	**7.0**	**7.3**	**5.3**	**7.3**	**0.0**
Thorax	**7.9**	**6.3**	**5.2**	**5.4**	**3.1**
Abdomen	**6.4**	**3.8**	**2.6**	**0.9**	**4.4**
Pelvis	**7.8**	**4.0**	**5.3**	**1.5**	**2.5**
Overall	**7.3**	**5.7**	**4.6**	**4.4**	**2.3**

The World SID 5th dummy was created by FTSS after the successful launch of the World SID 50th production dummy. This is a scaled down version of the World SID 50th dummy. Like the World SID 50th dummy, the World SID 5th dummy (representing a woman of small stature and a young adolescent) was also developed under the direction of the ISO through the APROSYS in consultation with the World SID Task Group (ISO). Under current efforts, both versions of the World SID dummies will endeavor to provide the foundation for future common and internationally accepted regulatory test procedures. This will also enable automakers and researchers worldwide to improve passenger safety by facilitating the comparison of crash test results.

The demand for virtual simulations of vehicle crash by CAE has seen rapid increases in recent years thanks to the large increase in computing power and decrease in cost. The usage of Finite Element (FE) dummy models has been increasing over the years in CAE simulations of crashworthiness analysis and occupant protection. FTSS has been making great efforts on the successful development of virtual (FE) dummies since 1995. The World SID 50th and 5th FE dummy models have been developed recently to add to the ever expanding FE dummy database.

NEW DEVELOPMENT IN FE DUMMY MODELS

The development of new dummy models have been keeping the pace with advancing of new technologies available both in computing technique and in engineering software such as Ls-dyna3d and Pamcrash. Many new FE modeling technologies have been adopted in the new virtual dummy model development such as laser scanning for accurate dummy geometry, finer mesh and increasing use of solid (Hexa) elements, more component level model-to-test validations and better material models.

In the World SID dummy hardware development, many new advanced materials were used. For example, Nitinol shape memory alloy was used for the rib to replace the high strength steel. The virtual dummy development also needs to match the new advances in hardware. Since no numerical material models for shape memory alloy (in solid elements) were available at the beginning of the virtual dummy model development, great effort has been made to work with the software developer and test the new material model to meet the challenge. The outcome is shown in Figure 1, the rib deflection in the virtual dummy model performed better and closer to test results when the new material model (for shape memory material) was used. Another example showing here is how to use of a numerical material model to describe the hyperlast material that was used for pelvis flesh. To decide what material model to use, firstly the material was tested at quasi-static and dynamic loading as well as stress relaxation. Then the material behavior was analyzed and identified as non-linear elastic with viscous (highly strain rate dependent with fast stress relaxation

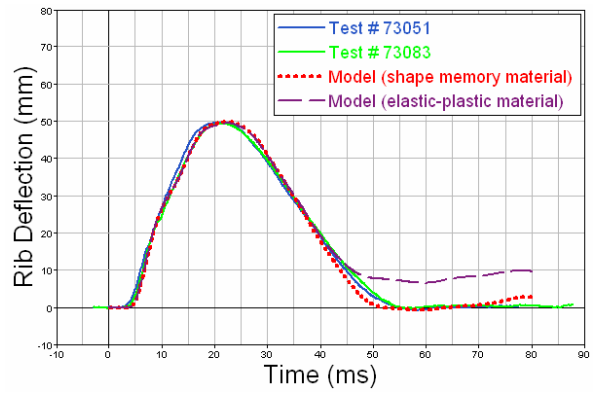

Figure 1. Rib deflection in dummy certification test – material model using latest technology

behavior). As a result, Ogden material model [2] was chosen to model the Hyperlast material in the virtual dummy models:

$$W = \sum_{i=1}^{3}\sum_{j=1}^{n}\frac{\mu_j}{\alpha_j}(\lambda_i^{*\alpha_j}-1)+K(J-1-\ln J) \qquad (1).$$

Here, λ is stretch, K is the bulk modulus, $J = \lambda_1\lambda_2\lambda_3$ and $\lambda_i^* = \lambda_i J^{-1/3}$, μ_i and α_I terms are non-integer values. The stress expression is

$$\sigma_i = \frac{1}{\lambda_j\lambda_k}\frac{\partial W}{\partial \lambda_i} = \frac{\lambda_i}{J}\frac{\partial W}{\partial \lambda_i}$$
$$= \sum_{j=1}^{n}\frac{\mu_j}{J}\left(\lambda_i^{*\alpha_j} - \sum_{k=1}^{3}\frac{\lambda_k^{*\alpha_j}}{3}\right) + K\frac{(J-1)}{J} \qquad (2).$$

This can be simplified further for the hyperlast material ($\nu \sim 0.5$):

$$\sigma_i = \sum_{j=1}^{n}\mu_j\left(\lambda_i^{\alpha_j} - \sum_{k=1}^{3}\frac{\lambda_k^{\alpha_j}}{3}\right) - p \qquad (3).$$

Here p is pressure. In uni-axial case, $\lambda_2 = \lambda_3 = \lambda_1^{-1/2}$,

and $p = -\frac{\sigma_1}{3}$, therefore

$$\sigma_1 = \sum_{j=1}^{n} \mu_j \left(\lambda_1^{\alpha_j} - \lambda_1^{-\alpha_j/2} \right) \quad (4).$$

A numerical procedure has been developed at FTSS to extract the Ogden parameters (up to 8 pairs of μ_i and α_i) for rubber and hyperlast materials by curve-fitting eq.(4) to the stress-stretch data obtained from uni-axial material tests.

MODEL VALIDATIONS

Before an FE model was released, it had to pass various certification tests. Typical certification tests for the World SID dummies include head drop, neck pendulum impact, and full dummy pendulum impact at different locations on the dummy. Besides the certification tests, more model-to-test validations were carried out such as sled impact tests, arm and rib cage drop tests.

The FE models were validated at three levels: material, component and whole dummy assembly. Table 2 and 3 list the material/component, dummy certification and bio-fidelity tests for World SID 50th and 5th dummies that have been used for the virtual dummy model development.

Table 2. Lab certification and bio-fidelity tests for the World SID 50th dummy

	Certification tests	Material/Component tests	Sled tests
Head	**200mm later drop (L+R) 376mm frontal drop**	**Head skin vinyl**	
Neck	**Lateral impact at 3.4m/s**	**Neck rubber**	
Shoulder	**Pendulum impact at 4.3m/s**	**Arm foam, Arm drop Rib drop at 3 velocities**	**WSU – 6.8m/s Heidelberg – 6.8m/s**
Thorax w/o arm	**Pendulum impact at 4.3m/s**	**Rib drop at 3 velocities**	
Thorax with half arm	**Pendulum impact at 6.7m/s**	**Rib drop at 3 velocities**	**WSU – 6.8m/s Heidelberg – 6.8m/s**
Abdomen	**Pendulum impact at 4.3m/s**	**Rib drop at 3 velocities**	**WSU – 6.8m/s Heidelberg – 6.8m/s**
Pelvis	**Pendulum impact at 6.7m/s**	**Pelvis hyperlast foam**	**WSU – 6.8m/s Heidelberg – 6.8m/s**

Table 3. Lab certification and bio-fidelity tests for the World SID 5th dummy

	Certification tests	Material/Component tests	Drop tests	Sled tests
Head	**200mm later drop (L+R) 376mm frontal drop**	**Head skin vinyl**		
Neck	**Lateral impact at 3.4m/s**	**Neck rubber**		
Shoulder	**Pendulum impact at 4.3m/s**	**Arm foam, Arm drop Rib drop at 3 velocities**		**WSU – 6.8m/s Heidelberg – 6.8m/s**
Thorax w/o arm	**Pendulum impact at 4.3m/s**	**Rib drop at 3 velocities**		
Thorax with half arm	**Pendulum impact at 6.7m/s**	**Rib drop at 3 velocities**	**1.0m 0.5m**	**WSU – 6.8m/s Heidelberg – 6.8m/s**
Abdomen	**Pendulum impact at 4.3m/s**	**Rib drop at 3 velocities**	**1.0m 0.5m**	**WSU – 6.8m/s Heidelberg – 6.8m/s**
Pelvis	**Pendulum impact at 6.7m/s**	**Pelvis hyperlast foam**	**1.0m 0.5m**	**WSU – 6.8m/s Heidelberg – 6.8m/s**

COMPONENT LEVEL VALIDATIONS

As a typical example, Figure 2 and 3 shows the model-to-test validation of the World SID 5th FE rib model. Three impact velocities were used in the validations that resulted the rib deflections in the range of 20 ~ 40 mm. Both the rib deflections and pendulum impact accelerations (forces) from the FE model are correlated very well with the tests. The 'shape memory' material model worked well in this case to represent the Nitinol shape memory material in the physical dummy as shown in the rib deflection plots. Other component level validations including head drop, neck pendulum and arm drop are detailed in the FTSS technical publications. [3]

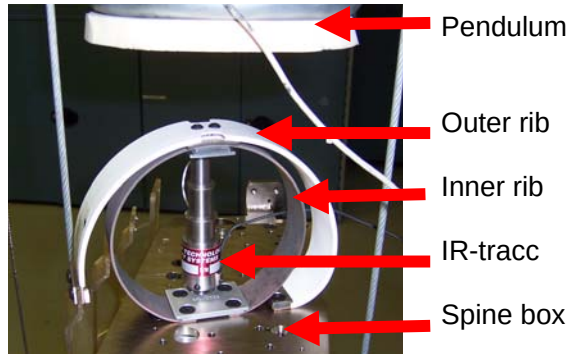

Figure 2. World SID 5th rib drop test set-up

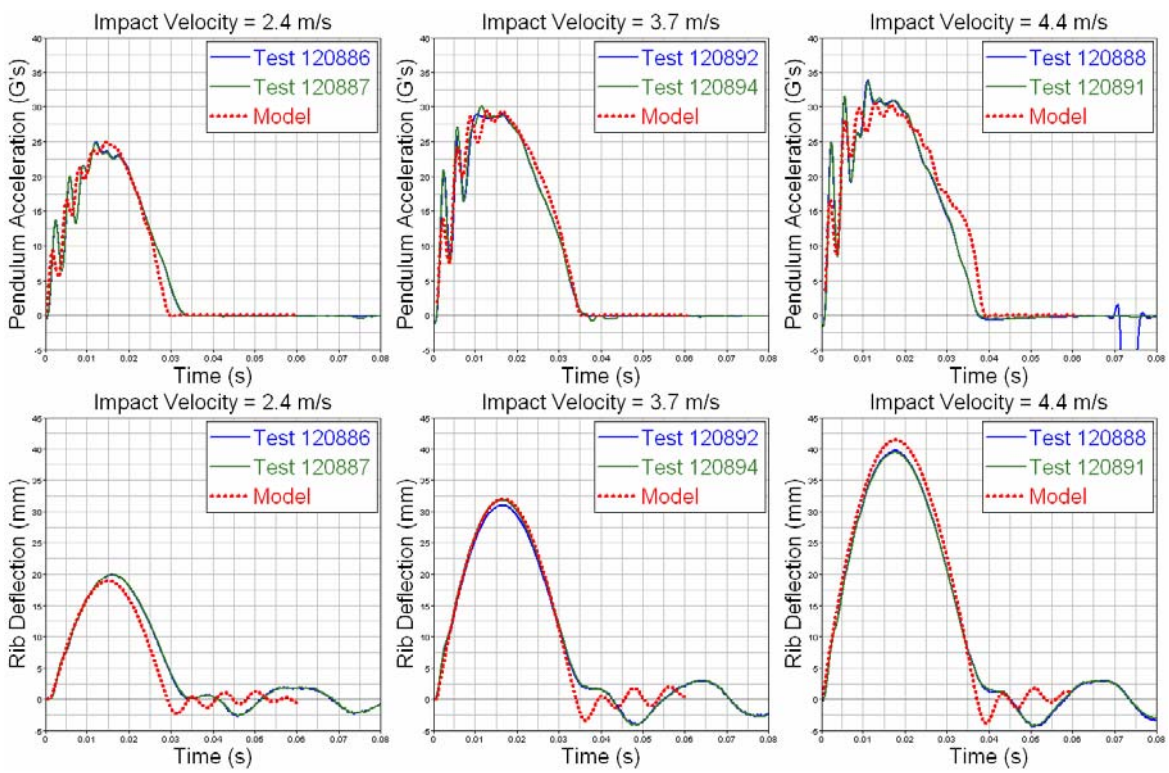

Figure 3. World SID 5th rib drop component level model-to-test validation

WHOLE DUMMY LEVEL VALIDATIONS

Whole dummy level validations including pendulum impact certification tests, sled tests and drop tests designed for biomechanics verification purposes.

Figure 4 and 5 show the model-to-test set-up and results of the World SID 50th thorax without arm impact. The certification corridors shown in the Figure 5 for such test have been specified by ISO based on biomechanics study on cadavers. [1]. It can be seen the current FE model (World SID 50th) correlates very well with the test results.

Pendulum mass: 23.4kg
Impact speed: 4.3 m/s

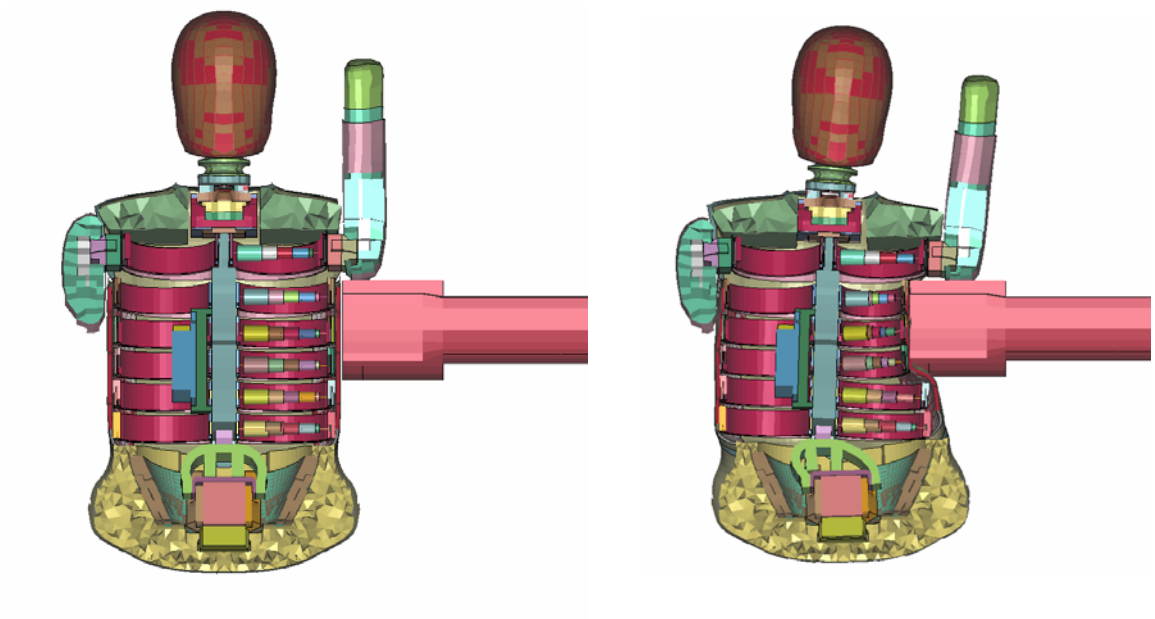

Initial position **Maximum rib deflection at 20ms**

Figure 4. World SID 50th pendulum impact FE model set-up

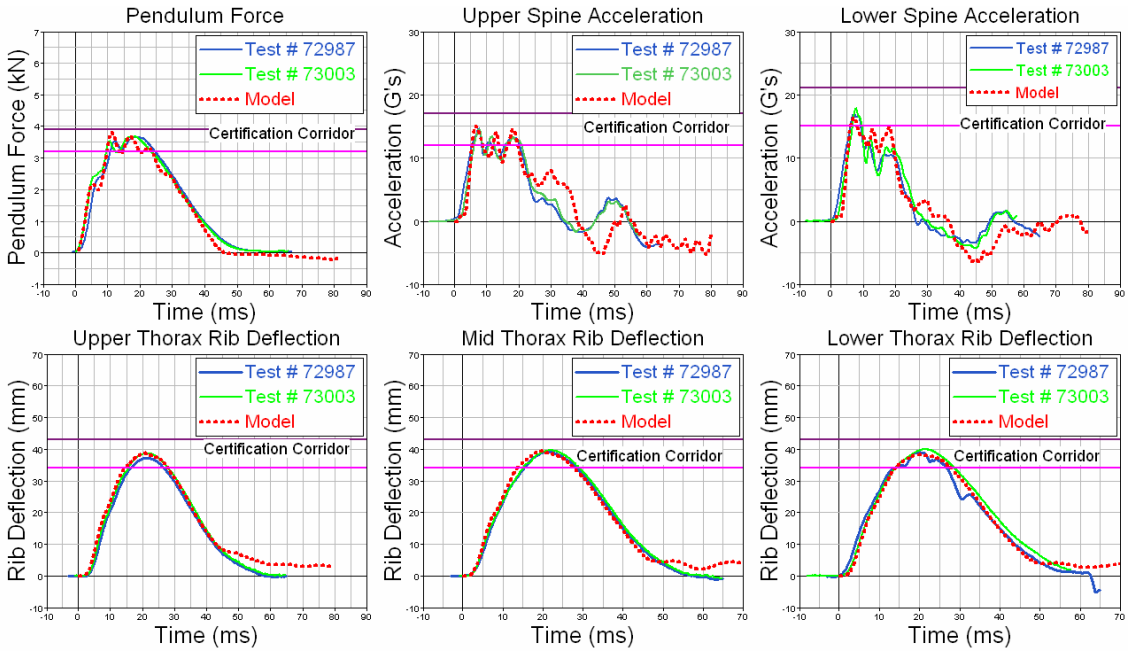

Figure 5. World SID 50th thorax without arm pendulum impact certification model-to-test validation

SLED TEST LEVEL VALIDATIONS

The World SID FE dummy models have been validated at sled level tests. These tests include Wayne State University (WSU) type sled test [4] and Heidelberg type sled test [5]. The World SID 50th Heidelberg sled test (6.7m/s impact) configuration and model-to-test validation results are shown in Figure 6 and 7. The FE model correlates with tests very well; as an example, the rib deflections correlations are shown in Figure 7. Other details of validations can be found in FTSS's technical publications [3].

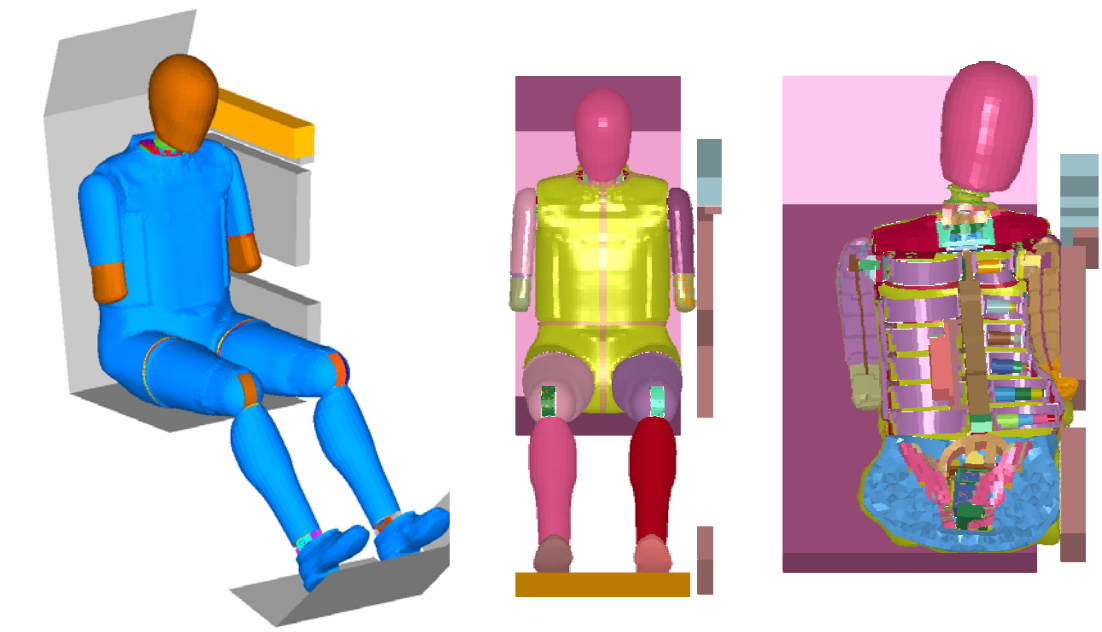

Heidelberg sled impact set-up **Time=0** **Time=25 ms**

Figure 6. World SID 50th FE dummy model Heidelberg sled test set-up

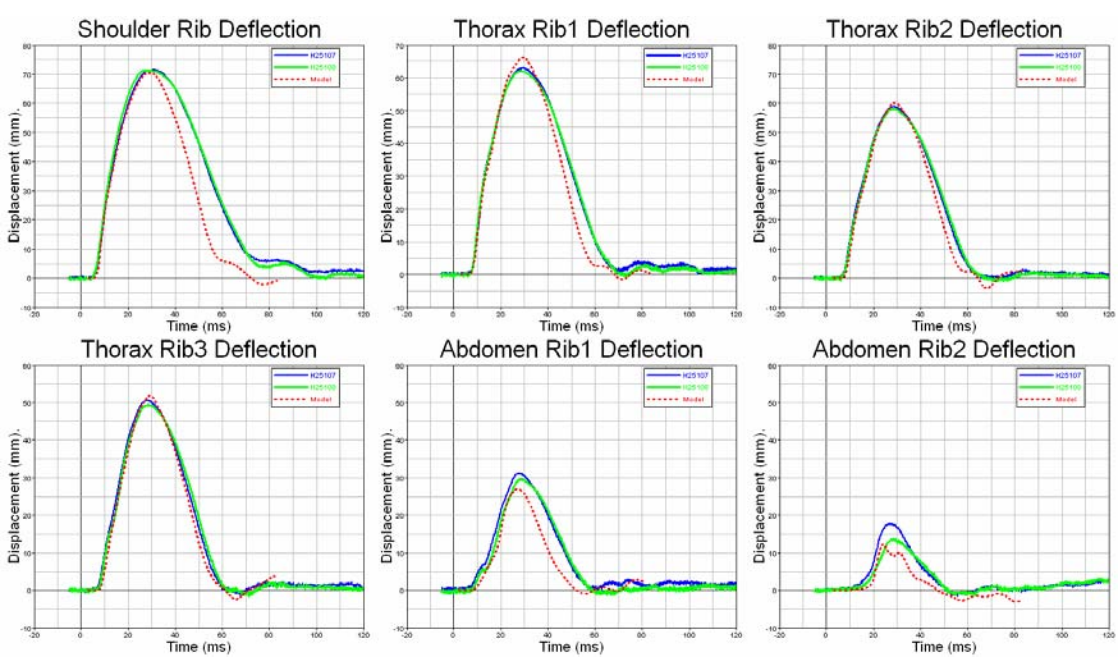

Figure 7. World SID 50th Heidelberg sled test model-to-test validation

DUMMY INJURY PREDICTION WITH VIRTUAL DUMMY MODELS

The occupant injury parameters can be extracted from the virtual dummy models after the simulation. Table 4 summaries the occupant injury parameters from the World SID and other side impact dummies such as SID-IIs and ES2 (ES2-re) that can be used to derive the occupant injury criteria as required by regulations, auto insurers and consumer oriented requirements.

Table 4. Dummy injury parameters extraction (√= available in current dummy)

Occupant injury parameters	World SID 5th and 50th	SID-IIs	ES2 (ES2-re)
HIC36/HIC15	√	√	√
Upper neck force&moment	√	√	√
Lower neck force&moment	√	√	√
Shoulder rib disp. and acc.	√	√	
Thorax rib 1 disp. and acc.	√	√	√
Thorax rib 2 disp. and acc.	√	√	√
Thorax rib 3 disp. and acc.	√	√	√
Abdomen rib 1 disp. and acc.	√	√	
Abdomen rib 2 disp. and acc.	√	√	
T1 acc.	√	√	√
T4 acc.	√		
T12 acc.	√		√
Arm upper&lower acc.		√	
Lumbar force&moment	√	√	
Pubic force	√	√	√
Illiac force	√	√	
Acetabulum force	√	√	
Shoulder force&moment	√		√
Pelvis acc.	√		√
Abdomen force			√
Back plate force&moment			√
T12 force&moment			√
Knee force	√	√	
Upper&lower femur force	√	√	
Upper&lower tibia force	√	√	

The World SID 50th and 5th dummy models have been tested in FMVSS214 oblique pole and moving deformable barrier (MDB) impact environments. Figure 8 shows the World SID 5th FE model simulated in a FMVSS214 MDB load case. The test configuration is that the occupant is seated in driver's seat in standard driving position as specified in FMVSS214. The MDB load case is applied to a mid-size car that equipped with a thorax airbag. The dummy and internal deformation at the peak of impact is depicted in Figure 8.

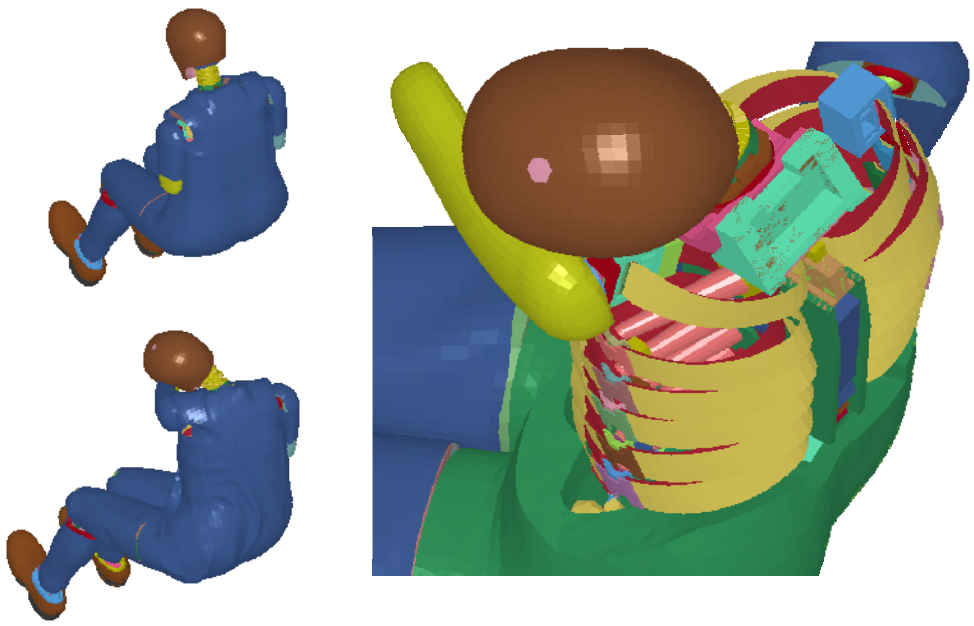

Figure 8. World SID 5th dummy model at peak impact under a FMVSS214 oblique pole impact simulation

As a comparison of performance a SID-IIs dummy model was also tested in exactly the same FMVSS214 MDB side impact environment as the World SID 5th dummy model. The occupant parameter outputs from the simulations are listed in Table 5 and the rib deflections from both models are shown in Figure 9. As shown in Figure 9, the maximum rib deflections for shoulder and top/middle thorax ribs from the 2 dummies are quite close**.** However the bottom thorax and abdomen rib deflections from the World SID 5th are generally lower. Other injury parameter comparisons between the 2 dummies can be found in Table 5.

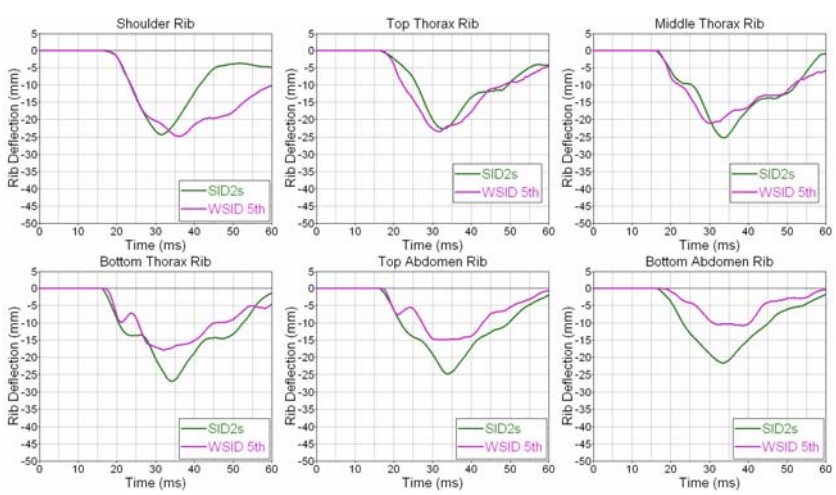

Figure 9. Rib deflections from World SID 5th and SID-IIs in FMVSS214 oblique pole impact

Table 5. Occupant injury parameters comparison: World SID 5th vs. SID-IIs in FMVSS214 MDB impact

Occupant Injury Parameters	World SID 5th	SID-IIs
HIC36	48.46	27.91
Upper Neck Fz+ (kN)	0.911	0.871
Upper Neck Fz - (kN)	-0.070	-0.222
Shoulder Rib Deflection (mm)	24.77	24.26
Top Thorax Rib Deflection (mm)	23.35	22.60
Middle Thorax Rib Deflection (mm)	20.99	25.18
Lower Thorax Rib Deflection (mm)	17.84	26.75
Upper Abdomen Rib Deflection (mm)	14.92	24.80
Lower Abdomen Rib Deflection (mm)	10.76	21.62
Upper Thorax Rib VC (max)	0.294	0.309
Middle Thorax Rib VC (max)	0.263	0.348
Lower Thorax Rib VC (max)	0.271	0.339
Upper Abdomen Rib VC (max)	0.174	0.309
Lower Abdomen Rib VC (max)	0.076	0.155
T12 Lower Spine Accel Resultant (G)	37.96	44.58
Pubic Load (kN)	0.688	0.172
Combined Illiac & Acetabulum Load (kN)	0.451	2.466
Shoulder Compression Force (kN)	0.784	1.223
Pelvis Acceleration (G)	48.81	32.69

CONCLUSIONS

- World SID 5th and 50th virtual dummy models have been developed that incorporated with latest advances in FE technology. The new models correlated very well at components, sub-assembly and full dummy level certification and sled tests.
- The models have been tested in FMVSS214 side collision environments. The injury parameters can be extracted from the dummy models to calculate occupant injury criteria as required by regulatory, insurers and consumer assessment programs.
- It has shown that the current virtual dummy models have performed and validated well against tests and the authors believe that these models are able to predict reasonable and reliable occupant injury in crashworthiness and safety analysis.

REFERENCES

1. "Road vehicles – Design and performance specifications for the World SID 50th percentile m al e side impact dummy (Part 1~ Part 4)", ISO TC 22/SC 12N, Oct. 2004.
2. Ogden, R.W., "Large Deformation Isotropic Elasticity – On the Correlation of Theory and Experiment for Incompressible Rubber like Solids," Proc. Royal Soc. London, A326, pp. 565-584, 1972.
3. FTSS FE Model Development Technical Report, "World SID 50th (ver. 2.0) and World SID 5th ", (ver 1.0), 2007.
4. Cavanaugh, J.M., Walilko, T.J., Malhotra, A., Zhu, Y., King, A.I., 1990, "Biomechanical Response and Injury Tolerance of the Thorax in Twelve Sled Side Impacts", Proceedings of the 34th Stapp Car Crash Conference, paper # 902307.
5. Marcus, J.H., Morgan, R.M. and EPPINGER, R. "Human responses and injury from lateral impact", SAE 831634 in Proceedings of the 27th Stapp car crash conference. Warrendale, PA, SAE 1983, pp419-433.

DEVELOPMENT OF A DOE/OPTIMIZATION CAE METHOD TO SIMULTANEOUSLY IMPROVE SIDE IMPACT OCCUPANT RESTRAINT SYSTEM PERFORMANCE FOR MULTIPLE TEST MODES

Sanjaya Fonseka
Honda R&D Americas Inc.
USA
Gaetan Van den Bergh
Noesis Solutions
Belgium
Paper Number 07-0476

ABSTRACT

The automotive industry today faces the challenge of developing a single side impact occupant restraint system to meet performance requirements for multiple crashworthiness test modes. The side air bag, door liner, and vehicle side body structure are key systems that affect the injury criteria of the occupant. This paper discusses how DOE/optimization methods are used to quickly develop a specification for the side air bag and door liner that meets occupant injury criteria for three different side impact test modes. The work detailed in this paper focuses on occupant protection assessment based on three different CAE side impact sled models using ES2-re, DOT-SID and SID-2s, dummy models to evaluate the new FMVSS 214, SINCAP and SICE test modes.

Ten design variables were selected from air bag and door liner parameters which include mass flow rates, vent areas, two variables that define the location of the bag, and material/thickness of the door liner. Occupant injury parameters such as rib deflections/accelerations, pelvis accelerations/forces, and abdomen forces were selected as the responses. As the first step, a latin hypercube DOE method was used to evaluate sensitivity of the design variables to occupant injury parameters. Based on the DOE dominant design variables, optimization criteria and methods were established for the next step. Key injury criteria for each test mode were selected as the constraints. A self adaptive evolution (SAE) global optimization method was used to carry out automated simultaneous simulations. Based on the optimization results eleven feasible design specifications were found. Out of these candidates the optimum design was selected for further evaluation.

INTRODUCTION

Government and insurance institutions have introduced many safety standards that auto manufacturers should comply with to reduce the risk of serious and fatal injury to occupants in side impact crashes. To achieve a desired crashworthiness the auto industry focuses on developing better side body structures and efficient occupant restraint systems.

Typically the vehicle is subjected to multiple side impact test modes to verify that it meets the required standards. The traditional approach is to tune the restraint system to each test mode separately. This is a very laborious process as a restraint system which is good for one test mode may not work for another. This may induces higher costs and large lead times to find a restraint system that is good for all test modes. Still the engineer may not find the optimum system.

Today the use of occupant simulation is an integral part of restraint system development process. This study introduces an occupant simulation based methodology to find an optimum restraint system in a multi test mode scenario.

This methodology employs design of experiments (DOE) and numerical optimization techniques. Design variables that are most sensitive to the responses and optimization technique were found based on the DOE. A latin hypercube sampling method was selected for the DOE. This is because the user can specify the number of experiments and it ensures the ensemble of random numbers as a good representative of the real variability.

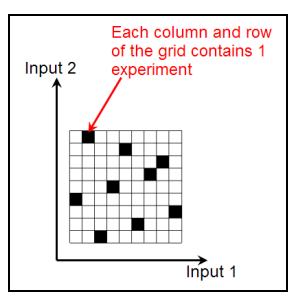

Figure 1. Latin Hypercube Technique

As shown in Figure 1 the Latin hypercube generates random experiments which are more uniform across the design space.

The numerical optimization method employed was self adaptive evolution. This is a global optimization method in which results are not depended on the starting point. Also iterations are calculated in parallel and tend to converge to a global optimum.

This paper also discusses the application of the response surface method (RSM). A response surface is a simplified multi-dimensional surface fit to what is usually a more complex function. Response surface functions were developed by fitting taylor polynomial models through the DOE results. This was done primarily to evaluate fidelity of such functions for future work and also to quickly find design trade offs.

SCOPE OF THE PROJECT

Moving deformable barrier impacts are key to evaluate side restraint system. Therefore side sled models derived from new FMVSS 214, SINCAP and SICE test modes were used in this study. Air bag and door liner spec were varied to optimize the restraint system. Occupant injury criteria for each test mode were selected as the responses.

General Outline of the Project

- Process Integration and Automation: Creation of a work flow that automatically generates executes and extracts results for multiple design iterations.
- Design of Experiments (DOE): Evaluate sensitivity of air bag and door liner design variables to occupant injury criteria.
- Optimization: Finding the optimal characteristics for airbag and door liner that meets all injury criteria targets.
- Response surface model generation based on the design of experiments to evaluate fidelity of such functions.

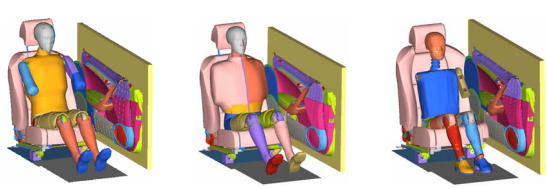

New FMVSS 214 with ES2-re **SINCAP with DOT-SID** **SICE with SID-2S**

Figure 2. Sled simulation models.

LS-DYNA dynamic code was used for sled test simulations.

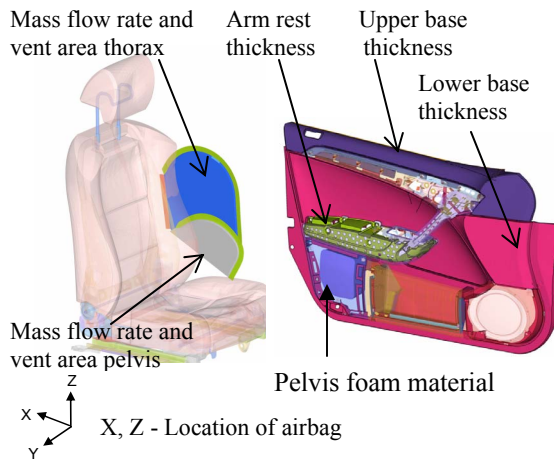

Figure 3. Design Variables.

OPTIMUS process automation software was used to integrate all 3 sled models into a single work flow which would make all simulations run in batch mode. This work flow automatically generates, executes input simulation files, and extracts results for multiple design iterations. This automation allows the user to evaluate multiple designs with little or no manual intervention.

DESIGN OF EXPERIMENTS

The number of experiments required in order to make valid conclusions is directly proportional to the number of design variables in the process. Therefore it is important to get the correct composition of design variables (some times referred as factors) that defines the problem which generally comes with experience. How much resources are available is a another important factor that effects the number of experiments to be conducted. Figure 4 shows the 10 design variables selected and their ranges normalized with respect to the upper bound.

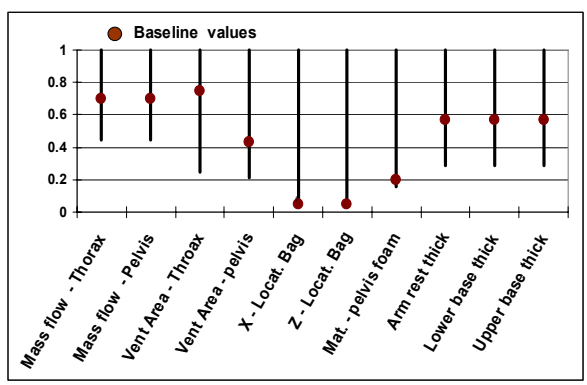

Figure 4. Air bag and door liner design variables.

For responses, rib deflections/acceleration, pelvis accelerations/forces, and abdomen forces were

measured. Injury criteria targets are based on the allowable response values dictated by each test mode. Figures 5,6,7 show baseline responses, normalized with respect to allowable levels.

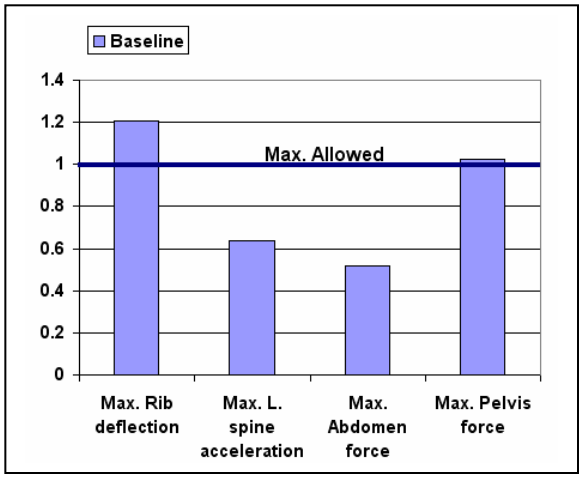

Figure 5. New 214 - Baseline injury responses

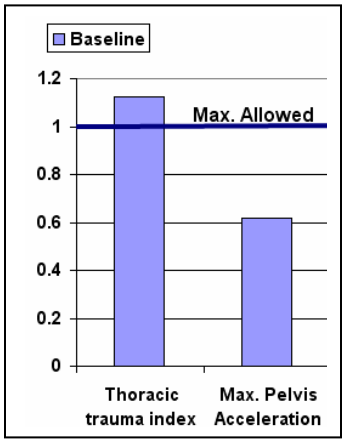

Figure 6. SINCAP - Baseline injury responses

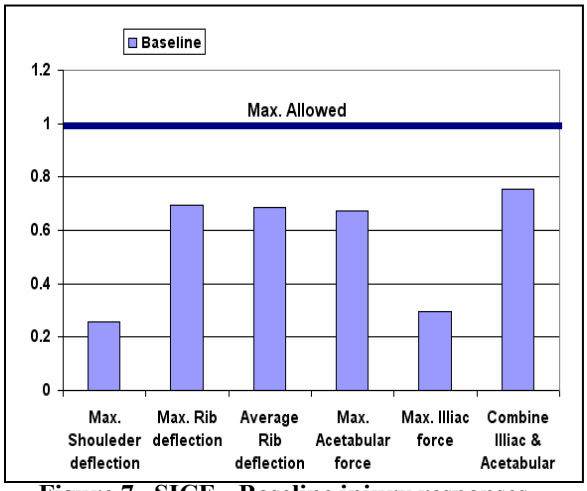

Figure 7. SICE - Baseline injury responses

Three baseline injury responses are above the maximum allowed. Therefore this is not a feasible design.

The primary goal of the DOE was to explore the design space to find the most dominant design variables for occupant injury criteria. Only these dominant design variables would be included in the optimization process. This would reduce computational time considerably as one additional design variable would require 12 additional experiments.

Based on the latin hypercube sampling method 96 experiments were simulated. That is a total of 288 simulations considering 3 test modes. 2 feasible designs were discovered based on the DOE. Injury responses for these designs are compared to the baseline in Figures 8,9,10.

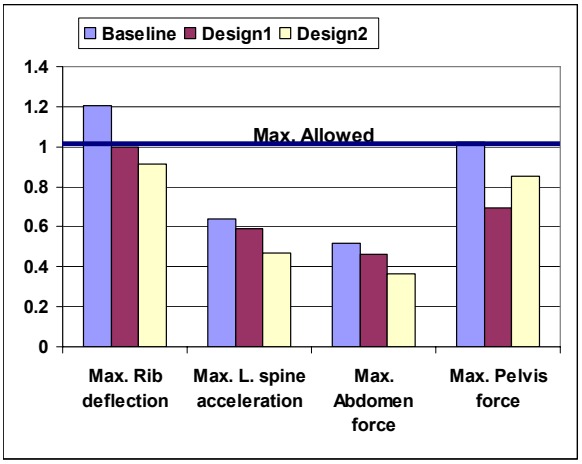

Figure 8. New 214 – Designs obtained from DOE compared to baseline.

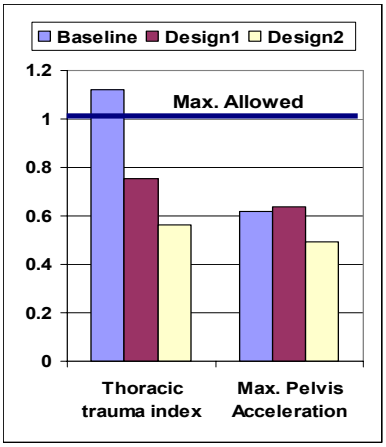

Figure 9. SINCAP – Designs obtained from DOE compared to baseline.

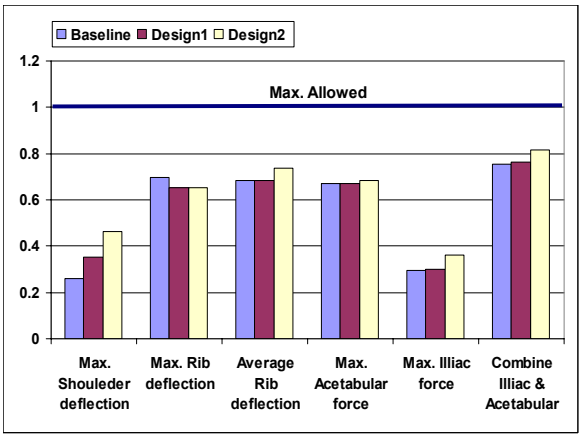

Figure 10. SICE – Designs obtained from DOE compared to baseline.

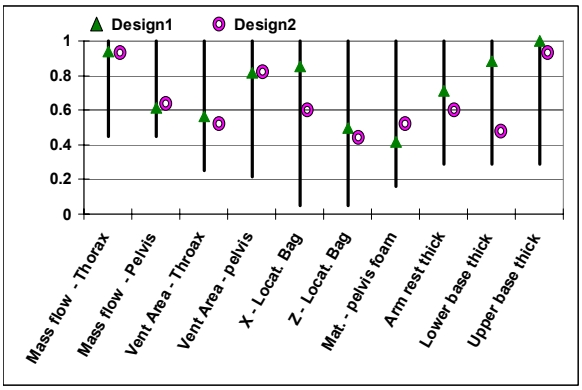

Figure 11. Feasible Design1, Design2.

Feasible Design1 and Design2 from the DOE have higher mass flow rate for thorax (see Figure 11). To achieve this level of mass flow rate, a higher pressure rated inflator would be necessary. This would be quite costly, thus not the anticipated solution.

A correlation value matrix which was generated based on the DOE gives information on the level of correlation between the design variables and the responses.

Table 1.
Sample correlation values

	Vent area - thorax	Z – location of the bag
Upper rib deflection - SINCAP	0.808	0.022
Thoracic Trauma Index - SINCAP	0.748	0.026
Average rib deflection - SICE	-0.701	0.060

The correlation value is always between +1 and -1. A correlation close to +1 or -1 signifies that responses and corresponding design variables are mostly linearly related, while a value close to zero indicates that they are fairly independent. Table 1 show that the upper rib deflection-SINCAP is linearly related to the vent area-thorax because of the higher correlation value between these. Therefore the best way to influence the rib deflection is to vary the vent area. On the other hand, the location of the bag in z-direction has almost no influence on any of the occupant injury responses. Thus this design variable can be neglected during the optimization. Based on the low correlation values seen, 4 design variables were taken out of the optimization process.

OPTIMIZATION

The noisy, non-linear nature related to crash analysis reduces the utilization of gradient-based optimization methods. Therefore the global optimization method 'Self-Adaptive Evolution' is selected to drive the optimization. The Self Adaptive Evolution (SAE) strategy is directly based on real valued vectors when dealing with continuous parameter optimization problems. It is a multi-recombinant scheme based on a population of designs and this algorithm's strategy is to imitate biological mutation and selection. Designs with the best fit from the current total population will be selected as the parents for the next generation. The multi-recombinant method used here selects multiple parents to generate one offspring. Mutation is independently applied to each design. This way old generation produces a new generation. The new generation fitness is then calculated and new offspring are made. The algorithm has convergence criteria, and for certain ranges, algorithm parameter values have been determined for improved performance.

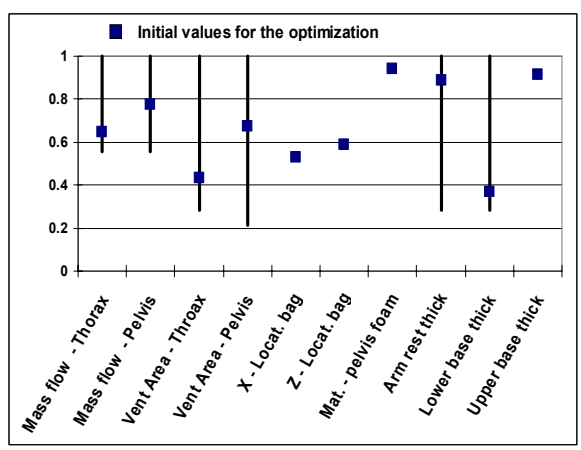

Figure 12. Based on correlation values. x, z-location of the bag, mat-pelvis foam and upper base thickness were taken out of the optimization.

The design range for the mass flow rate was reduced so that the same air bag inflator could be used. The list of experiments with this new range was found from the DOE without any additional computations. Out of these best doe experiment was selected as the starting point for the optimization. Although the global optimization method does not necessarily depend on the starting point, this will enable a faster convergence. At the start of the optimization 2 responses violate the constraints.

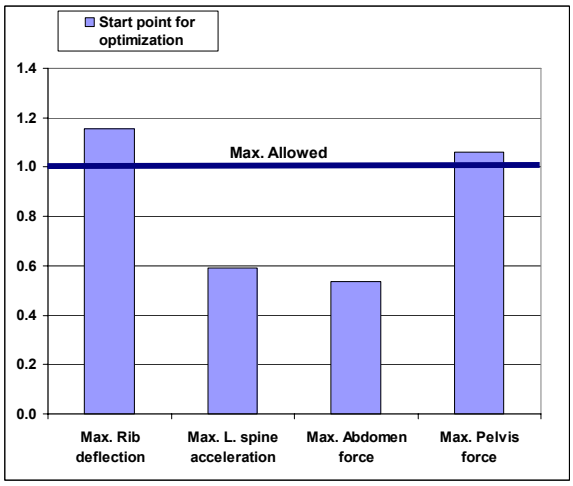

Figure 13. Two constraints were violated for New 214. SINCAP and SICE responses were with in the allowable range at the start of optimization.

The objective function for the optimization was based on the most critical responses. The responses selected for the objective function were thoracic trauma index from sincap, and max. rib deflection, max. pelvis force from new 214.

Objective Function: Normalized (Thoracic Trauma Index + Max. rib deflection + Max. pelvis force).

Six iterations were carried out for the optimization. A single iteration consists of 12 experiments. Therefore 72 experiments (a total of 216 simulations considering 3 test modes) were simulated. Following mass flow rate thorax vs pelvis section plots shows the optimization progress (Figure 14-19). The first and second iterations could not find any feasible design. The third iteration finds 2 feasible designs. The fourth iteration will focus more on these optimal regions. This leads to discovery of 2 more feasible designs. In fifth and sixth iteration the algorithm keeps focusing on this region and it discovers 7 feasible designs. Some of the iterations contain fewer experiments than the population size. This was due to some experiments failed due to model instabilities and was ignored by the optimization.

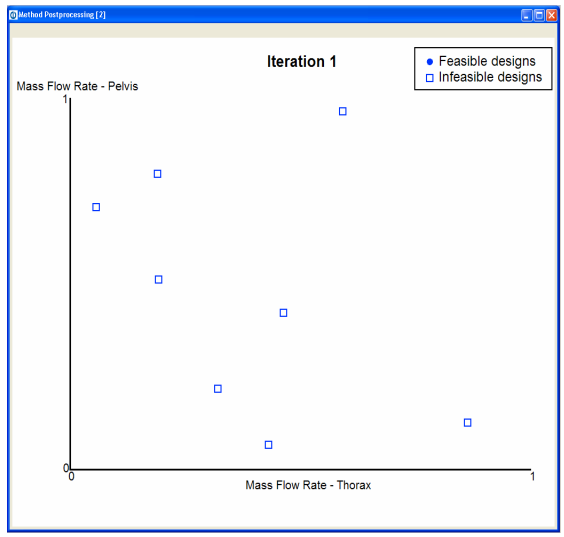

Figure 14. Optimization iteration1. No feasible designs were found.

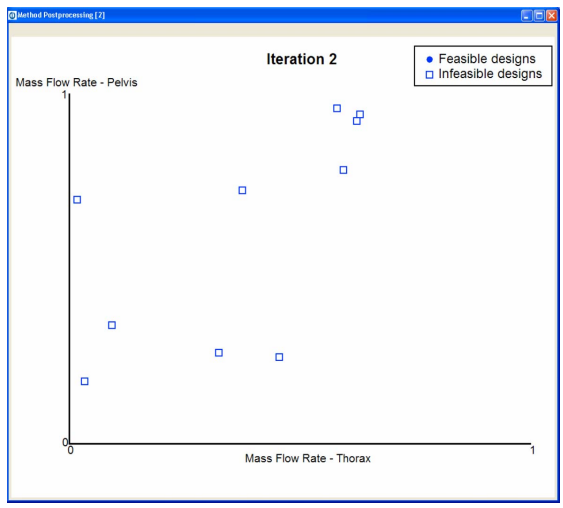

Figure 15. Optimization iteration2. No feasible designs were found.

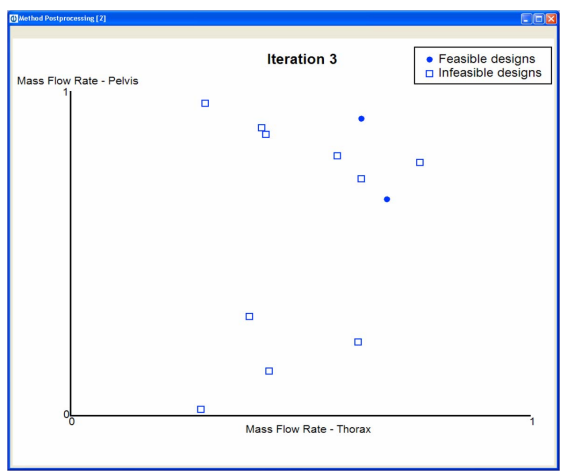

Figure 16. Optimization iteration3. 2 feasible designs were found.

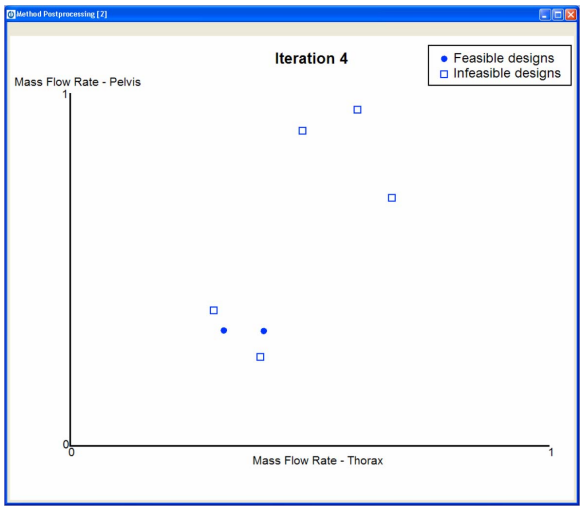

Figure 17. Optimization iteration4. 2 feasible designs were found.

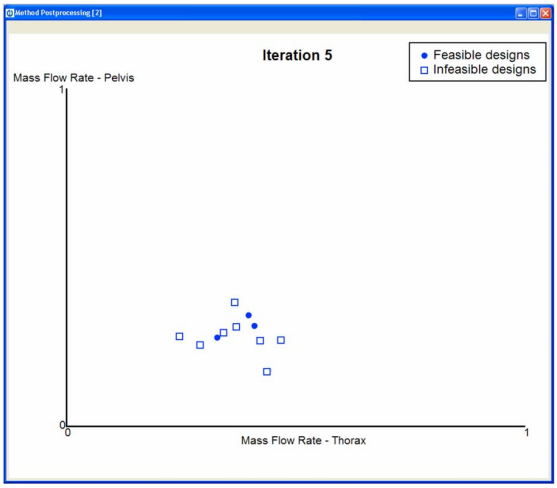

Figure 18. Optimization iteration5. 3 feasible designs were found.

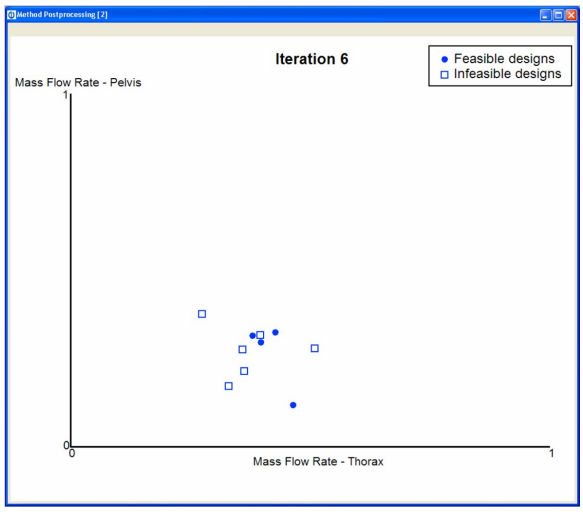

Figure 19. Optimization iteration6. 4 feasible designs were found.

The injury responses for baseline vs optimum design are compared;

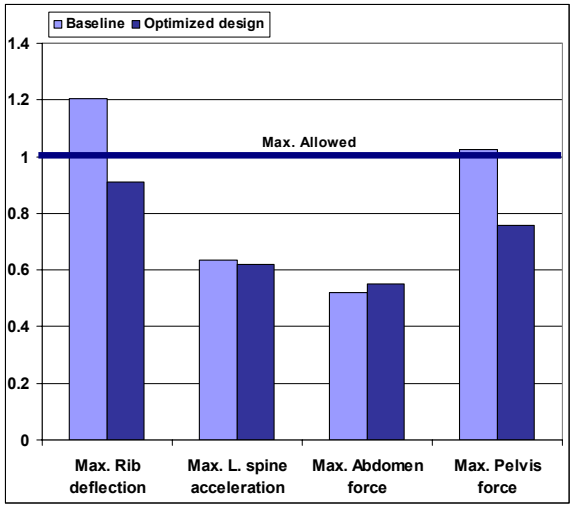

Figure 20. New 214: Baseline vs Optimized design.

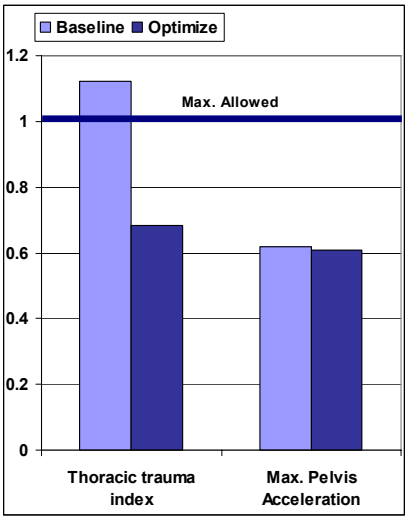

Figure 21. SINCAP: Baseline vs Optimized design.

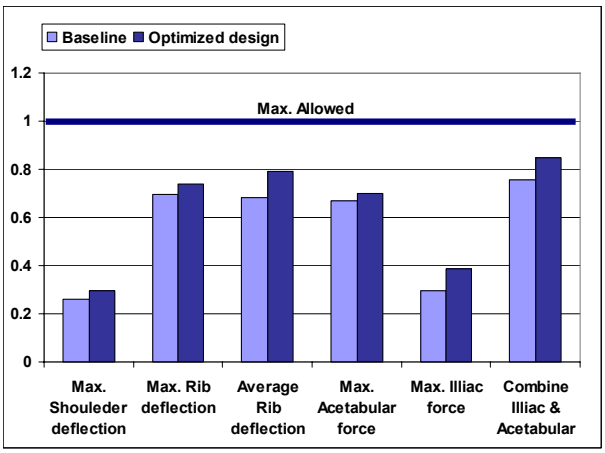

Figure 22. SICE: Baseline vs Optimized design.

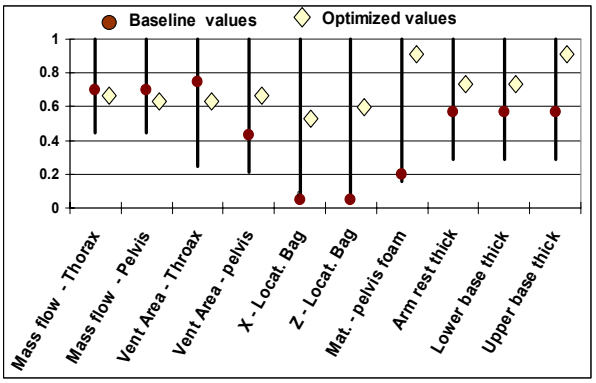

Figure 23. Comparison of baseline and optimized design.

Out of 11 feasible designs the most optimized design is compared to the baseline as shown in Figure 23. This optimized design does not require major modifications to the baseline design. Specially, the costly option of going for a new inflator is avoided. (Baseline and optimized design have similar mass flow rates). This optimum design was selected for further evaluation.

RESPONSE SURFACE METHOD

Response surface functions were developed by fitting taylor polynomial models through the DOE results for each of the occupant injury responses. AIC (Akaike's Information Criterion) procedure is utilized to optimize the quality of the models. These models were developed primarily to evaluate the fidelity of such functions for future work.

$$\hat{Y} = \sum_{i=1}^{p} a_i F_i(x_1,\ldots\ldots\ldots,x_n)$$

$\hat{Y}$ = Response

a_i = model coefficients are calculated based on the least squares criterion

x_i = Design variables

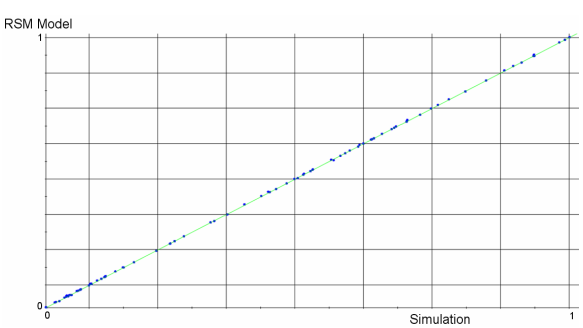

Figure 24. Scatter plot: Compares response values between simulation and RSM model.

The scatter plot assesses the quality of the models. Model is accurate when the sample points are close to the diagonal as shown in figure 24.

These models are quite handy to quickly identify design trade-offs. Once an anticipated design is found it should be verified by actual simulations. The optimized design was used as a sample point to check the RSM functions. Comparison is made between the actual and RSM prediction as shown below.

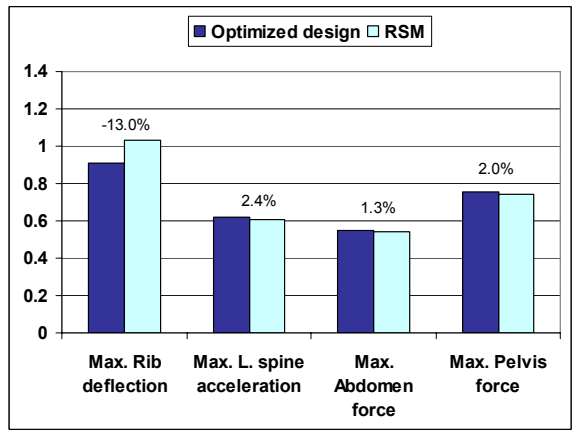

Figure 25. New 214: Optimized design vs RSM.

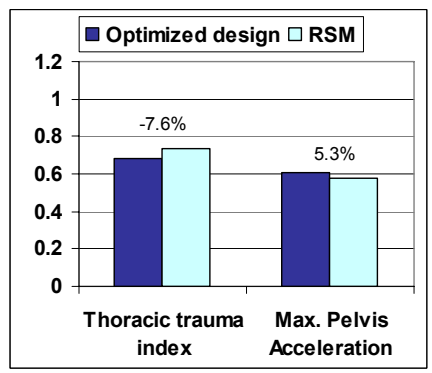

Figure 26. SINCAP: Optimized design vs RSM.

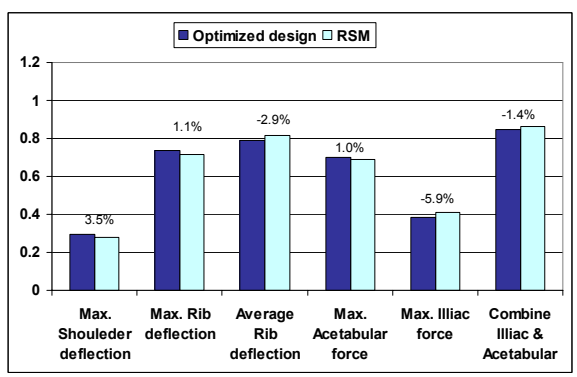

Figure 27. SICE: Optimized design vs RSM.

RSM predictions are acceptable for most of the injury responses except for max rib deflection (new 214) and thoracic trauma index.

RSM based optimization techniques were not explored in this study because crash analysis tends to be quite noisy and non-linear. Although reasonably good response surface functions were developed for many of the injury responses, they tend to be accurate along certain regions only. Therefore they are not recommend to be used with global optimization techniques.

CONCLUSION

The method presented in this paper shows how to employ DOE and optimization techniques to find a optimum restraint system that meets all injury requirements in a multi test mode scenario. Around 500 LS-DYNA simulations were needed to complete the study. OPTIMUS process automation software was used to integrate all 3 sled models into a single work flow which would make all simulations run in batch mode. A few simulations did not complete correctly due to model instabilities that occurred when extremes of the design space is explored. OPTIMUS was very flexible to incorporate safe guards that detect and eliminate the failed experiments from the optimization process. This is very important in optimization because successive iterations will depended on previous ones.

The methodology presented in this paper can be applied to any simulation based development work. DOE and Optimization technique that should be employed may vary depending on the nature of the application.

REFERENCE

1. Rodriguez, D.L., “Response Surface Based Optimization with a Cartesian CFD Method”, AIAA -2003-0465, Sept. 2003.
2. Schwefel, H. P., “Numerical Optimization of Computer Models”, (John Wiley & Son Chicester, New York).
3. Khuri, A., Cornell, J., “Response Surfaces, Design and Analyses”, (Marcel Dekker, New York).
4. Box, G., Hunter, W., Hunter, S., “Statistics for Experiments”, (Wiley, New York).
5. Papalambros, P. Y., Wilde, D. J., “Principles of Optimal Design”, Cambridge University Press.
6. Noesis Solutions NV, OPTIMUS Documentation.
7. LS-DYNA version 970 Keyword user’s Manual